

FILE COPY
NO. I-W

MR No. A5J12

NATIONAL ADVISORY COMMITTEE FOR AERONAUTICS

WARTIME REPORT

ORIGINALLY ISSUED

October 1945 as
Memorandum Report A5J12

AERODYNAMIC CHARACTERISTICS OF A 1/8-SCALE POWERED
MODEL OF A HIGH-SPEED BOMBER WITH A DUAL PUSHER

PROPELLER AFT OF THE EMPENNAGE

By James A. Weiberg and Alfred W. Schnurbusch

Ames Aeronautical Laboratory
Moffett Field, California

FILE COPY
To be returned to
the files of the National
Advisory Committee
for Aeronautics
Washington, D. C.



WASHINGTON

NACA WARTIME REPORTS are reprints of papers originally issued to provide rapid distribution of advance research results to an authorized group requiring them for the war effort. They were previously held under a security status but are now unclassified. Some of these reports were not technically edited. All have been reproduced without change in order to expedite general distribution.

NATIONAL ADVISORY COMMITTEE FOR AERONAUTICS

MEMORANDUM REPORT

for the

Air Technical Service Command, U. S. Army Air Forces

AERODYNAMIC CHARACTERISTICS OF A 1/8-SCALE POWERED

MODEL OF A HIGH-SPEED BOMBER WITH A DUAL PUSHER

PROPELLER AFT OF THE EMPENNAGE

By James A. Weiberg and Alfred W. Schnurbusch

SUMMARY

Wind-tunnel tests were made to determine the aerodynamic characteristics of a 1/8-scale model of a high-speed bomber with a dual pusher propeller aft of the empennage. In this report the results of these tests are discussed with respect to the longitudinal, lateral, and directional stability and control, the empennage design, and ground effects on the aerodynamic characteristics.

The test results indicated that, because of the location of the propeller, the configuration of this airplane has several advantages with regard to stability and control over the conventional-type single-engine airplane configuration. The effect of power is to increase both the longitudinal and directional stability. Power has negligible effect on the dihedral characteristics. The effectiveness of the empennage and the control surfaces agreed well with computed values, and the ground-plane results indicated an increase in longitudinal stability and lift-curve slope that compared favorably with computed values.

INTRODUCTION

At the request of the Air Technical Service Command, U.S. Army Air Forces, tests were made on a 1/8-scale powered model of a high-speed bomber having a dual pusher propeller aft of the empennage. These tests were made in the Ames 7- by 10-foot wind tunnel to determine the aerodynamic characteristics of the model.

This report discusses the longitudinal, lateral, and directional stability and control of the model. Included are model characteristics with a braking propeller and ground effects in the simulated take-off and landing attitudes. This discussion is based on the results of tests made during the period from December 27, 1943 to January 31, 1944 and March 22, 1944 to April 8, 1944. An analysis of the flying qualities of the airplane is presented in reference 1.

COEFFICIENTS AND SYMBOLS

All data are presented as standard NACA coefficients corrected for support tares, tunnel-wall interference, and stream inclination. Rolling-moment coefficients are given about the stability axes; all other coefficients are referred to the wind axes. Moments are presented about a center-of-gravity position located at 25 percent of the M.A.C. and 6.8 percent of the M.A.C. above the fuselage reference line. The trunnion and center-of-gravity locations with respect to the model geometry are shown in figure 7. The angles of attack and yaw are referred to the fuselage reference line and the plane of symmetry, respectively. Wind-tunnel-wall corrections and configuration symbols used on the figures are given in appendixes A and B, respectively. Coefficients and symbols used throughout the report are defined as follows:

- C_L lift coefficient (L/qS_W)
- C_D drag coefficient (D/qS_W)
- C_Y side-force coefficient (Y/qS_W)
- C_l' rolling-moment coefficient referred to stability axis ($L/qS_W b$)
- C_m pitching-moment coefficient ($M/qS_W \bar{c}$)
- C_n yawing-moment coefficient ($N/qS_W b$)
- C_{h_e} elevator hinge-moment coefficient ($HM_e/qS_e t_e$)
- C_{h_r} rudder hinge-moment coefficient ($HM_r/qS_r t_r$)
- HM_e elevator hinge moment, pound-feet
- HM_r rudder hinge-moment, pound-feet
- F control force, pounds

- S area (for hinge-moment coefficients, area aft of hinge line), square feet
- b span, feet
- \bar{c} mean aerodynamic chord, feet
- t M.A.C. of control-surface area aft of hinge line, feet
- A aspect ratio
- l_H tail length from $0.25\bar{c}_W$ to $0.25\bar{c}_H$, feet
- l_V tail length from $0.25\bar{c}_W$ to $0.25\bar{c}_V$, feet
- l_{He} tail length from $0.25\bar{c}_W$ to aerodynamic center of incremental lift due to elevator deflection
- l_{Vr} tail length from $0.25\bar{c}_W$ to aerodynamic center of incremental lift due to rudder deflection, feet
- S_{He} horizontal-tail area affected by elevators, square feet
- S_{Vr} vertical-tail area affected by rudders, square feet
- q dynamic pressure ($\frac{1}{2}\rho V^2$), pounds per square foot
- R Reynolds number ($\rho V l / \mu$)
- V velocity, feet per second
- ρ air density, slugs per cubic foot
- μ coefficient of viscosity
- T_c thrust coefficient $\left(\frac{\text{effective thrust}}{\rho V^2 D^2} \right)$
- V/nD advance diameter ratio
- n propeller rotational speed, revolutions per second
- D propeller diameter, feet
- $\Delta P/q$ pressure coefficient (pressure below the elevator nose seal minus the pressure above or the pressure to the left of the rudder seal minus the pressure to the right divided by free-stream dynamic pressure)

α_u	geometric angle of attack of fuselage reference line (uncorrected), degrees
α	angle of attack of fuselage reference line (corrected for wind-tunnel-wall interference and stream inclination), degrees
α_H	angle of attack of horizontal tail (measured from zero tail lift line), degrees
a	lift curve slope ($dC_L/d\alpha$)
i_H	horizontal-tail incidence (measured from fuselage reference line to horizontal-tail reference plane), degrees
ψ	angle of yaw of fuselage plane of symmetry, degrees
δ	control-surface deflection, degrees

Subscripts

W	wing
H	horizontal tail
V	vertical tail
e	elevator
r	rudder

DESCRIPTION OF THE AIRPLANE AND MODEL

The airplane is a three-place light bomber. Major airplane dimensions are listed in Appendix C and tables I and II. A three-view drawing of the airplane and line drawings of the wing and empennage are given in figures 1, 2, and 3, respectively. The airplane is of unconventional design in that the dual pusher propeller is aft of the empennage. Each set of three propeller blades is gear-driven by one of two engines submerged in the fuselage. The airplane has sealed internally balanced control surfaces (see figs. 2 and 3 for cross-sectional views), a tricycle landing gear retractable into the fuselage, and double-slotted partial-span flaps. The small split flap on the wing adjacent to the fuselage (fig. 2) operates in

conjunction with the landing gear in that it is retracted when the gear is up and deflects to 40° after the gear is extended. This linkage is necessary in order to provide a flap between the double-slotted flaps and the fuselage and still allow the double-slotted flap to be operated for any position of the gear. The vertical tail extends both above and below the fuselage with the lower half also acting as a propeller guard.

The model is shown mounted in the tunnel in figure 4. The model is 1/8-scale and is scaled from the airplane with the following exceptions:

1. There are no ailerons or elevator trim tabs on the model.
2. There are flap brackets on the model wing which do not exist on the prototype.
3. The wing gun turrets on the model are not an exact simulation of those on the airplane.
4. The model has no wing leading-edge ducts, flush-type fuselage carburetor scoop, engine exhaust or propeller-bearing oil-cooler scoop.
5. There are no main wheel-well doors on the model. The doors on the airplane were considered to be closed when the main gear was extended.
6. The inboard end of the model lower rudder is 1.094 inches full scale farther outboard than on the airplane. This represents a decrease in lower rudder area of 0.198 square foot full scale (2.2 percent).
7. The control-surface balance and balance-plate spans on the model differed from those on the prototype airplane as shown by the following table:

Control surface	^a Geometric balance	^b Effective balance	Balance-plate span full scale (ft)
Airplane Elevators	^c 0.45 _{c_e} to .50 _{c_e}	^{c&d} 0.40 _{c_e} to .45 _{c_e}	18.00
Upper rudder	.47 _{c_r}	^d .396 _{c_r}	5.08
Lower rudder	.47 _{c_r}	^d .396 _{c_r}	3.42
Model Elevators (original balance)	^e .365 _{c_e}	.358 _{c_e}	17.15
(revised balance)	^f .45 _{c_e}	.443 _{c_e}	17.65
Upper rudder (original balance)	.355 _{c_r}	.335 _{c_r}	4.47
(revised balance)	.47 _{c_r}	.465 _{c_r}	4.94
Lower rudder (original balance)	.355 _{c_r}	.346 _{c_r}	3.12
(revised balance)	.47 _{c_r}	.458 _{c_r}	3.12

^aThe geometric balance is the ratio of c_b/c_f where c_b is the distance from the hinge line to the center line of the seal and c_f is the chord of the control surface aft of the hinge line. The balance plate chord c_b and control surface chord c_f are, for each control surface, a constant percent of the total surface chord. The estimated control-surface effective balance on the airplane is less than the geometric balance because of the effects of cut-outs for hinges, cut-offs for cover-plate ribs, and leakage through drainage holes. The model effective balance is less than the geometric because of the short balance-plate spans.

^bThe effective balance is an equivalent geometric balance of constant percent elevator chord with no seal leaks and with a balance-plate span scaled from the airplane.

^cAdjustable.

^dEstimated.

^eBalance on original empennage used during series of tests from December 27, 1943 to January 31, 1944. This empennage is referred to as HV in the report. (See configuration key.)

^fCorresponds to empennage with balance increased so that the geometric balance was the same on both the model and the airplane. Used on the series of tests from March 22, 1944, to April 8, 1944. This empennage is referred to as H₁V₁ in the report. (See configuration key.)

The model control surfaces were equipped with resistance-type electrical strain gages for measuring hinge moments. Pressure tubes were installed on the original empennage HV in the balance cells of the rudders and elevators for obtaining the increment of pressure coefficient $\Delta P/q$ across the nose seals at about the 40-percent spanwise stations of the balance-plate spans. Elevator and rudder deflections were set by means of templates with an estimated accuracy of $\pm 0.25^\circ$. The horizontal stabilizer settings were set by fixed brackets.

Power for the dual propeller was supplied by two 25-horsepower water-cooled induction motors mounted in the fuselage. Each motor drove a set of three propeller blades through its own separate gear system. The model propeller was scaled from the propeller on the airplane and was set at a blade angle (at 0.75R) of 20° when operating at positive thrust and -25° for negative thrust. Power conditions were set using the computed variation of T_c with C_L for the airplane given in figure 5.

The necessary loads for operating the motors and strain gages were brought into the model through the support struts. (See fig. 6.)

RESULTS AND DISCUSSION

The results presented herein include elevator and rudder hinge-moment coefficients for both the original HV and a revised H₁V₁ model control-surface balance. In general, the tests for the estimation of the flight characteristics were made with the control-surface balances revised to conform with those on the airplane. Other tests were made with the original balances. The percent effective balance for which the hinge-moment coefficients are

presented is given in each figure. Where the hinge-moment coefficients are presented for the original balance, the pressure coefficient $\Delta P/q$ is also given so that the coefficients may be corrected for the balances corresponding to those on the airplane.

Lateral- and Directional-Stability and -Control Characteristics

Lateral stability.-- The variation of rolling moment with angle of yaw $C_l'_{\psi}$ shown in figures 8 to 12 is, for the angle-of-attack range tested, unaffected by changes in the thrust coefficient T_c or by the addition of the horizontal and vertical tail surfaces. The lateral-stability derivative $C_l'_{\psi}$ is not dependent on T_c because the slipstream does not pass over any lifting surface and because the propeller forces have negligible moment arms for providing rolling moment. The tail surfaces also have negligible moment arms for developing rolling moment. At high positive or negative angles of attack the effect of the propeller and the tail surfaces on $C_l'_{\psi}$ may become large.

It may also be noted from figures 8 to 12 that the variation of $C_l'_{\psi}$ with flap deflection is very small for the angle-of-attack range tested ($\alpha_{fl} = 2^\circ$ for flaps up and flaps 30° , $\alpha_{fl} = -1^\circ$ for flaps 50°). This latter characteristic may be attributed to the plan-form geometry of the wing (85-percent line straight) as indicated by the results of reference 2.

Directional stability.-- The effect on directional stability of varying the thrust coefficient T_c is shown by the curves of C_n plotted against ψ in figures 8 to 12. To provide a more exact comparison, these results have been summarized in figure 13 in the form of curves of $C_n'_{\psi}$ ($\partial C_n / \partial \psi$) plotted against T_c average from -6° to 10° angle of yaw.

From figure 13 it may be seen that the addition of the propeller, operating at zero thrust, to the tail-removed configuration produces a stabilizing increase in $C_n'_{\psi}$. Operation of the propeller increases this increment at positive values of T_c and decreases it at negative values. The variation with T_c of the yawing moment due to the propeller, with the empennage removed, is dependent on the variation with T_c of the angle of flow into the propeller as regulated by the fuselage sidewash angle, the dynamic pressure over the aft end of the fuselage and the side force resulting from the yawed propeller.

Addition of the vertical tail to the model produces the normal

stabilizing increase in $C_{n\dot{\psi}}$. Inspection of figure 13 indicates, however, that the increase resulting from the addition of the tail is less when the propeller is operating at zero T_c than it is when the propeller is removed. This reduction may be accounted for by the reduced angle of flow into the propeller due to the sidewash of the vertical tail (corresponding to downwash on a lifting surface). Thus, location of the tail just forward of the propeller results in mutual interference that reduces the effectiveness of the combination in producing directional stability.

Positive values of T_c have no effect on the increment in $C_{n\dot{\psi}}$ due to the addition of the vertical tail but negative T_c reduces this increment. The variation with T_c of the yawing moment, due to the propeller with the empennage on, is governed by the variation with T_c of the angle of flow into the tail as regulated by the fuselage sidewash angle, the angle of flow into the propeller as regulated by the tail sidewash angle, the dynamic pressure over the tail, and the side force resulting from the yawed propeller. (This analysis assumes that the addition of the tail does not affect the variation with T_c of the angle of flow into the propeller as regulated by the fuselage sidewash angle and the dynamic pressure over the aft end of the fuselage.) Because of the number of variables involved, it is not possible to determine from the existing data the magnitude of each of the variables.

It may be noted from figure 13 that the tail yawing-moment derivative (tail on $C_{n\dot{\psi}}$ minus tail off $C_{n\dot{\psi}}$) is reduced as the flaps are deflected. This reduction exists with both propeller on and propeller off. The reduction is due to either a decrease in velocity over the tail or an increase in rate of change of fuselage-wing sidewash angle resulting from flap deflection.

Figures 8 to 12 show a break occurring in the propeller-removed tail-on curve of C_n plotted against ψ at an angle of yaw of approximately 15° . With the application of power, particularly positive thrust, this break is removed. It is believed that this straightening of the curve is the result of the sudden increase of the angle of flow into the propeller when the vertical tail stalls.

Vertical-surface effectiveness.— In order to obtain an indication of the effectiveness of the vertical surface with propeller removed, comparison is made of the flaps-retracted experimental and computed values of the tail yawing-moment derivative $(C_{n\dot{\psi}})_V$. From figures 8 and 9 for propeller removed and flaps retracted, $(C_{n\dot{\psi}})_V$ through zero ψ is -0.0020 . Calculation gives for the tail yawing moment

$$(C_{n\psi})_V = - \frac{S_V l_V}{S_W b_W} a_V (q_V/q) \eta_V \left(1 - \frac{d\alpha}{d\psi} \right)$$

where

$$a_V = \frac{0.11A}{A + 3} = 0.059 \quad (\text{reference 3})$$

Thus the tail yawing moment is

$$(C_{n\psi})_V = - \frac{(86.98)(20.23)}{(554.6)(70.5)} (0.059) \left(\frac{q_V}{q} \right) \eta_V \left(1 - \frac{d\alpha}{d\psi} \right)$$

Substitution of the experimental value of $(C_{n\psi})_V$ of -0.0020 gives

$$(q_V/q) \eta_V \left(1 - \frac{d\alpha}{d\psi} \right) = 0.77$$

This value is reasonable when compared with the results of reference 4.

Rudder effectiveness.— The results of tests for the determination of rudder effectiveness are summarized in figures 14 and 15. These figures show the effect of power and flap deflection on the yawing moment due to rudder deflection at zero sideslip. In order to better show the variation of rudder effectiveness with thrust coefficient T_C , values of $C_{n\delta_r}$ ($\partial C_n / \partial \delta_r$) averaged through 0° to -10° , δ_r from figures 14 and 15 for flaps 0° , 30° , and 50° are presented as a function of T_C in figure 16. From this figure it may be seen that $C_{n\delta_r}$ is reduced when the propeller, operating at zero thrust, is added to the propeller-removed configuration. With increase in positive thrust $C_{n\delta_r}$ increases. Negative thrust reduces $C_{n\delta_r}$. This variation of rudder effectiveness $C_{n\delta_r}$ with T_C and the reduction in $C_{n\delta_r}$ resulting from the addition of the propeller ($T_C = 0$) are seen to be essentially independent of flap deflection or model attitude for the angle range tested ($\alpha_{fl} = 2^\circ$ for flaps up and 30° , $\alpha_{fl} = -1^\circ$ for flaps 50°). When the rudder is deflected the tail sidewash angle and consequently the flow into the propeller and the resultant propeller side force are changed. The subsequent variation of C_n with T_C is dependent upon several other variables as was pointed out in the discussion of $C_{n\psi}$ under

directional stability, but because of the number of variables involved it is not possible to determine from the existing data the magnitude of each of the variables.

In order to show the variation of directional-control characteristics with angle of yaw, typical curves showing the variation with angle of yaw of C_n , C_{hr} , and $\Delta P/q$ with the rudder deflection varied are presented for flaps deflected 50° in figure 17 for propeller removed and in figures 18 and 19 for propeller operating at thrust coefficients of 0 and 0.75, respectively. The rudder effectiveness is essentially constant with angle of yaw within the sideslip-angle range to which the airplane can be balanced by the rudder. Thus the ability of the rudder to balance the airplane in steady sideslips for any flap position or power condition can be determined from the directional-stability curves of figures 8 to 12 and the rudder-effectiveness curves of figures 14 and 15. The pressure coefficient $\Delta P/q$ and rudder-hinge-moment coefficient C_{hr} were both essentially independent of flap deflection. Thus these coefficients may be determined for various power conditions from figures 17 to 19.

With flaps 50° and propeller removed (fig. 17) the relationship between directional stability, rudder effectiveness and rudder hinge moments is such that if the propeller-removed configuration were a condition of flight, there would exist on the airplane a reversal of rudder position and rudder-pedal force for balance as the angle of sideslip was increased. The effect of power, however, is to remove this rudder-angle and pedal-force reversal as shown by the curves of C_n , C_{hr} , and $\Delta P/q$ for propeller operating at zero thrust in figure 33.

In order to determine the contribution of each rudder to the yawing moment produced by rudder deflection, tests were made with only the lower rudder deflected. The results are presented in figures 20 and 21 for flaps 0° and 50° , respectively. The variation of yawing moment with lower rudder deflection at zero sideslip is shown in figure 22 for comparison with the data for both rudders deflected. The lower rudder has an area of 42 percent of the total rudder area and produces 37 percent of the total rudder yawing moment. The moment arms of the two rudders producing a yawing moment are essentially the same. Tests indicated that the lower-rudder hinge moments and balance-cell pressures were independent of upper rudder deflection.

In order to compare the effectiveness of the rudders as determined

experimentally with the computed effectiveness, computations are made of the yawing moment due to rudder deflection $C_{n\delta_r}$. From figure 22, $C_{n\delta_r}$ for flaps retracted and propeller off is -0.0007 for the upper rudder and -0.0004 for the lower rudder. Computation gives for the yawing moment resulting from rudder deflection

$$\frac{\partial C_n}{\partial \delta_r} = \frac{S_{V_r}}{S_W} \frac{l_{V_r}}{b_W} \frac{\partial a_V}{\partial \delta_r} a_V \frac{q_V}{q} \eta_{V_r}$$

where

$$\frac{\partial a_V}{\partial \delta_r} = -0.071 \quad (\text{reference 5})$$

$$a_V = \frac{0.11A}{A + 3} = 0.059 \quad (\text{reference 3})$$

Thus, for the upper rudder the yawing moment due to rudder deflection is

$$\begin{aligned} \frac{\partial C_n}{\partial \delta_r} &= \frac{31.35 (21.34)}{554.6 (70.5)} (-0.71)(0.059) \left(\frac{q_V}{q} \right) \eta_{V_r} \\ &= -0.0007 \left(\frac{q_V}{q} \right) \eta_{V_r} \end{aligned}$$

or

$$\left(\frac{q_V}{q} \right) \eta_{V_r} = 1.0$$

For the lower rudder, the yawing moment due to rudder deflection is

$$\begin{aligned} \frac{\partial C_n}{\partial \delta_r} &= \frac{22.95 (21.34)}{554.6 (70.5)} (-0.71)(0.059) \left(\frac{q_V}{q} \right) \eta_{V_r} \\ &= -0.0005 \left(\frac{q_V}{q} \right) \eta_{V_r} \end{aligned}$$

or

$$\left(\frac{qY}{q}\right) \eta_{Vr} = 0.8$$

Thus the upper rudder appears to be more effective in producing a yawing moment. The reduced effectiveness of the lower rudder may be attributed to disturbed flow over the lower vertical surface due to flow separation off the lower surface of the aft part of the fuselage.

Longitudinal-Stability and -Control Characteristics

Longitudinal stability.— As the power loading of conventional single-engine tractor airplanes is increased, the problem of maintaining longitudinal stability at low speeds with flaps down and the engine delivering considerable power and still having adequate maneuverability at high speeds becomes acute. The major destabilizing effect of power at low speeds on conventional airplanes arises from the large change in downwash over the tail when power is applied. When the propeller is placed aft of the empennage as on this airplane, unfavorable slipstream effects on the tail can be avoided. Location of the propeller aft of the center of gravity also results in the normal force on the pitched propeller producing a stabilizing moment when operating at positive thrust.

An indication of the effect of power on longitudinal stability for the model can be obtained from the pitching moment resulting from operating the propeller with elevator undeflected shown in figures 23 to 25 for flaps 0° , 30° , and 50° . Addition of the propeller, operating at zero thrust, to the propeller-removed configuration with flaps retracted (fig. 23) results primarily in a change in elevator angle required for balance amounting to approximately 0.5° of down-elevator with little change in dC_{M1}/dC_L . With flaps deflected, addition of the propeller operating at zero thrust results in an increase in dC_{M1}/dC_L of approximately 0.01 and 0.03 for flaps 30° (fig. 24) and 50° (fig. 25), respectively, as well as a change in elevator required for balance of approximately 2.5° down-elevator at a $C_L = 1.0$ for both flap deflections. An increase in power for both flaps up and flaps down results in a stabilizing increase in dC_{M1}/dC_L with elevators neutral.

The variation of longitudinal stability with power is governed by several factors (similar to those discussed under directional

stability). These include the flow into the tail as affected by the downwash from the wing-fuselage combination, the angle of flow into the propeller as affected by the tail downwash angle, the moment produced by the thrust force, the normal force resulting from the pitched propeller, and the dynamic pressure at the tail. Because of the number of variables involved it is not possible to determine from the existing data the contribution of each of the variables to longitudinal stability.

The longitudinal characteristics with elevator deflected are presented in figures 26 to 34 for flaps 0° , 30° , and 50° with the propeller removed and operating at zero thrust and military power. From these figures, the center-of-gravity positions for neutral stability for flaps up and deflected 50° are presented in figure 35 for elevator free and fixed. From this figure, it is seen that increasing power results in a rearward or favorable shift in neutral-point location. The location of the neutral points is such that both stick-fixed and stick-free longitudinal stability with propeller operating exists for center-of-gravity locations back to 35 percent M.A.C. (the most aft design center of gravity of the airplane).

It will be noted that, for flaps deflected 50° with propeller removed (fig. 32), a break in the pitching-moment curve occurs at a $C_L = 1.2$. This break is traceable to a stall of the horizontal tail. As the lift coefficient decreases, the negative tail angle of attack increases. Tail stall occurs at $C_L = 1.2$ ($\alpha_H = -11^\circ$). When power is applied (figs. 33 and 34), the acuteness of this break is reduced especially at the higher up-elevator deflections. This effect of power on the break in the power-off pitching-moment curve may be attributed to a change in propeller normal force resulting from a change in flow into the propeller when the tail stalls. With flaps retracted, the tail angle of attack does not reach the point where it stalls so that the above-mentioned type of break does not occur with flaps retracted.

The longitudinal characteristics as affected by Reynolds number are presented for flaps 0° and 50° in figures 36 and 37 for tail off and tail on, respectively. At a lift coefficient of approximately 0.6 for flaps 0° and 1.3 for flaps 50° , a change in lift-curve slope occurs. Figures 36 and 37 show that increasing Reynolds number increases the lift-curve slope above where this change in slope occurs and increases $C_{L_{max}}$ but has only a negligible effect on elevator hinge moments. Increased Reynolds number has little effect on pitching moment with flaps retracted but results in a large

shift in tail-on C_m with flaps 50° and a slight shift in tail-on C_m such that the tail pitching moment is increased. However, there is practically no change in stability. By the use of a rope mesh in front of the model, the stream turbulence, and hence the effective Reynolds number, was increased. Although the data (figs. 38 and 39) are qualitative only, they do indicate the same effect on lift curve and $C_{L_{max}}$ as increasing q . With flaps retracted (fig. 38), the increased effective Reynolds number resulted in an increase in dC_{he}/dC_L in a positive direction.

Horizontal-surface effectiveness.-- A determination of the effectiveness of the horizontal tail was made by obtaining the longitudinal characteristics, flaps retracted, for three tail settings 0° , 3.0° , and 5.8° . The results are plotted in figure 40 which shows the variation of C_m and C_{he} with uncorrected angle of attack α_u . The data in this figure cross-plotted at the value of α_u corresponding to zero tail angle of attack with 3.0° incidence (fig. 41) give a value of $\partial C_m / \partial i_H = -0.033$. A computed value can be determined from

$$\left(\frac{\partial C_m}{\partial i_H} \right)_\alpha = - \frac{l_H S_H}{c_W S_W} a_H \left(\frac{q_H}{p} \right) \eta_H$$

where

$$a_H = \frac{0.11A}{A + 3} = 0.066 \quad (\text{reference 3})$$

Thus, the horizontal-tail effectiveness is

$$\begin{aligned} \left(\frac{\partial C_m}{\partial i_H} \right)_\alpha &= - \frac{(19.86)(139.3)}{(8.56)(554.6)} (0.066) \left(\frac{q_H}{p} \right) \eta_H \\ &= -0.0385 \left(\frac{q_H}{p} \right) \eta_H \end{aligned}$$

or

$$\left(\frac{q_H}{p} \right) \eta_H = \frac{-0.033}{-0.0385} = 0.86$$

This value is a reasonable interference factor for the horizontal tail.

Elevator effectiveness.— In order to get an indication of the relative efficiency of the elevator, comparison is made of the propeller-removed experimental pitching moment resulting from elevator deflection $\partial C_m / \partial \delta_e$ with that computed. The data of figure 26, for flaps retracted and propeller removed, cross-plotted for $\alpha_H = 0^\circ$ in figure 42 give a value of $\partial C_m / \partial \delta_e = -0.0222$. The elevator effectiveness may be computed from the following:

$$\left(\frac{\partial C_m}{\partial \delta_e} \right)_\alpha = \frac{l_{H_e} S_{H_e}}{\bar{c}_W S_W} a_H \left(\frac{\partial \alpha_H}{\partial \delta_e} \right) \left(\frac{q_H}{q} \right) \eta_{H_e}$$

where

$$a_H = \frac{0.11A}{A + 3} = 0.066 \quad (\text{reference 3})$$

$$\frac{\partial \alpha_H}{\partial \delta_e} = -0.66 \quad (\text{reference 5})$$

Thus, the elevator effectiveness is

$$\begin{aligned} \left(\frac{\partial C_m}{\partial \delta_e} \right)_\alpha &= \frac{(21.47)(107.2)}{(8.56)(554.6)} (0.066) (-0.66) \left(\frac{q_H}{q} \right) \eta_{H_e} \\ &= -0.0211 \left(\frac{q_H}{q} \right) \eta_{H_e} \end{aligned}$$

Computations by the method of reference 6 indicate that $q_H/q = 1.0$. Therefore the elevator efficiency factor will be

$$\eta_{H_e} = \frac{-0.0222}{-0.0211} = 1.05$$

This value is in the direction that might be expected because of the low ratio of S_{H_e}/S_H . For this airplane $S_{H_e}/S_H = 0.77$ is low in comparison with values for other airplanes.

Negative thrust.— It is intended to use the propeller on the airplane as a brake in retarding the ground roll after contact has been made with the ground. However, for the purpose of indicating the effect on stability if the propeller were to be used as a brake

in dives or maneuvers, tests were made on the 1/8-scale model without a ground plane with the propeller operating at negative thrust.

The results showing the longitudinal characteristics with the propeller operating at negative thrust with military power at sea level are shown in figure 43 for flaps retracted. The large change in stability below $C_L = 0.3$ is attributed to the large dT_c/dC_L variation at low lift coefficients (fig. 5).

Tests of the Model in the Presence of a Ground Plane

Tests on the model included a determination of the aerodynamic characteristics of the model mounted in the presence of a ground plane to ascertain landing and take-off characteristics of the airplane. A side view of the model mounted in the 7- by 10-foot tunnel showing the location of the model in relation to the ground plane is shown in figure 44. Photographs of the installation in the tunnel are shown in figure 45.

Experimental and computed ground effects.— The effect of a ground plane on the lift-curve slope and the pitching-moment characteristics of the model is shown in figures 46 and 47 for flaps 0° and 30° . Included in these figures are computed ground effects on lift-curve slope and pitching moment as determined by the methods of reference 7. The effect of the ground is to increase the stability and slope of the lift curve.

The methods for computing ground effects on wing and tail angle of attack (reference 7) do not include the change in wing pitching moment. Reference to figures 46 and 47 shows that the ground effect on wing pitching moment is of appreciable value. If this experimentally determined change in wing pitching moment is applied to the computed tail on pitching moment in the presence of a ground plane, the computed and experimental results can be compared.

Figure 46 shows that, for flaps retracted, the slopes of the computed and experimental pitching-moment curves agree up to $C_L = 0.6$; however, the computed curve is shifted such that the up-elevator deflections required for balance near the ground are greater than those determined from the ground plane results. The data for flaps 30° (fig. 47) are presented for gear retracted because of the limited angle-of-attack range obtainable with the gear down in the presence of the ground plane. The effect of the

gear is to cause a shift in pitching moment without a change in stability and is essentially the same with tail on and off. The computed and experimental pitching-moment curves (flaps 30°) show reasonable agreement up to $C_L = 1.3$. Above $C_L = 1.3$ the curves diverge such that the computed up-elevator deflections required for balance near the ground are less than experimental elevator deflections.

The computed and experimental ground effect on lift-curve slope for flaps retracted (fig. 46) show excellent agreement throughout the angle-of-attack range. With flaps 30° at the higher lift coefficients near the stall, the computed and experimental lift curves are not in agreement because of a reduction in the lift-curve slope near the stall obtained from the ground plane tests.

Ground effects on maximum lift.— Tests of the model with the flaps deflected to the landing position (50°) in the presence of a ground plane gave abnormal lift characteristics (fig. 48) in that C_{Lmax} with flaps at 40° was greater than C_{Lmax} with flaps 50° . Further tests at increased Reynolds number obtained through increased stream turbulence by use of a turbulence screen in front of the model indicated that the airplane lift will be greater with flaps deflected 50° than with flaps 40° . (See fig. 48.) From the tail-off lift curves presented in figures 46 and 47 for flaps 0° and 30° , it can be seen that maximum lift is unaffected by the presence of the ground with flaps retracted but is reduced by approximately $\Delta C_L = 0.15$ with flaps deflected 30° .

Longitudinal control.— The adequacy of the elevator control is usually determined by its ability to hold the airplane at the landing attitude near the ground. As was shown in the discussion above, the ground-plane tests of the model with the flaps deflected to the landing position (50°) showed abnormal lift characteristics. In order to get an indication of the sufficiency of the elevator control in landing, tests were made with the flaps deflected 30° and 40° . (See figs. 49 and 50, respectively.) The data presented in reference 1 on the estimated flying qualities of the airplane showed that by extrapolation of the data of figures 49 and 50 there would be sufficient elevator control to land the airplane with flaps full down 50° with full forward center of gravity (0.20 M.A.C.).

The aerodynamic characteristics of the model in the take-off configuration (flaps 30°) with the propeller operating at take-off power in the presence of a ground plane are shown in figure 51. Comparison of this figure with figure 49 shows the effect of power

on the longitudinal characteristics of the model in the take-off configuration.

Horizontal-surface effectiveness.-- The horizontal-tail effectiveness in the presence of a ground plane was determined for flaps 0° , 30° , and 40° . The results, presented in figure 52, show the variations of C_m and C_{H_e} with angle of attack for tail settings of 0° , 3.0° , and 5.8° . A cross plot of this figure at the value of α_u corresponding to $\alpha_H = 0^\circ$ for $i_H = 3^\circ$ in figure 53 gives a value of $(\partial C_m / \partial i_H)_\alpha = -0.034$ for flaps retracted, which is slightly higher than the value of -0.033 obtained with no ground. Deflection of the flaps results in a small reduction of $(\partial C_m / \partial i_H)_\alpha$ and also a variation of $(\partial C_m / \partial i_H)_\alpha$ with angle of attack. This change may be due to the wing wake passing closer to the tail as the flaps are deflected.

Elevator effectiveness.-- The aerodynamic characteristics in the presence of a ground plane for flaps retracted with the elevator deflected and propeller removed are presented in figure 54. For comparison with the elevator effectiveness with no ground, the pitching moment resulting from elevator deflection (fig. 54) cross-plotted for zero tail angle of attack is given in figure 55. Up to -15° elevator deflection $\partial C_m / \partial \delta_e$ is unaffected by the presence of the ground.

Directional and lateral stability.-- The directional and lateral characteristics of the model in the presence of a ground plane are shown in figures 56 and 57 for flaps 30° and 50° , respectively. Comparison of these figures with the data of figures 11 and 12 for no ground plane indicates that the tail yawing moment and the yawing moment due to the propeller are unaffected by the ground. The directional stability of the complete model, however, is somewhat reduced due to the effect of the ground on the wing and fuselage. This increment change in stability $(\Delta C_n / d\psi)$ is 0.0001 and 0.0002 for flaps deflected 30° and 50° , respectively. The dihedral effect as shown by the variation of rolling moment with angle of yaw is increased in the presence of the ground. The change in $\Delta C_l' / d\psi$ is 0.0002 for either flap deflection.

CONCLUSIONS

The results of the model tests discussed in this report indicate the following:

1. With the propeller located aft of the empennage there is a mutual interference between the tail and the propeller. The interference is such that the effectiveness of the tail surfaces in producing stability and control is less with propeller on than with propeller off.

2. With increase in power, the effect of the propeller forces is such as to increase both the longitudinal and directional stability. Power has negligible effect on dihedral characteristics.

3. For both power on and off, longitudinal stability with elevator fixed and free exists for center-of-gravity positions back to 35 percent M.A.C. (the most aft design center-of-gravity location).

4. The effectiveness of the empennage and the control surfaces with propeller removed shows reasonable agreement with computed results.

5. The ground-plane results indicate an increase in longitudinal stability and lift-curve slope that compare favorably with computed values.

Ames Aeronautical Laboratory,
National Advisory Committee for Aeronautics,
Moffett Field, Calif.

APPENDIX A

Wind-Tunnel-Wall Corrections

Tunnel-wall corrections were applied to the drag, pitching moment, and angle of attack. The corrections are additive and were computed by the methods of reference 8 as follows:

For the model mounted in the center of the tunnel

$$\Delta\alpha_T = \delta_W \left(\frac{S_W}{C} \right) C_{Lu} \quad (57.3)$$

$$\Delta C_{DT} = \delta_W \left(\frac{S_W}{C} \right) C_{Lu}^2$$

$$\Delta C_{mT} = -\delta_{a.c.s.} \left(\frac{S}{C} \right) C_{Lu} \quad (57.3) \left(\frac{\partial C_m}{\partial i_H} \right)_\alpha$$

where

$$\delta_W = 0.127$$

$$\delta_{a.c.s.} = 0.067$$

$$S_W = \text{wing area} = 8.674 \text{ square feet}$$

$$C = \text{cross-sectional area of test section} \\ = 70 \text{ square feet}$$

$$\left(\frac{\partial C_m}{\partial i_H} \right)_\alpha = -0.033$$

For the model mounted in the presence of a ground plane

$$\Delta\alpha_T = \delta_W \left(\frac{S_W}{C} \right) C_{Lu} \quad (57.3)$$

$$\Delta C_{DT} = \delta_W \left(\frac{S_W}{C} \right) C_{Lu}^2$$

$$\Delta C_{mT} = 0$$

where

$$\delta_W = 0.026$$

$$S_W = 8.674 \text{ square feet}$$

$$C = 65 \text{ square feet}$$

APPENDIX B

Configuration Key

W_2	wing, including flaps
f_5	design partial-span flap with vane fixed to flap
f_6	split flap over landing gear
B	fuselage with bomber nose (includes dummy tail cone for tail-off configuration)
H	horizontal tail with $0.365c_e$ geometric balance elevators
H_1	horizontal tail with $0.45c_e$ geometric balance elevators and adjustable stabilizer
V	vertical tail with $0.355c_r$ geometric balance rudders
V_1	vertical tail with $0.47c_r$ geometric balance rudders
X_2	wing-fuselage fillet
E_3	pilot enclosure
Z_c	propeller spinner
G_3	wing guns
N_a	attack nose
N_b	bomber nose
P_1	front propeller operating with right-hand rotation
P_2	rear propeller operating with left-hand rotation
L	main gear
L_N	nose gear
S	standard configuration $W_2 G_3 B X_2 E Z_e H V$
S_1	standard configuration with tail having control surface balances corresponding to airplane $W_2 G_3 B X_2 E Z_e H_1 V_1$
GP	ground plane

APPENDIX C

Specifications of the Airplane

Engines (operated side by side for driving
dual propeller) Two Allison
V-1710-93 (E 11)

Gear ratio 0.361

Engine ratings (each) bhp/rpm/alt

War emergency power 1500/3000/SL

Take-off power 1325/3000/SL

Military power 1325/3000/SL to
1200/3000/22,500

Maximum rated power 1050/2600/SL to
20,000

Propeller Hamilton Standard
pusher

	Front (right hand)	Rear (left hand)
Blades (three each)	2C15B1-24	2C15B2-24
Diameter (ft)	13.167	13.0

Loading conditions	Gross weight (lb)	wing loading (lb/sq ft)	c.g. position* (percent M.A.C.)
Design	25,000	45	25
Attack	25,000	45	25 to 35
Bomber	34,580	62.2	25.3
Landing	21,500	38.8	26

*Vertical location of center of gravity for design condition is 6.8 percent M.A.C. above fuselage reference line or 13.3 percent M.A.C. below thrust line (same vertical location used for other conditions).

Tail lengths

l_H , ft	19.86
l_V , ft	20.23
l_{H_e} , ft	21.47
l_{V_r} , ft	21.34

Over-all dimensions

Length, ft	53.64
Height, ft	18.79

REFERENCES

1. Weiberg, James A., and Schnurbusch, Alfred W.: Flying Qualities of a Bomber Airplane with Engines in the Fuselage as Estimated from Tests of a 1/8-Scale Powered Model. NACA CMR No. A4K04, 1944.
2. Teplitz, Jerome: Effects of Sweep and Dihedral on Stalling and Lateral Characteristics of the Wind-Fuselage Combination of a Model of the XA-26 Airplane with Partial- and Full-Span Flaps. NACA ACR No. L4E20, 1944.
3. Wood, K.D.: Aspect Ratio Corrections. Jour. of the Aero. Sci., vol. 10, no. 8, Oct. 1943, pp. 270-272.
4. Pass, H.R.: Analysis of Wind-Tunnel Data on Directional Stability and Control. NACA TN No. 775, 1940.
5. Sears, Richard I.: Wind-Tunnel Data on the Aerodynamic Characteristics of Airplane Control Surfaces. NACA ACR No. 3L08, 1943.
6. Silverstein, Abe, and Katzoff, S.: Design Charts for Predicting Downwash Angles and Wake Characteristics Behind Plain and Flapped Wings. NACA Rep. No. 648, 1939.
7. Katzoff, S., and Sweberg, Harold H.: Ground Effect on Downwash Angles and Wake Location. NACA Rep. No. 738, 1943.
8. Swanson, Robert S., and Schuldenfrei, Marvin J.: Jet-Boundary Correction to the Downwash Behind Powered Models in rectangular Wind Tunnels with Numerical Values for 7- by 10-Foot Closed Wind Tunnels. NACA ARR, Aug. 1942.

TABLE I.— GENERAL GEOMETRIC DIMENSIONS OF THE AIRPLANE

Dimension	Wing	Horizontal tail	Vertical tail
Area (sq ft)	554.6	139.28	86.98
Span (ft)	70.5	25.0	17.4
M.A.C. (ft)	8.56	5.78	5.29
Aspect ratio	8.96	4.49	3.48
Taper ratio	.333	.57	-----
Geometric twist	2.07° (washout)	-----	-----
Dihedral from reference plane	4.0	0	-----
Incidence from reference plane	0	0	-----
Incidence from α_{L_0}	-----	1.89°	-----
Section profile (constant)	Douglas G-17	Douglas F ₁	Douglas H
Maximum percent thickness	17.02	13.45	15.55
Root chord (ft)	11.83	7.17	6.33
Tip chord (ft)	3.94	4.08	^a 4.25
Percent-chord line straight	85	65	60

^aDimension given is for upper vertical. Lower vertical has irregularly shaped bumper on tip.

TABLE II.-- MOVABLE SURFACE GEOMETRIC DIMENSIONS
OF THE AIRPLANE

Dimension	Ailerons	Elevators	Rudders		^a Double slotted flap	Split flap
			Upper	Lower		
Area (sq ft)	-----	-----	-----	-----	57.98	11.66
Area aft hinge line (sq ft)	26.34	37.50	12.54	8.99	----	----
Span (ft)	23.62	20.34	6.25	4.72	29.82	^b 2.88 ^c 3.42
Percent balance	^d 0.43 _{ca}	^d 0.45 _{ce} to 0.50 _{ce}	^d 0.47 _{cr}		----	----
^e Percent chord	22	35	40		25	34.7
Percent span	33.5	81.5	63		42.3	^b 4.08 ^e 4.85
^s aft ^t aft (ft ³)	31.34	71.6	26.08	16.57	----	----
Control travel	±6°	10° down 25° up	±20°		50° down	40° down
ⁱ F/HM	^f 3.142	^f .60	^f 1.003		----	----
Area affected by movable surfaces (sq ft)	-----	107.2	62.70	45.90	----	----
Area aft hinge line affected by balance (sq ft)	23.78	34.42	10.78	6.84	----	----
^h Trim tab area (sq ft)	-----	3.38	-----		----	----
Tab travel	-----	10° up 20° down	-----		----	----

^aDoes not include vane.^bMeasured along hinge line.^cMeasured along trailing edge.^dCorresponds to geometric balance on airplane.^eRatio of chord aft of hinge line to total surface chord.^fThese values are for cockpit control motions which allow for cable stretch^gWheel moment/hinge moment.^hRudder and aileron are trimmed with a apring.ⁱControl system mechanical advantage.

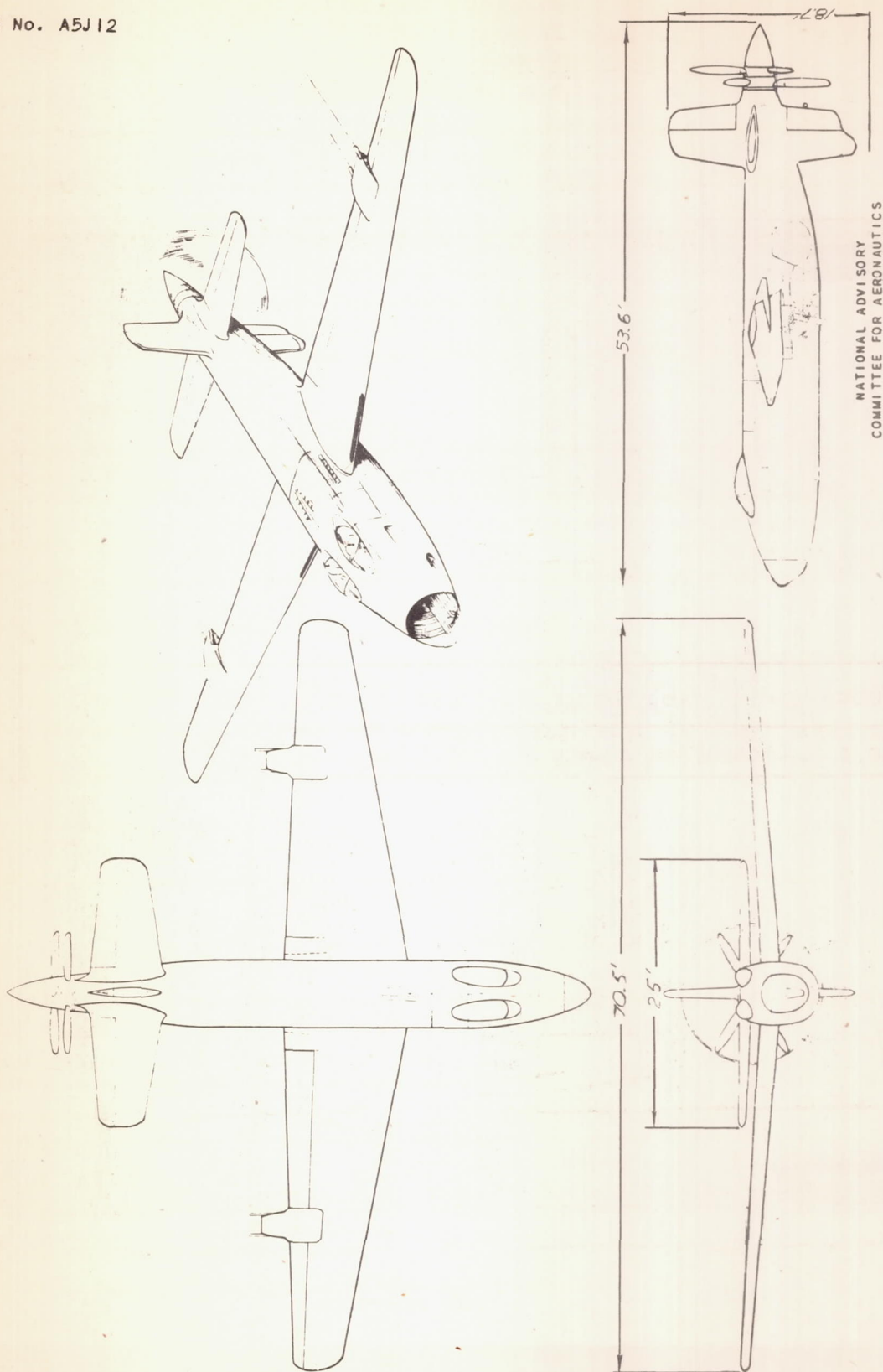
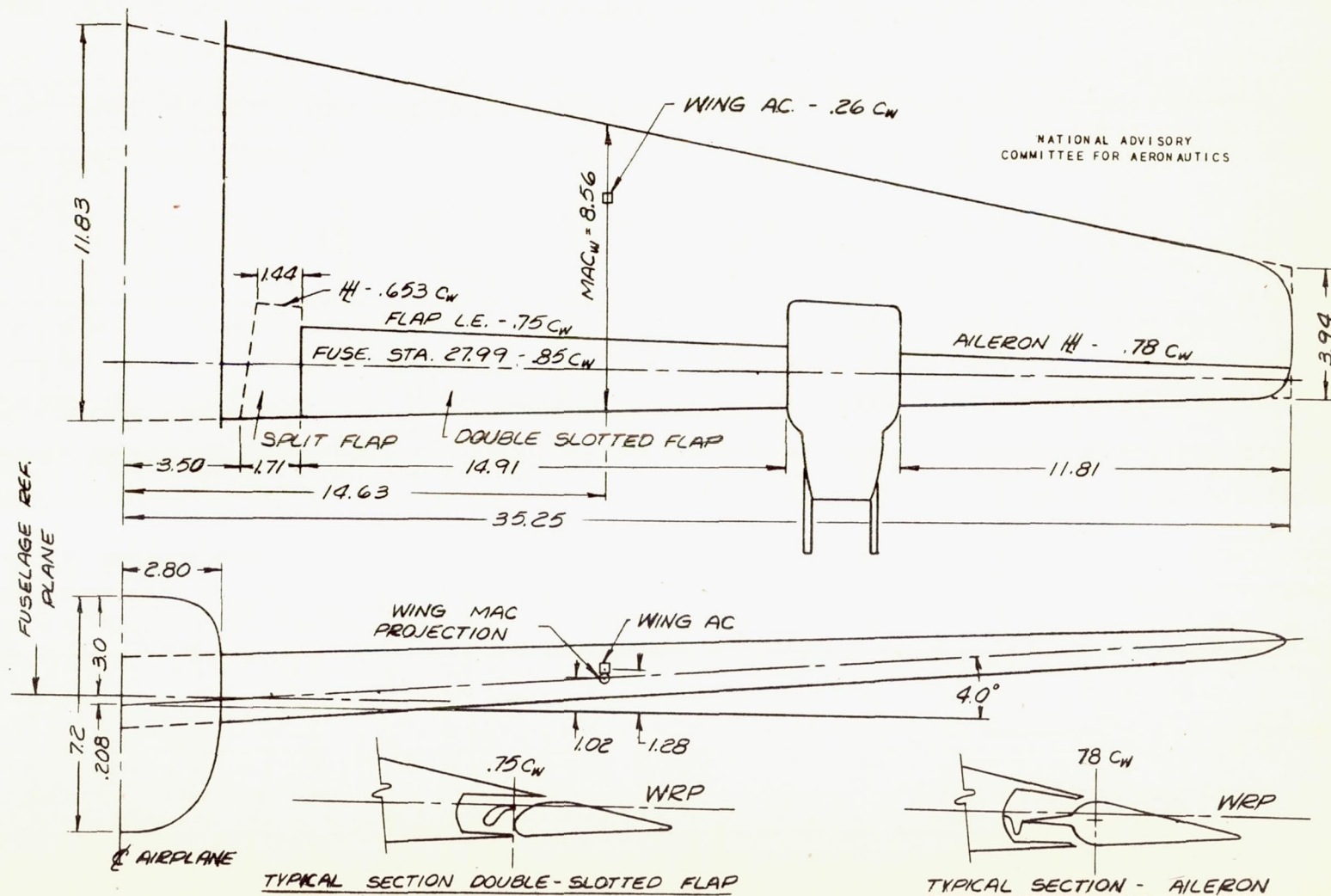
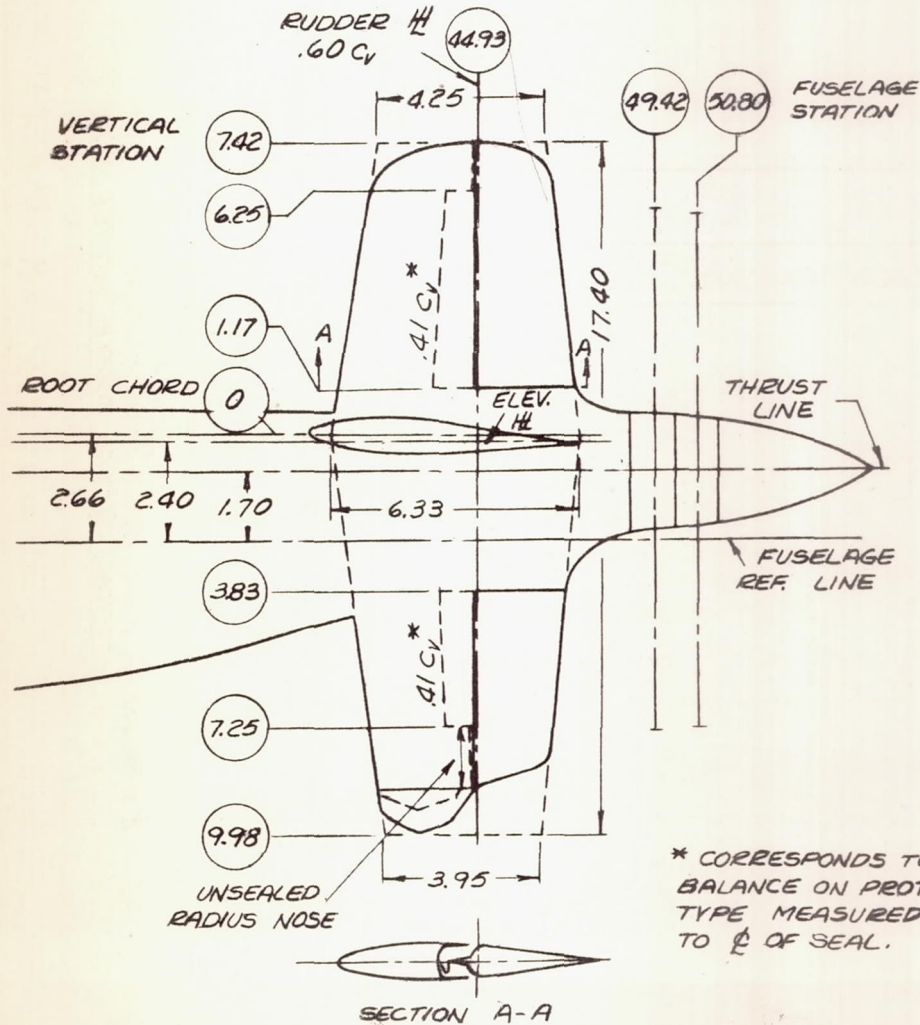
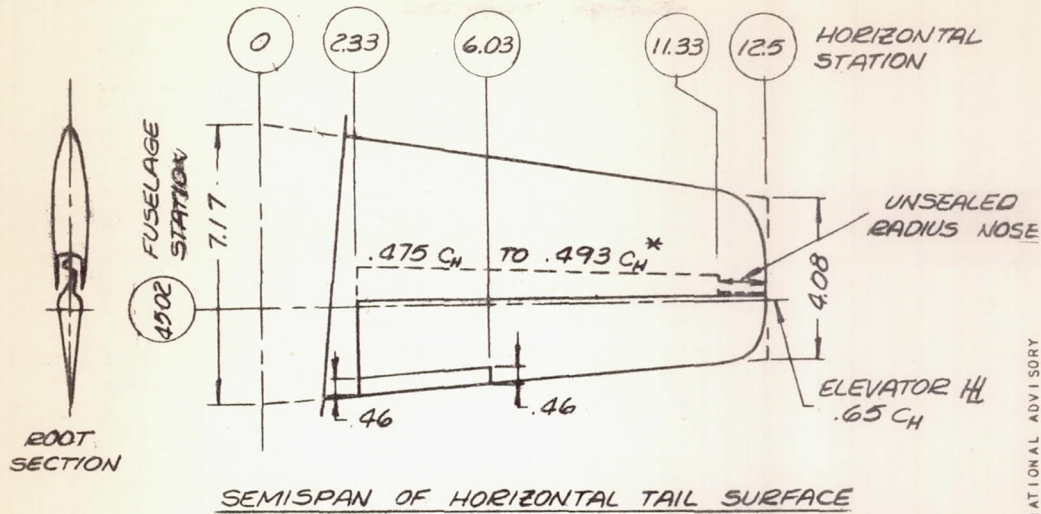


Figure 1.- Three-view drawing of the airplane.



DIMENSIONS FEET FULL SCALE $\frac{1}{100}$ SCALE

FIGURE 2.- LINE DIAGRAM C - WING SEMISPAN OF THE AIRPLANE.



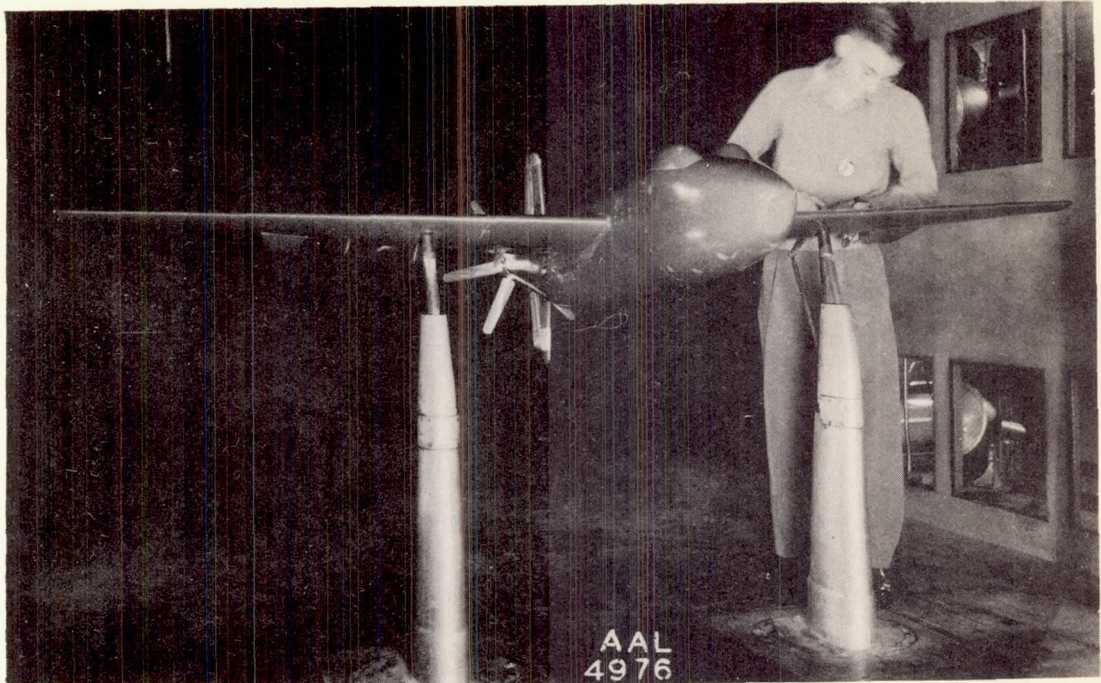
* CORRESPONDS TO BALANCE ON PROTO-TYPE MEASURED TO $\frac{1}{2}$ OF SEAL.

ALL DIMENSIONS FEET FULL SCALE
 $\frac{1}{40}$ SCALE

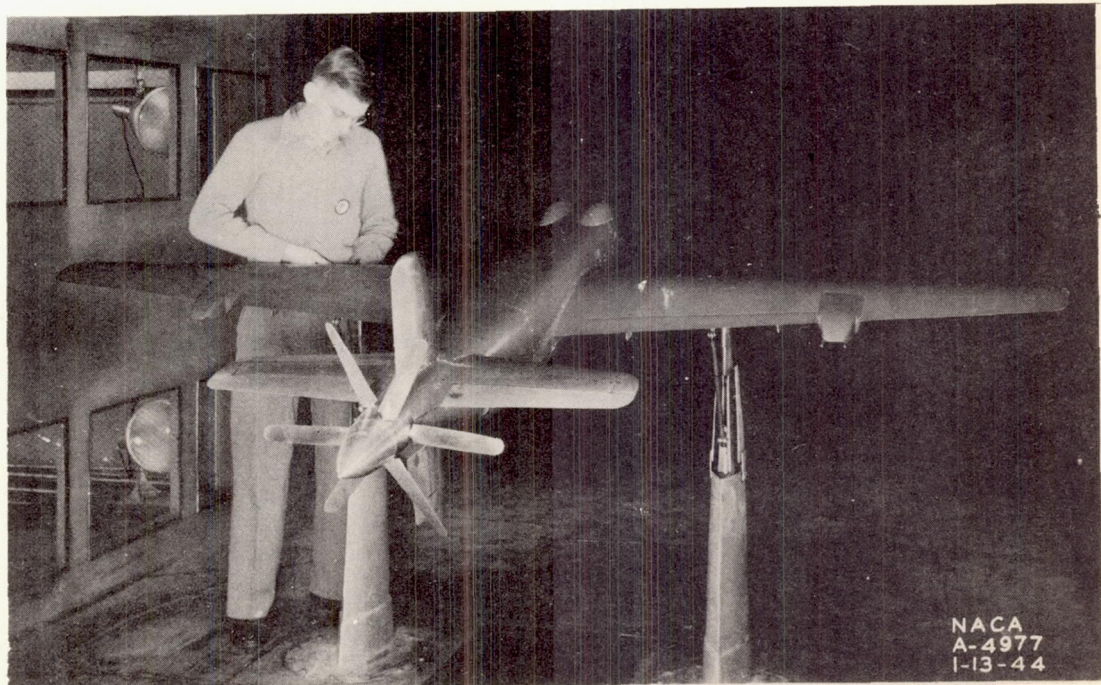
NATIONAL ADVISORY
COMMITTEE FOR AERONAUTICS

FIGURE 3.- LINE DIAGRAM OF EMPENNAGE OF THE AIRPLANE.

VERTICAL TAIL SURFACE

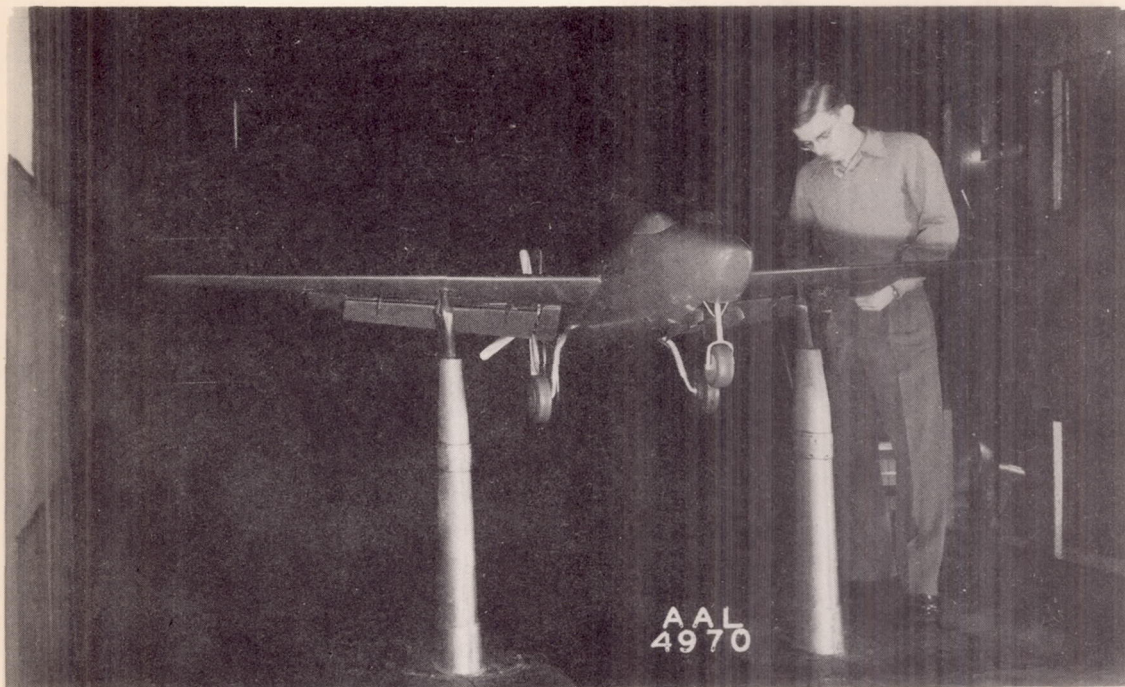


(a) Three-quarter front view. Standard configuration with propeller on. (S+P₁P₂)

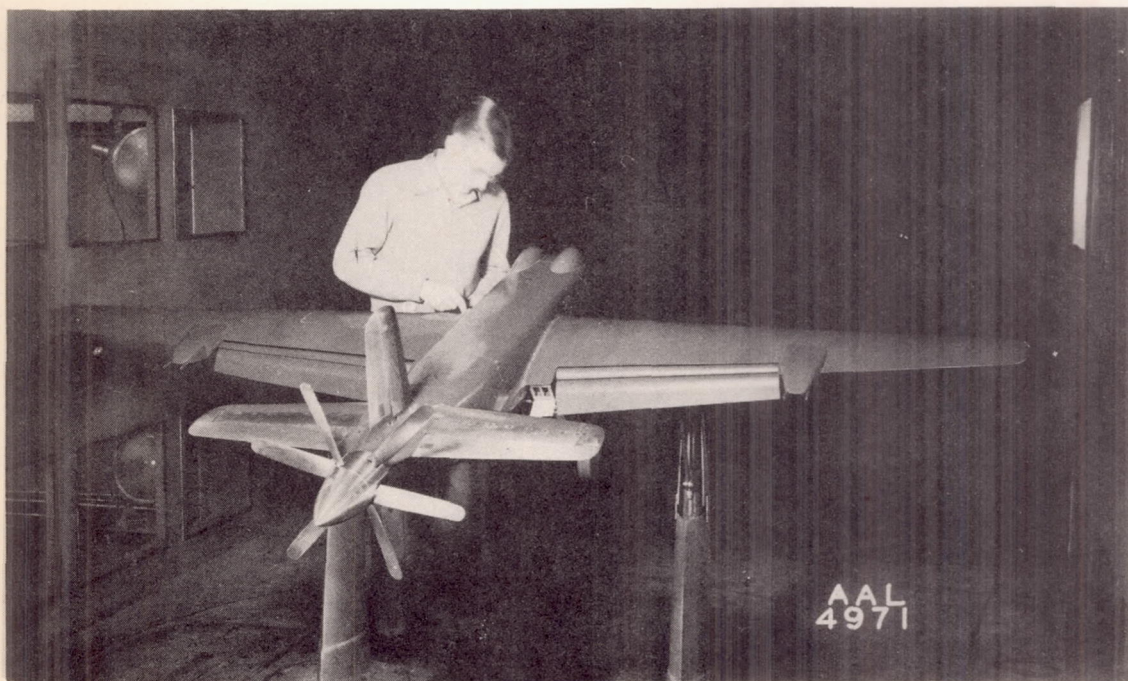


(b) Three-quarter rear view. Standard configuration with propeller on. (S+P₁P₂)

Figure 4.- Views of the model mounted in the Ames 7- by 10-foot wind tunnel.



(c) Three-quarter front view. Landing configuration
($S + f_5^{50} f_6^{40} LL_N P_1 P_2$).



(d) Three-quarter rear view. Landing configuration
($S + f_5^{50} f_6^{40} LL_N P_1 P_2$).

Figure 4.- Concluded.

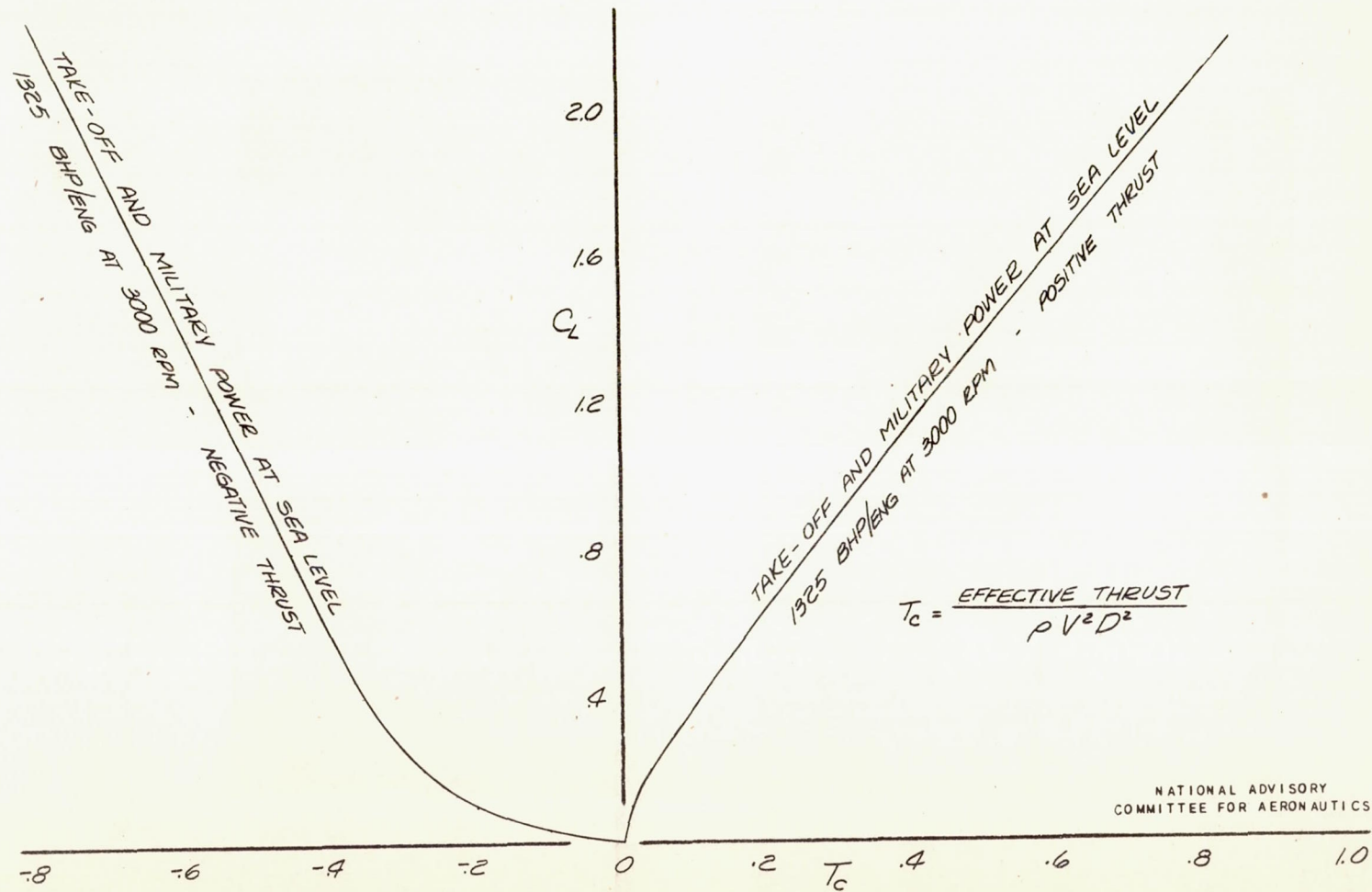


FIGURE 5.- VARIATION OF THRUST WITH LIFT COEFFICIENT OF THE AIRPLANE.
TWO ENGINES OPERATING, GEAR RATIO = 0.361, GROSS WEIGHT = 25,000 LB.

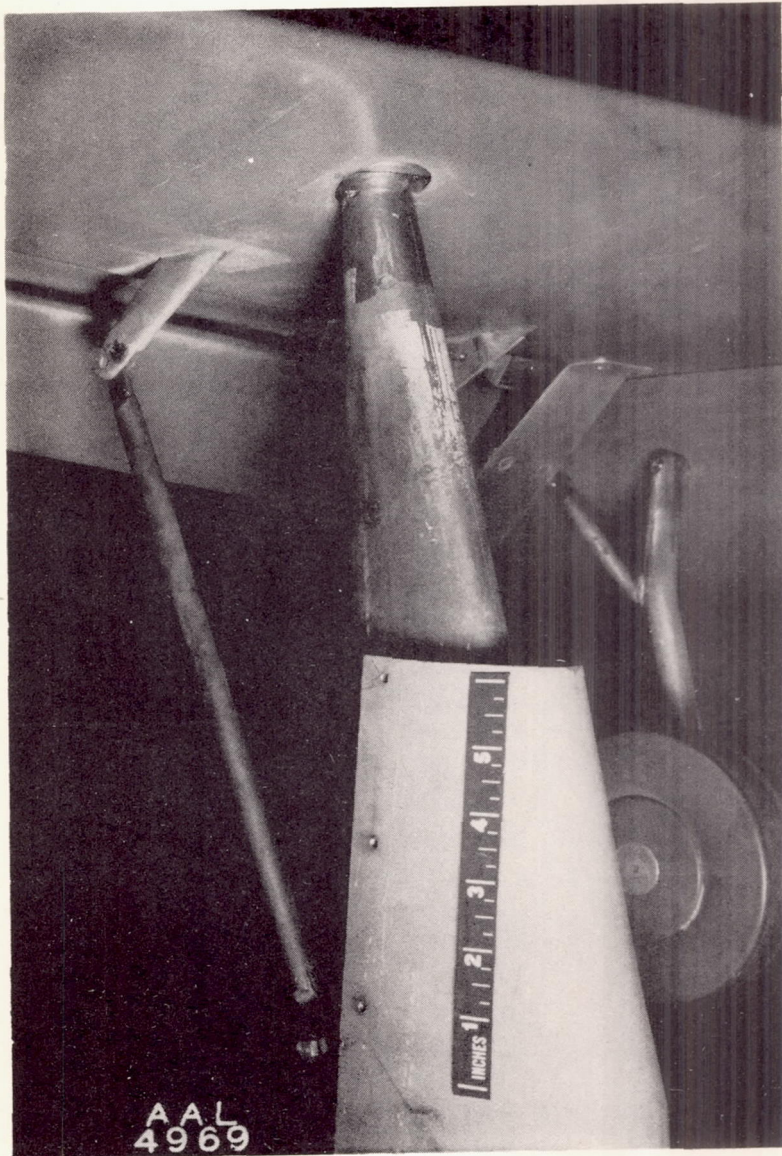
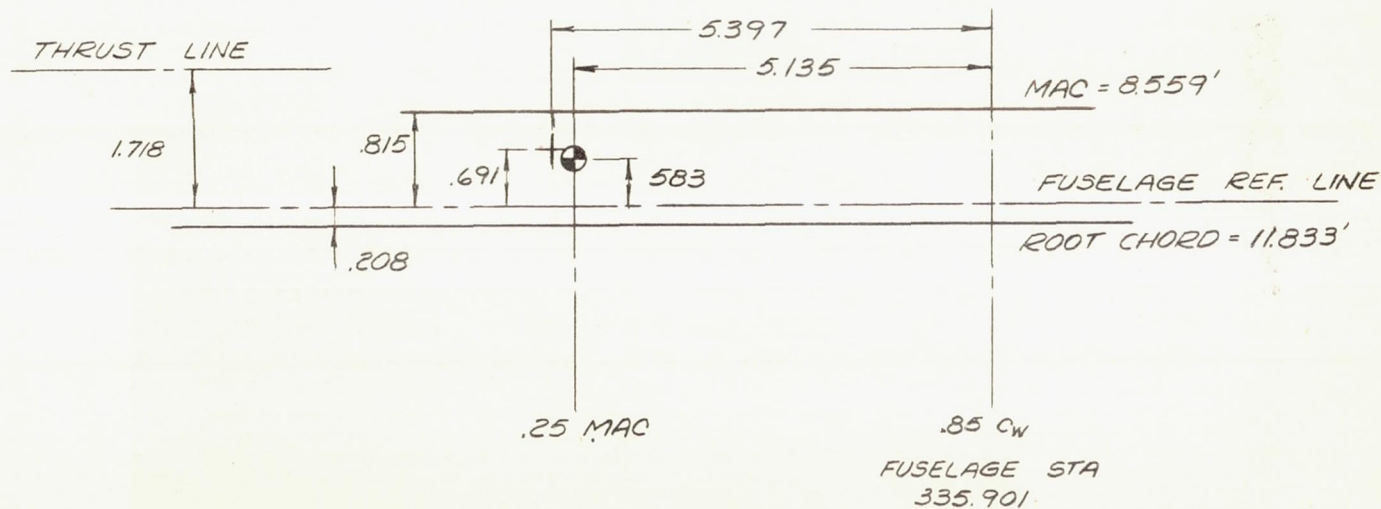


Figure 6.- Detail of support strut used for the model.

+ TRUNNIONS

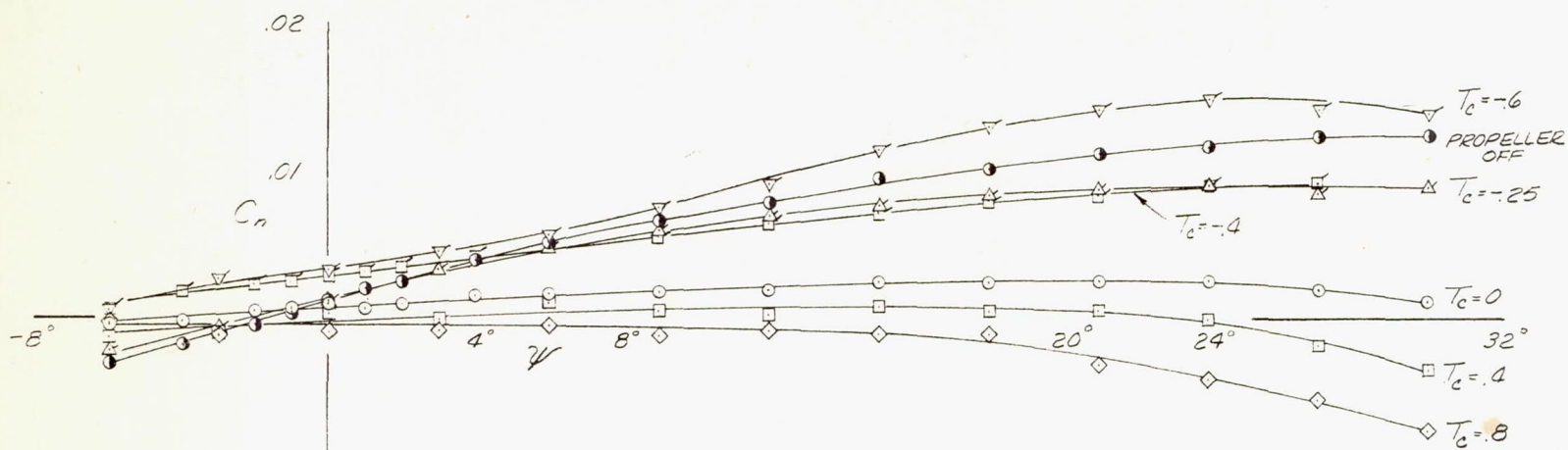
⊕ CENTER OF GRAVITY ABOUT WHICH
MOMENTS ARE PRESENTED



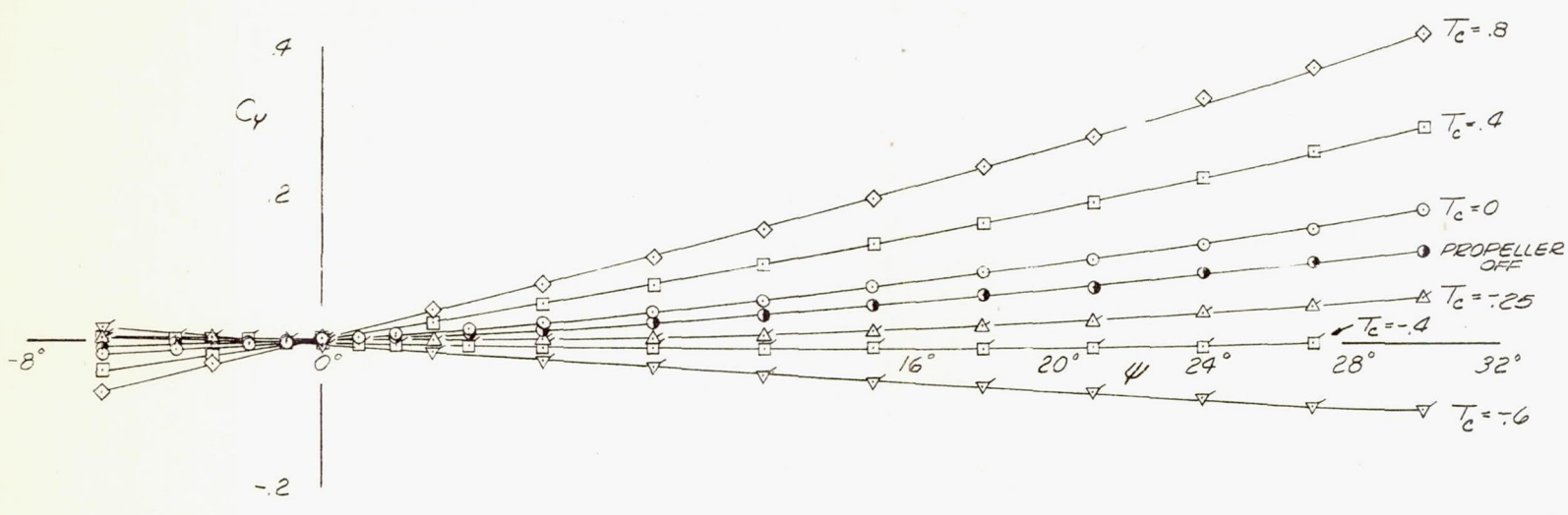
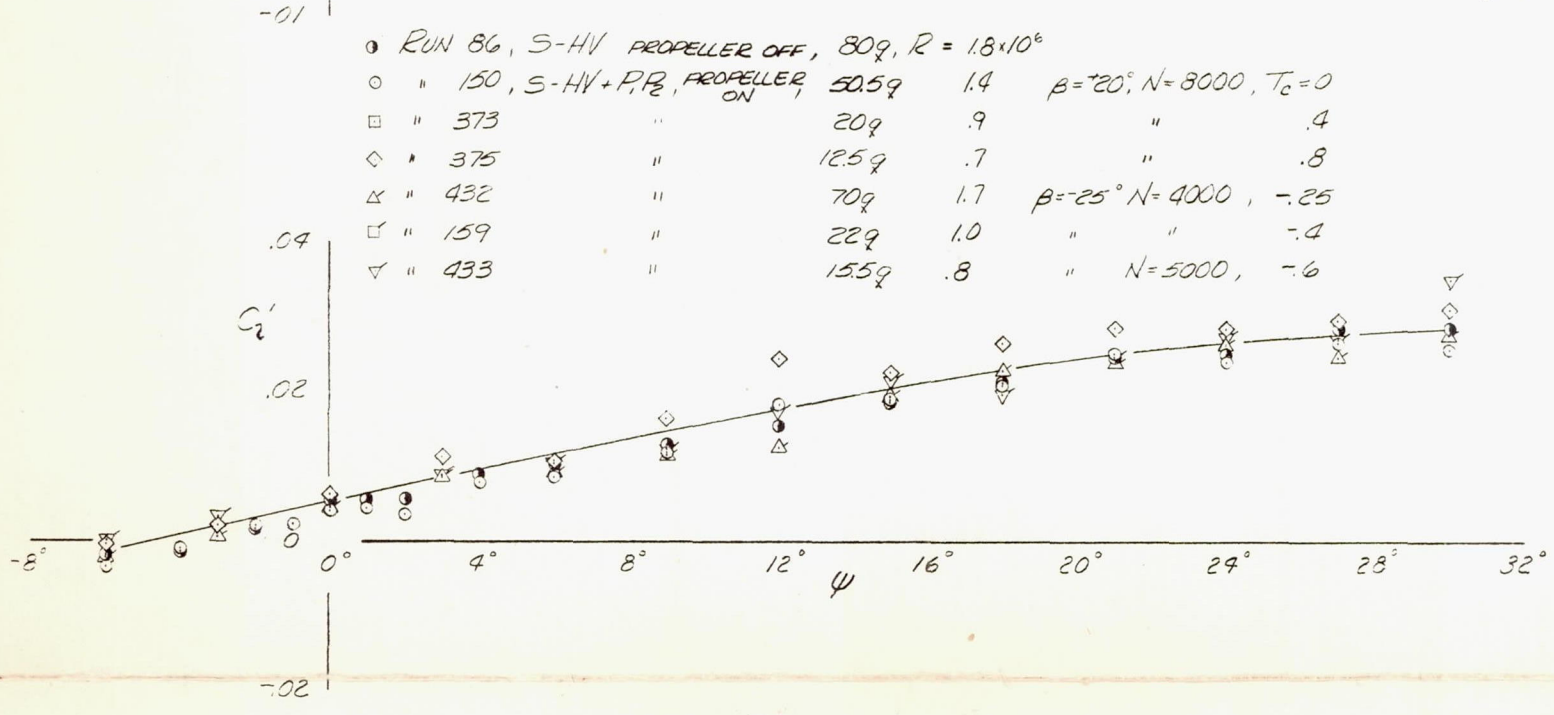
ALL DIMENSIONS ARE FEET FULL SCALE

NATIONAL ADVISORY
COMMITTEE FOR AERONAUTICS

FIGURE 7.- MOMENT CENTER LOCATION ON THE MODEL.

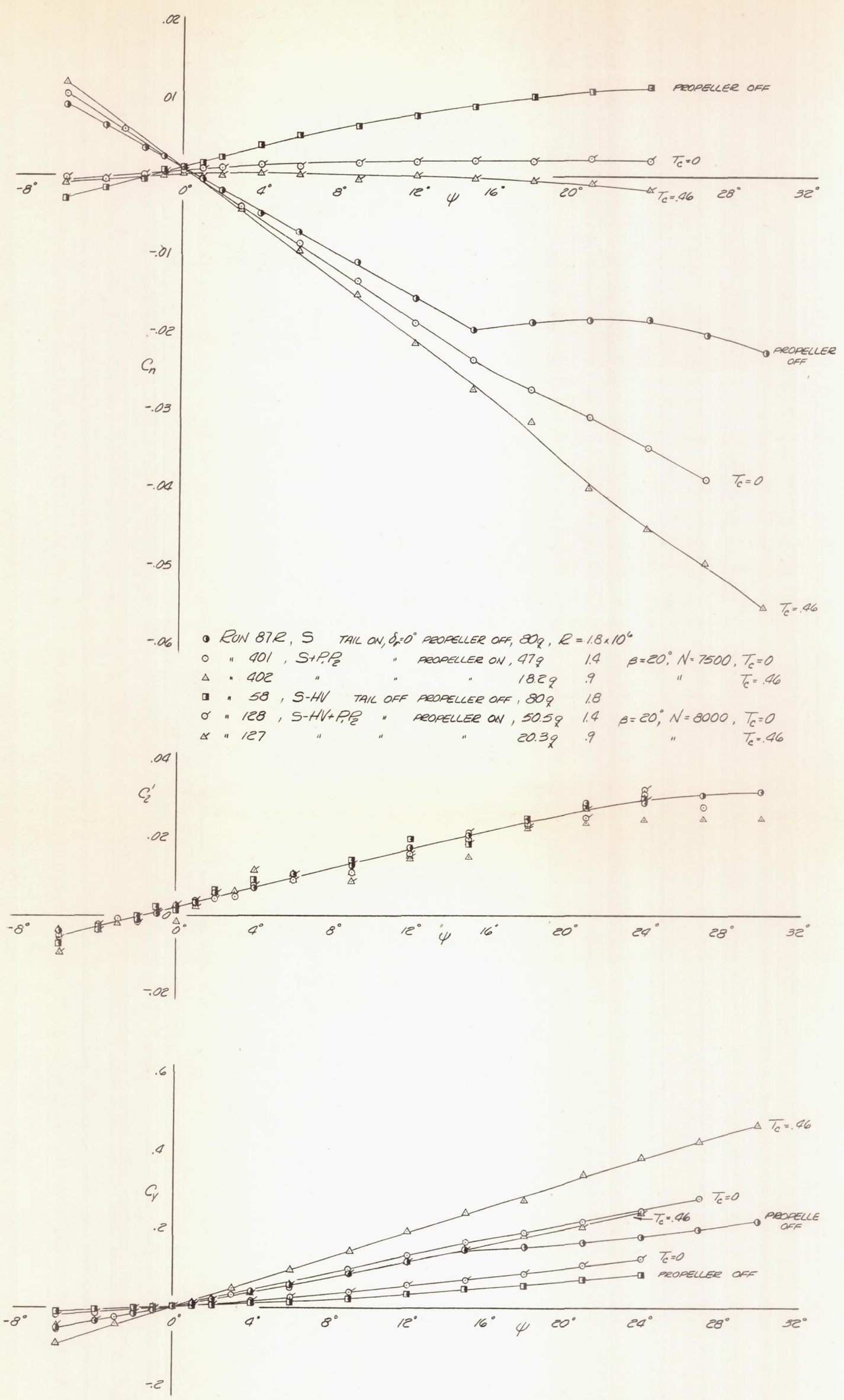


● RUN 86, S-HV PROPELLER OFF, 80g, $R = 1.8 \times 10^6$
 ○ " 150, S-HV + P, P₂, PROPELLER ON, 50.5g 1.4 $\beta = 20^\circ, N = 8000, T_c = 0$
 □ " 373 " " 20g .9 " " .4
 ◇ " 375 " " 12.5g .7 " " .8
 △ " 432 " " 70g 1.7 $\beta = 25^\circ, N = 4000, -0.25$
 ◻ " 159 " " 22g 1.0 " " -.4
 ▽ " 433 " " 15.5g .8 " $N = 5000, -.6$



NATIONAL ADVISORY COMMITTEE FOR AERONAUTICS

FIGURE 9.-EFFECT OF THRUST COEFFICIENT ON THE VARIATION OF AERODYNAMIC CHARACTERISTICS WITH ANGLE OF YAW. MODEL $(C_{L_{TRIM}})_{\psi=0^\circ} = 0.66, \alpha_w = 2^\circ$, FLAPS AND GEAR UP, TAIL OFF.



NATIONAL ADVISORY COMMITTEE FOR AERONAUTICS

FIGURE 10.-EFFECT OF THRUST COEFFICIENT ON THE VARIATION OF AERODYNAMIC CHARACTERISTICS WITH ANGLE OF YAW. MODEL $(C_{L\text{TRIM}})_{\psi=0^\circ} = 0.93$, $\alpha_0 = 6^\circ$, FLAPS AND GEAR UP.

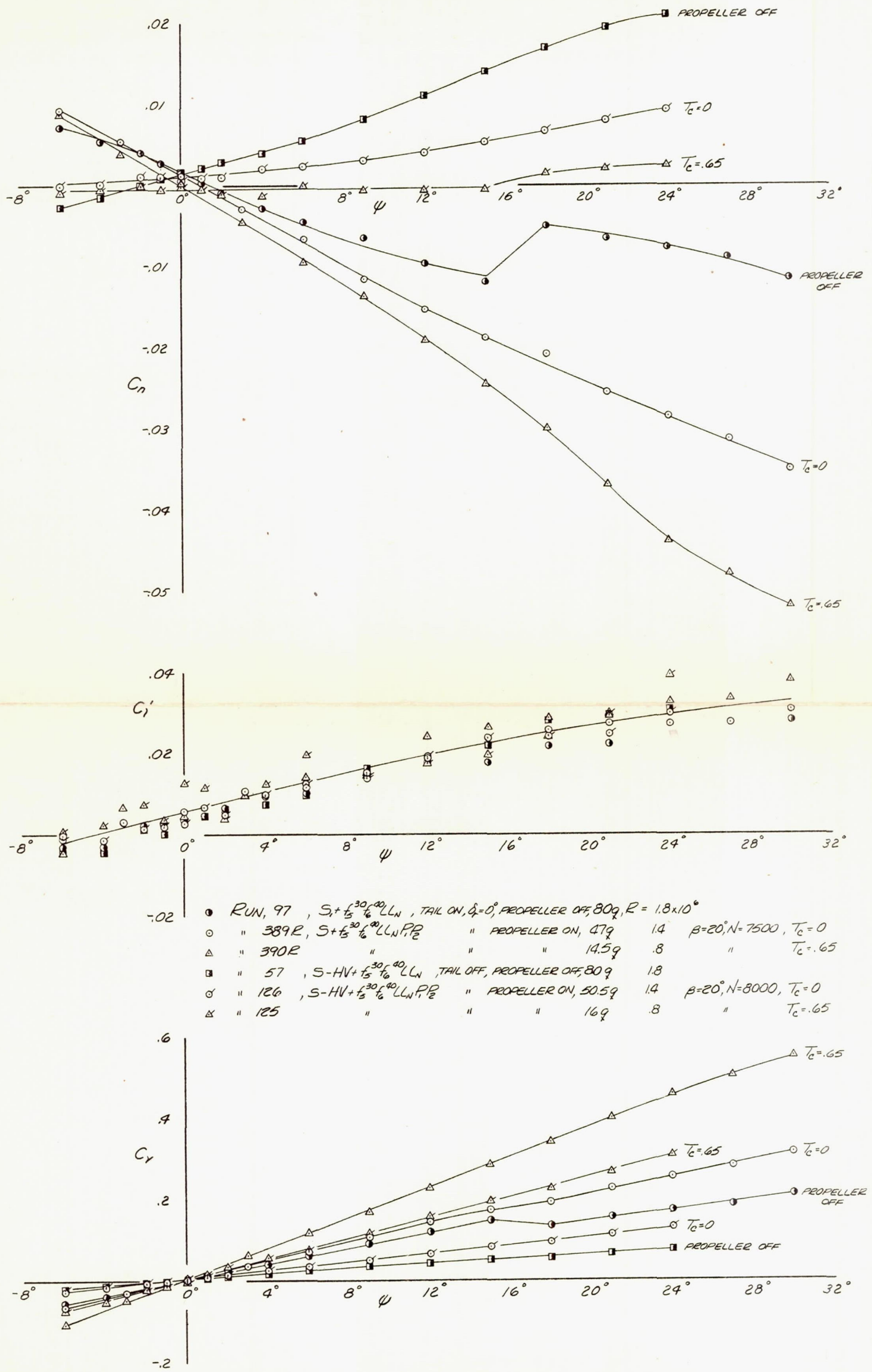
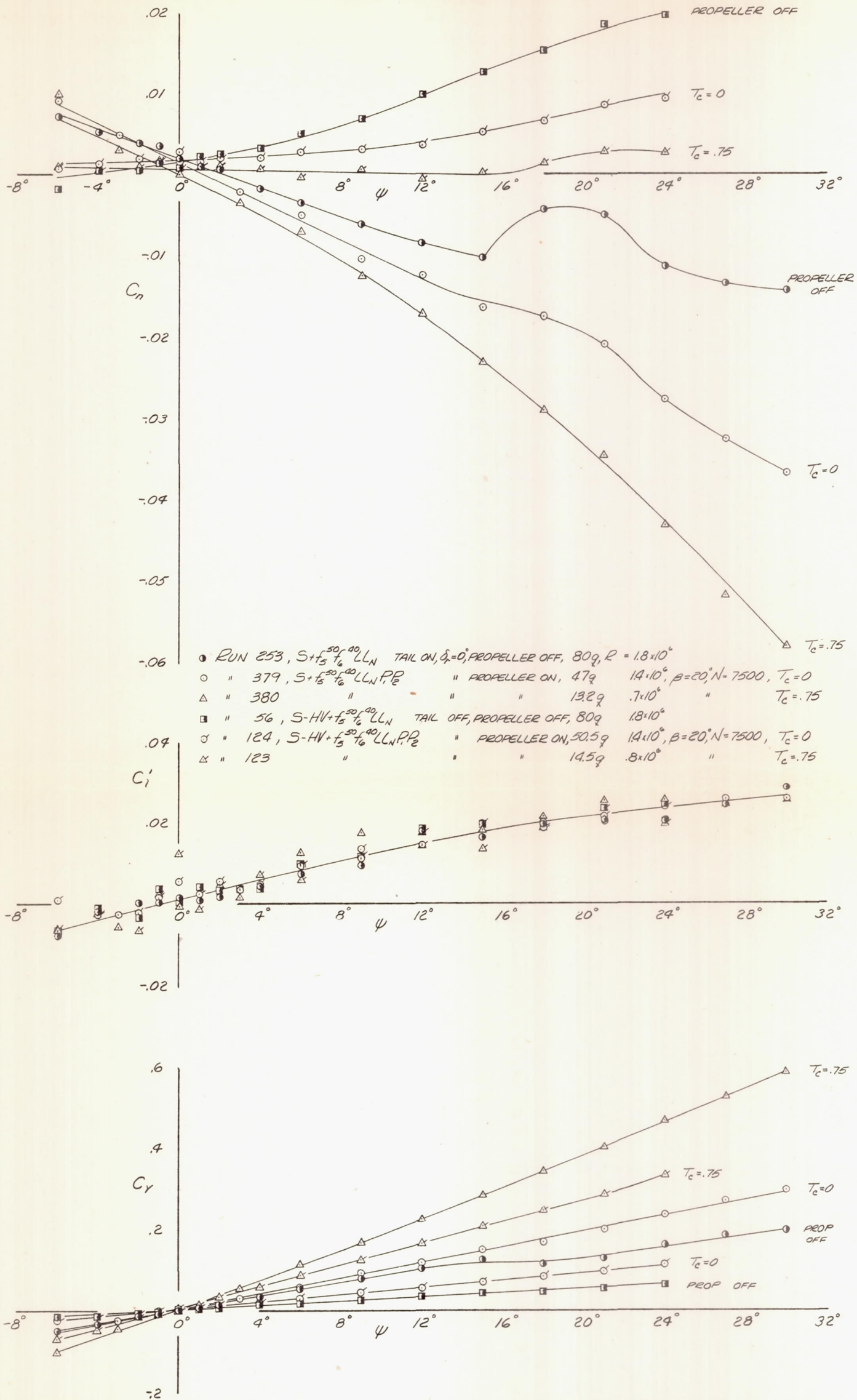
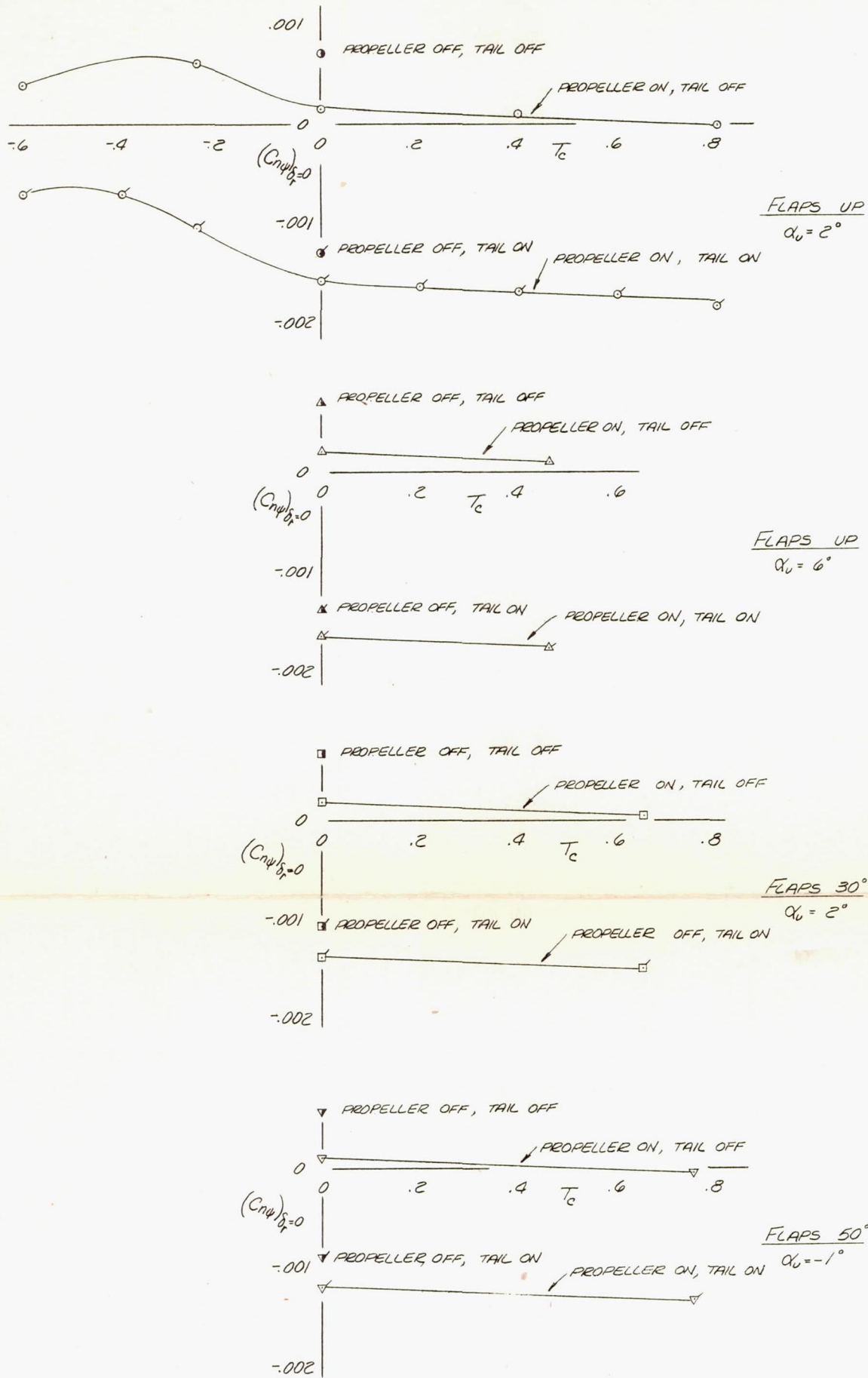


FIGURE 11.-EFFECT OF THRUST COEFFICIENT ON THE VARIATION OF AERODYNAMIC CHARACTERISTICS WITH ANGLE OF YAW. MODEL $(C_{L_{TRIM}})_{\psi=0^\circ} = 1.44, \alpha_u = 2^\circ$, FLAPS 30° , GEAR DOWN.



NATIONAL ADVISORY COMMITTEE FOR AERONAUTICS

FIGURE 12.-EFFECT OF THRUST COEFFICIENT ON THE VARIATION OF AERODYNAMIC CHARACTERISTICS WITH ANGLE OF YAW. MODEL $(C_{L_{TRIM}})_{\psi=0^\circ} = 1.50, \alpha_v = 1^\circ$, FLAPS 50° , GEAR DOWN.



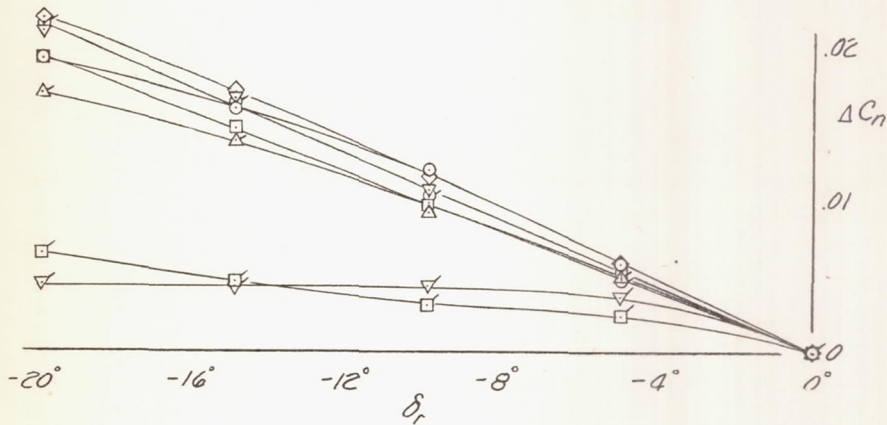
- | | | | |
|----------------------|----------------------|--|-----------------------|
| $\alpha_0 = 2^\circ$ | $\alpha_0 = 6^\circ$ | | |
| ○ | △ | S | |
| ○ | △ | S-HV | |
| ○ | △ | S+PP ₂ | |
| ○ | △ | S-HV+PP ₂ | |
| □ | | S+ $f_5^{30} f_6^{40}$ LLN | $\alpha_0 = 2^\circ$ |
| □ | | S-HV+ $f_5^{30} f_6^{40}$ LLN | " |
| □ | | S+ $f_5^{30} f_6^{40}$ LLN, PP ₂ | " |
| □ | | S-HV+ $f_5^{30} f_6^{40}$ LLN, PP ₂ | " |
| ▽ | | S+ $f_5^{50} f_6^{40}$ LLN | $\alpha_0 = -1^\circ$ |
| ▽ | | S-HV+ $f_5^{50} f_6^{40}$ LLN | " |
| ▽ | | S+ $f_5^{50} f_6^{40}$ LLN, PP ₂ | " |
| ▽ | | S-HV+ $f_5^{50} f_6^{40}$ LLN, PP ₂ | " |

NATIONAL ADVISORY
COMMITTEE FOR AERONAUTICS

FIGURE 13. VARIATION OF THE DIRECTIONAL STABILITY DERIVATIVE C_{ny} WITH THRUST COEFFICIENT T_c .

$\alpha_0 = 2^\circ \quad (C_{L_{TRIM}})_{\psi=0^\circ} = 0.66$

○	S	PROPELLER OFF, 80g, R = 1.8 × 10 ⁶			
△	S + P ₁ P ₂	PROPELLER ON, 47g	1.4	β = 20°, N = 7500, T _c = 0	
□	"	" 28g	1.1	" "	.2
▽	"	" 20g	.9	" "	.4
◇	"	" 15.3g	.8	" "	.6
⊙	"	" 12.7g	.7	" "	.8
△	"	" 70g	1.7	β = -25, N = 4000, -25	
□	"	" 20.5g	.9	" N = 4000, -4	
▽	"	" 15.5g	.8	" N = 5000, -6	



NATIONAL ADVISORY
COMMITTEE FOR AERONAUTICS

$\alpha_0 = 6^\circ \quad (C_{L_{TRIM}})_{\psi=0^\circ} = 0.93$

○	S	PROPELLER OFF, 80g, R = 1.8 × 10 ⁶			
△	S + P ₁ P ₂	PROPELLER ON, 47g	1.4	β = 20°, N = 7500, T _c = 0	
□	S + P ₁ P ₂	18.2g	.9	" "	T _c = .46

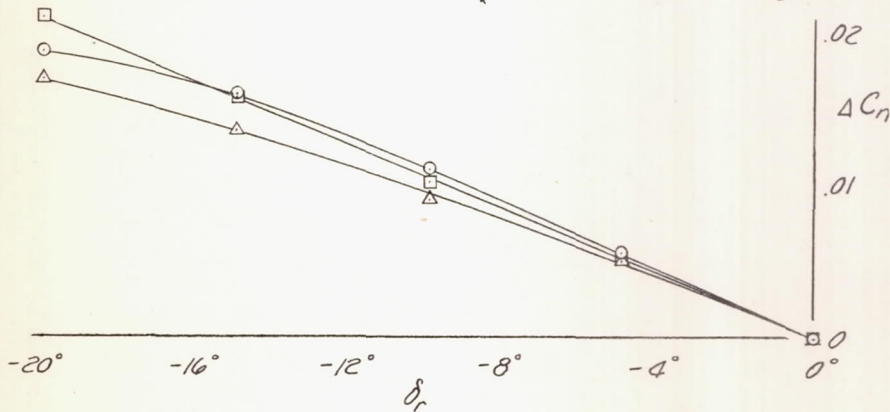
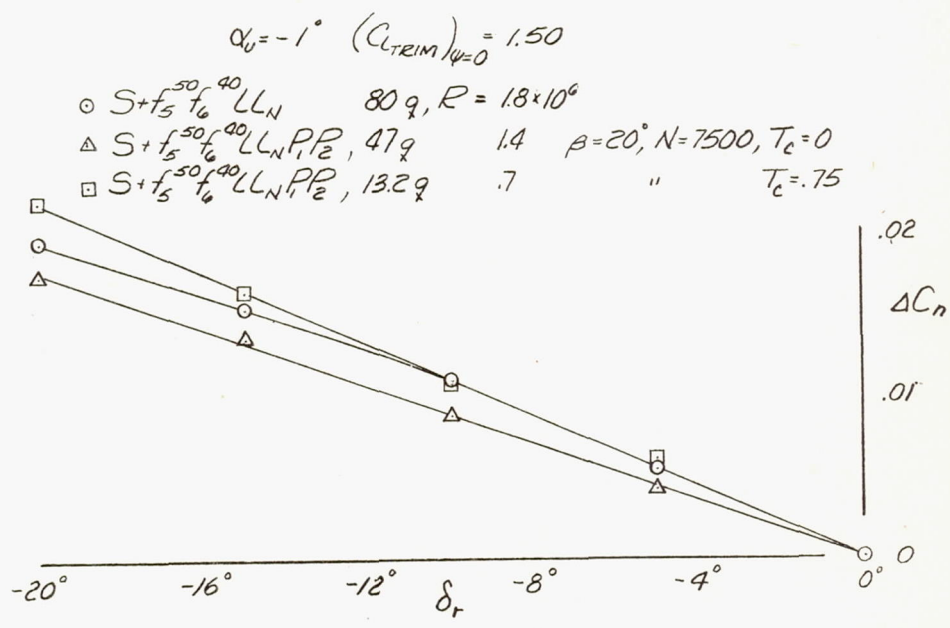
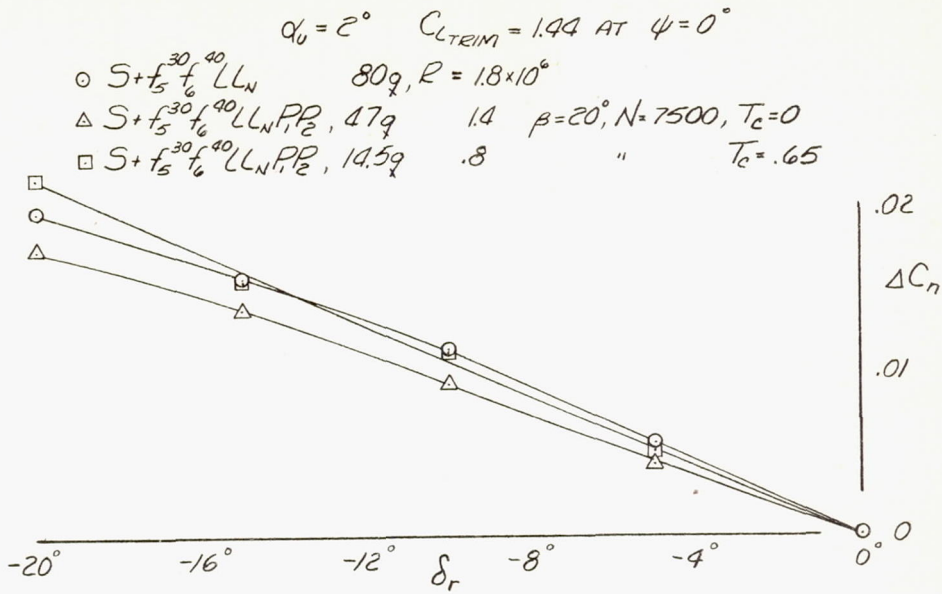
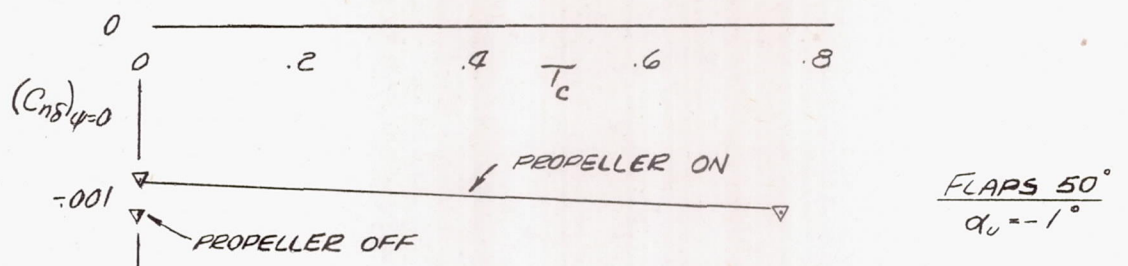
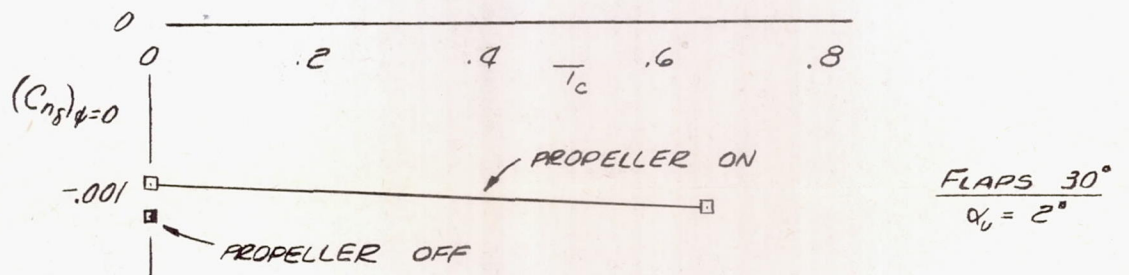
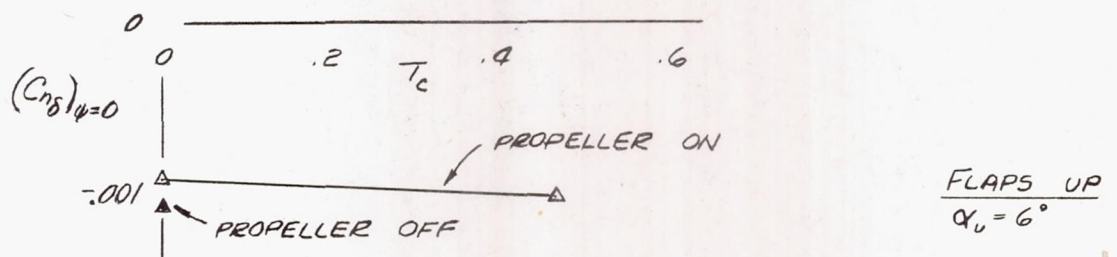
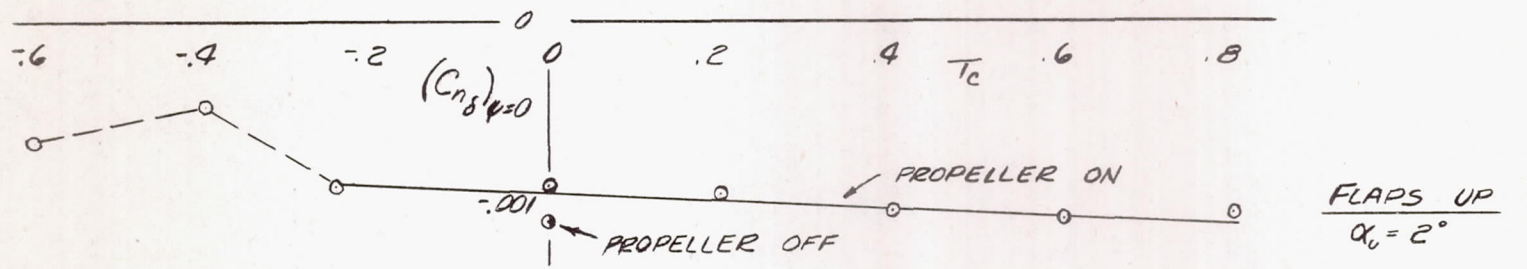


FIGURE 14. - VARIATION OF YAWING-MOMENT COEFFICIENT WITH RUDDER DEFLECTION. FLAPS AND GEAR UP, $\psi = 0^\circ$.



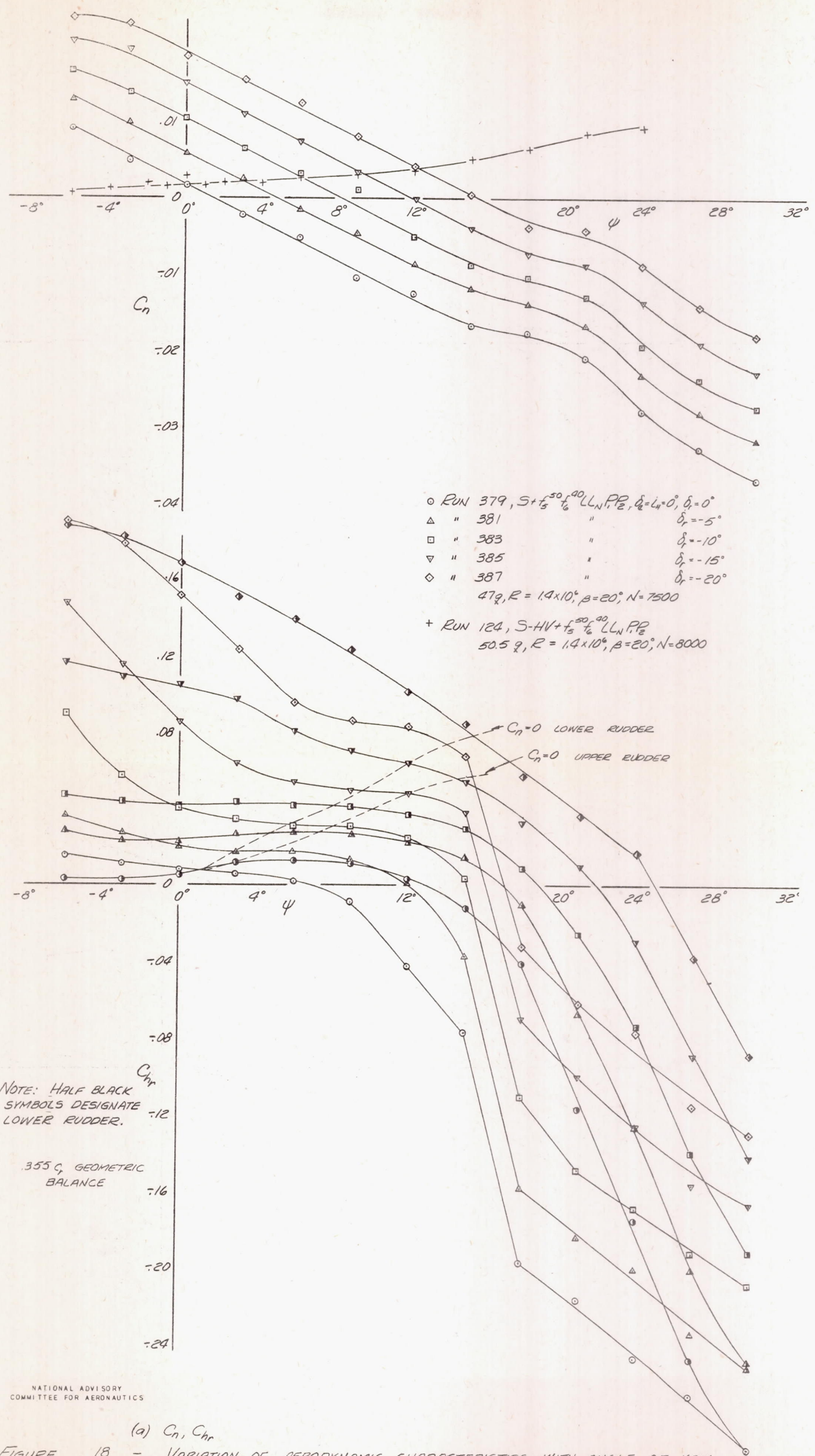
NATIONAL ADVISORY
COMMITTEE FOR AERONAUTICS

FIGURE 15. - VARIATION OF YAWING-MOMENT COEFFICIENT WITH RUDDER DEFLECTION.
FLAPS 30° AND 50°, GEAR DOWN, $\psi = 0^\circ$.



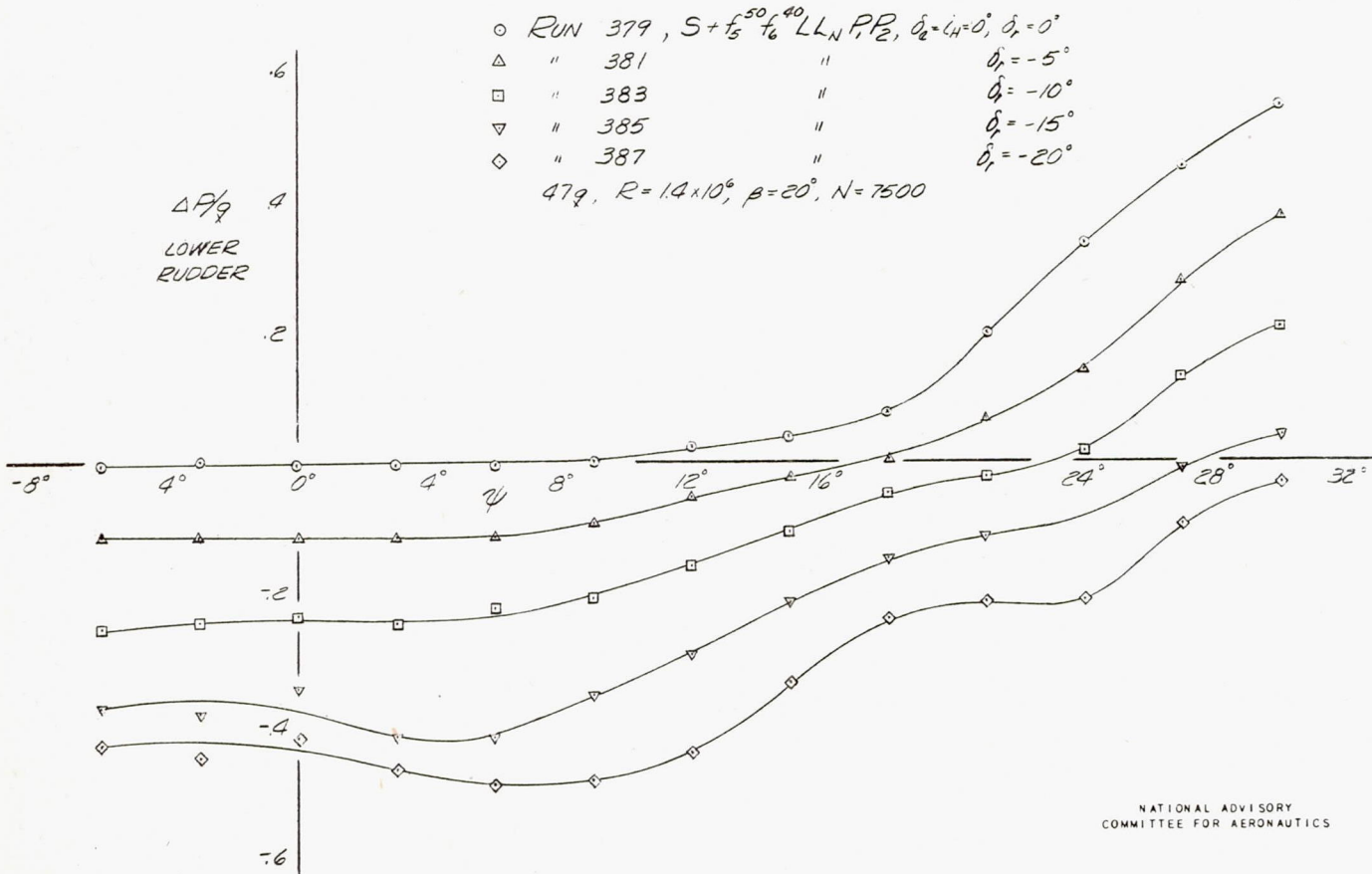
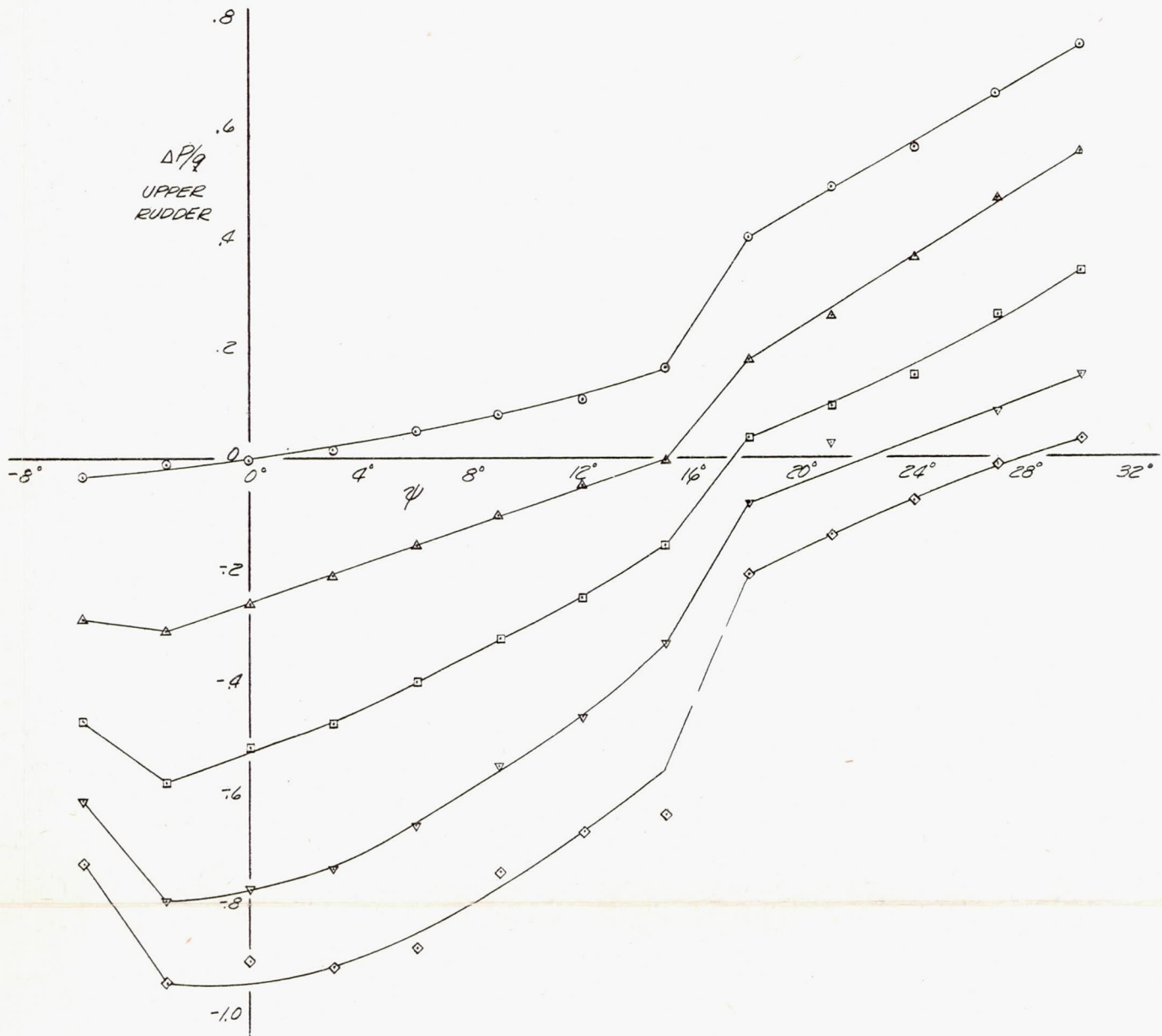
- $\alpha_v = 2^\circ$ $\alpha_v = 6^\circ$
- ▲ S
- △ S + P, P₂
- S + f₅³⁰ f₆⁴⁰ LLN $\alpha_v = 2^\circ$
- S + f₅³⁰ f₆⁴⁰ LLN, P, P₂ "
- ▼ S + f₅⁵⁰ f₆⁴⁰ LLN $\alpha_v = -1^\circ$
- ▼ S + f₅⁵⁰ f₆⁴⁰ LLN, P, P₂ "

FIGURE 16 .- VARIATION OF RUDDER EFFECTIVENESS WITH THRUST COEFFICIENT T_c .



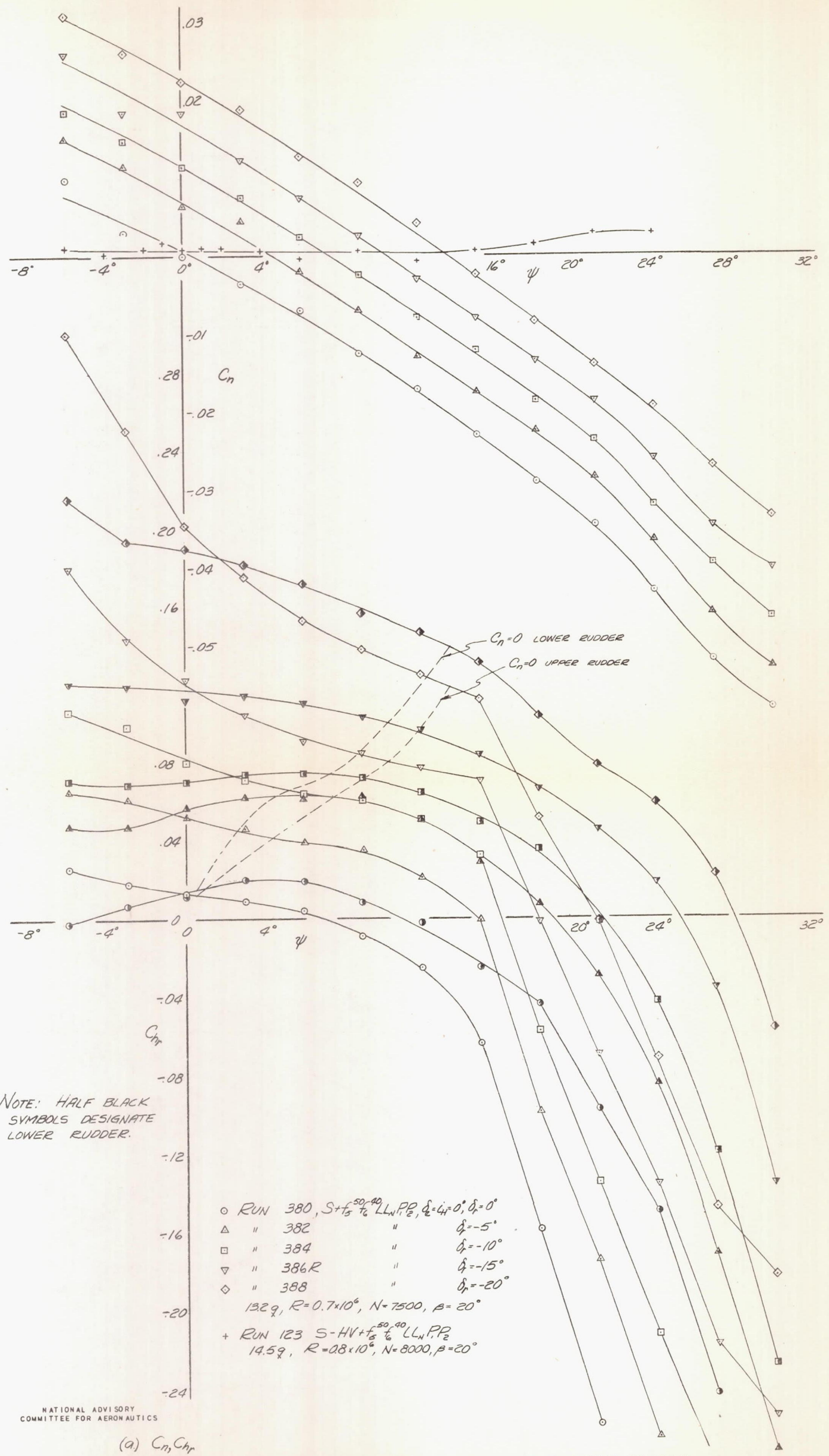
NATIONAL ADVISORY COMMITTEE FOR AERONAUTICS

(a) C_n, C_{nr}
FIGURE 18. - VARIATION OF AERODYNAMIC CHARACTERISTICS WITH ANGLE OF YAW. MODEL ($C_{L_{trim}})_{\psi=0^\circ} = 1.50, \delta_v = -1^\circ, FLAPS 50^\circ, GEAR DOWN, POWER OFF (T_0 = 0)$



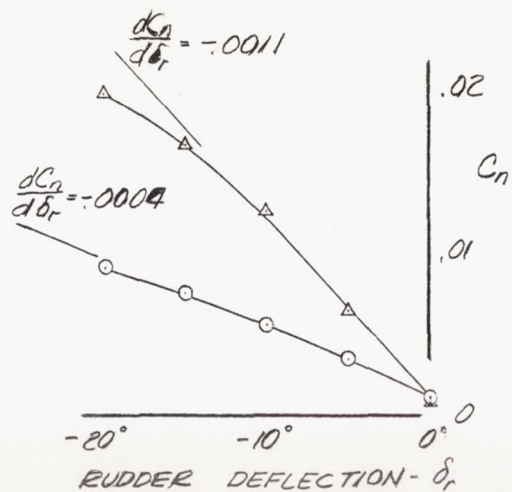
NATIONAL ADVISORY
COMMITTEE FOR AERONAUTICS

(b) $\Delta P/q$
FIGURE 18 - CONCLUDED.



NATIONAL ADVISORY COMMITTEE FOR AERONAUTICS

(a) C_n, C_{np}
FIGURE 19.- VARIATION OF AERODYNAMIC CHARACTERISTICS WITH ANGLE OF YAW.
MODEL ($C_{L_{trim}})_{\alpha=0} = 1.50$, $\alpha_0 = -1^\circ$, FLAPS 50° , GEAR DOWN, POWER ON ($T_c = 0.75$).



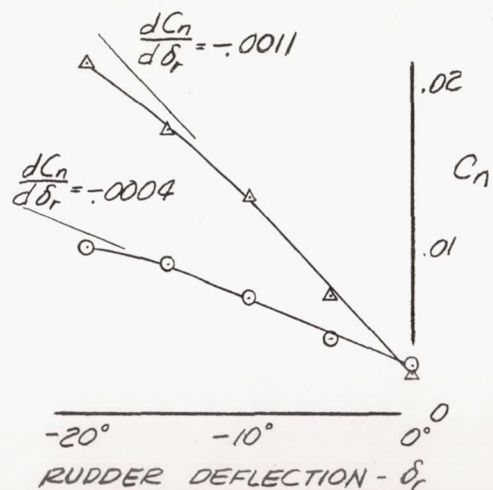
S

- LOWER RUDDER, FIG. 20
- △ BOTH RUDDERS, FIG. 14

FLAPS AND GEAR UP

$$\alpha_0 = 2^\circ \quad C_{L_{TRIM}} = 0.66$$

$$80g, R = 1.8 \times 10^6$$

S + f₅⁵⁰ f₆⁴⁰ LL_N

- LOWER RUDDER, FIG. 21
- △ BOTH RUDDERS, FIG. 15

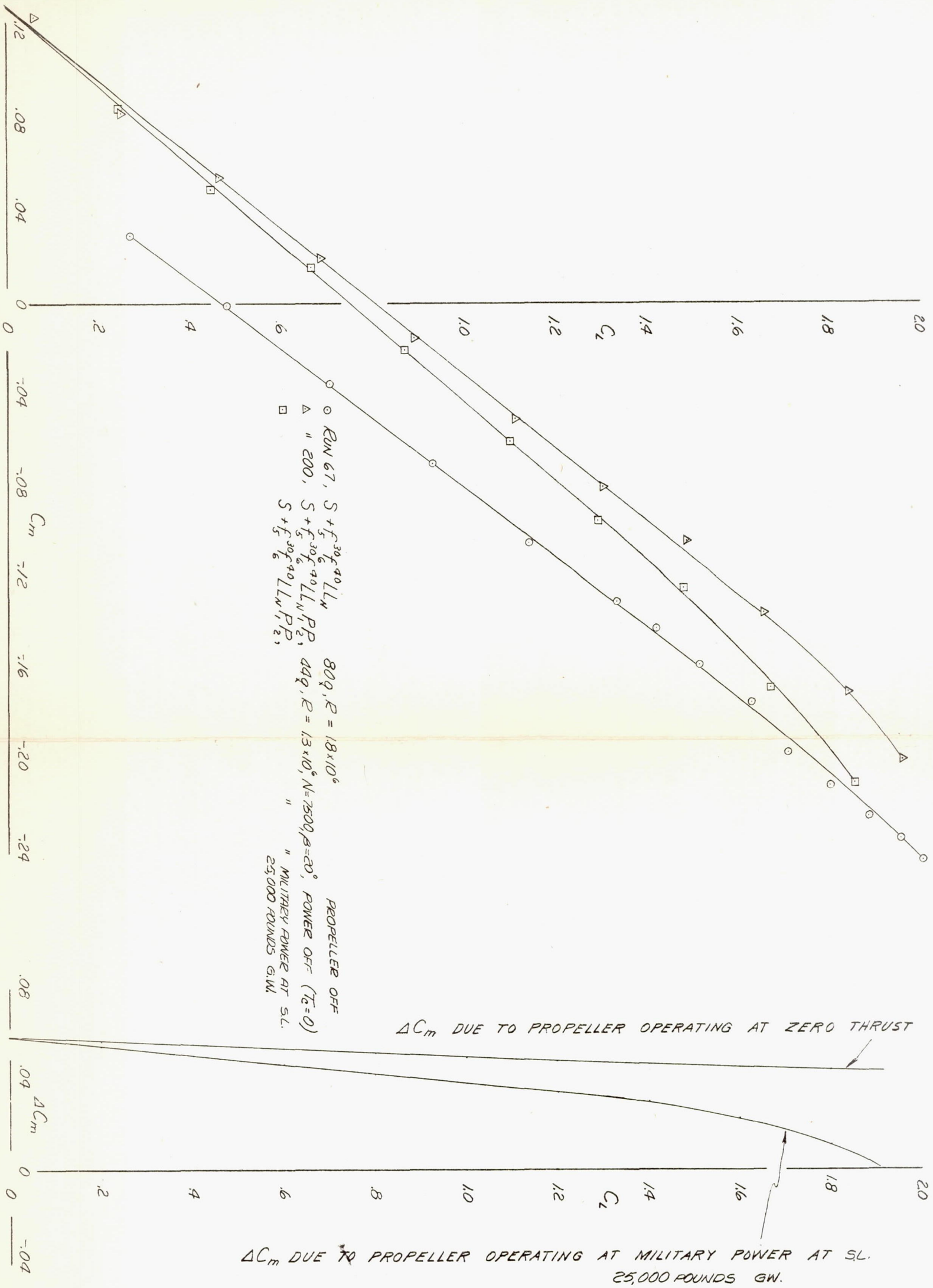
FLAPS 50° GEAR DOWN

$$\alpha_0 = -1^\circ \quad C_{L_{TRIM}} = 1.50$$

$$80g, R = 1.8 \times 10^6$$

NATIONAL ADVISORY
COMMITTEE FOR AERONAUTICS

FIGURE 22.- COMPARISON OF THE EFFECTIVENESS OF THE UPPER AND LOWER RUDDERS AT ZERO ANGLE OF YAW. PROPELLER OFF.



NATIONAL ADVISORY COMMITTEE FOR AERONAUTICS

FIGURE 24.- EFFECT OF POWER ON LONGITUDINAL STABILITY
 FLAPS 30°, GEAR EXTENDED, ELEVATOR 0°.

MR No. A5J12

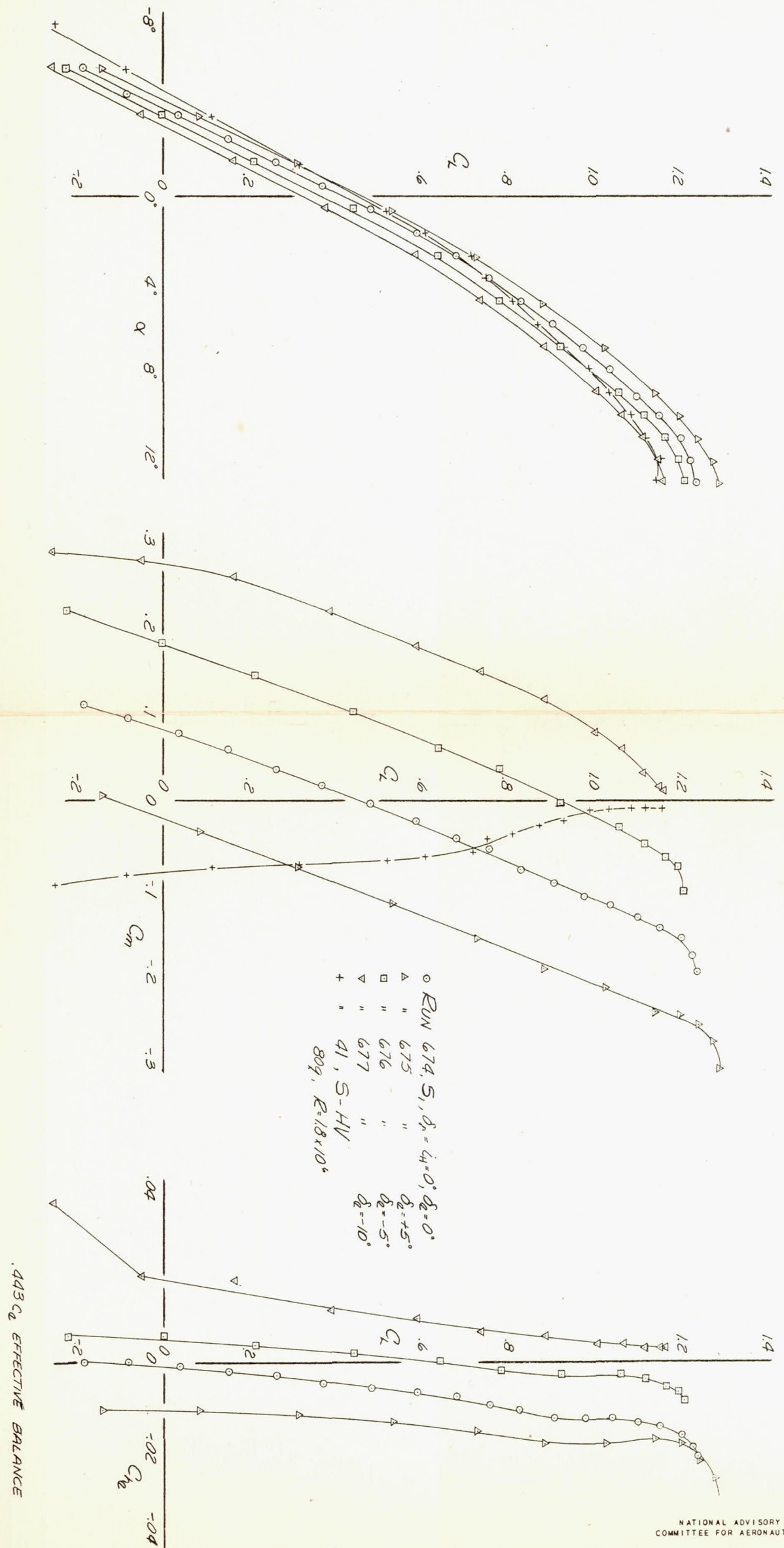


FIGURE 26.- VARIATION OF AERODYNAMIC CHARACTERISTICS WITH LIFT COEFFICIENT. FLAPS AND GEAR UP, PROPELLER OFF.

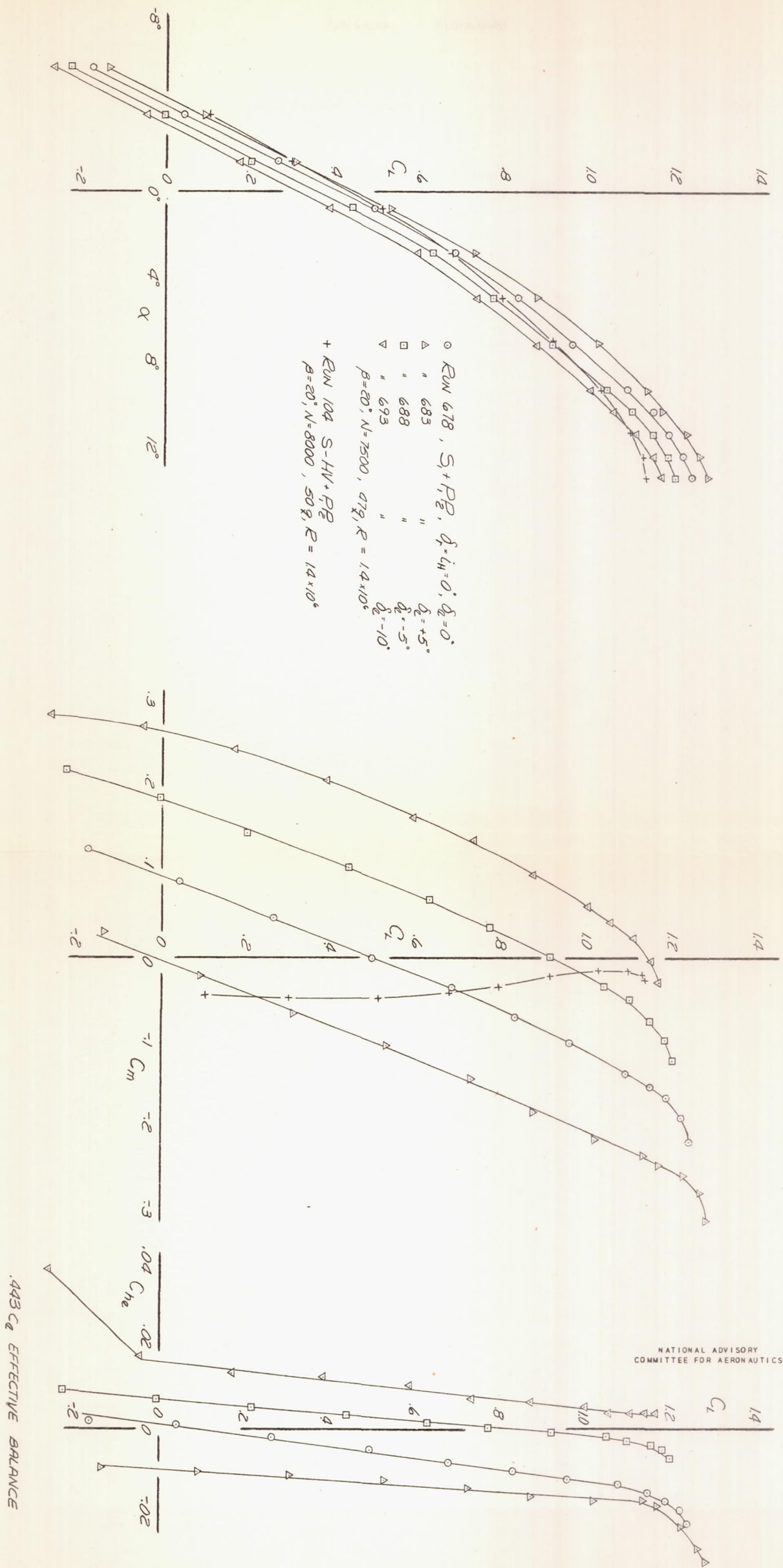
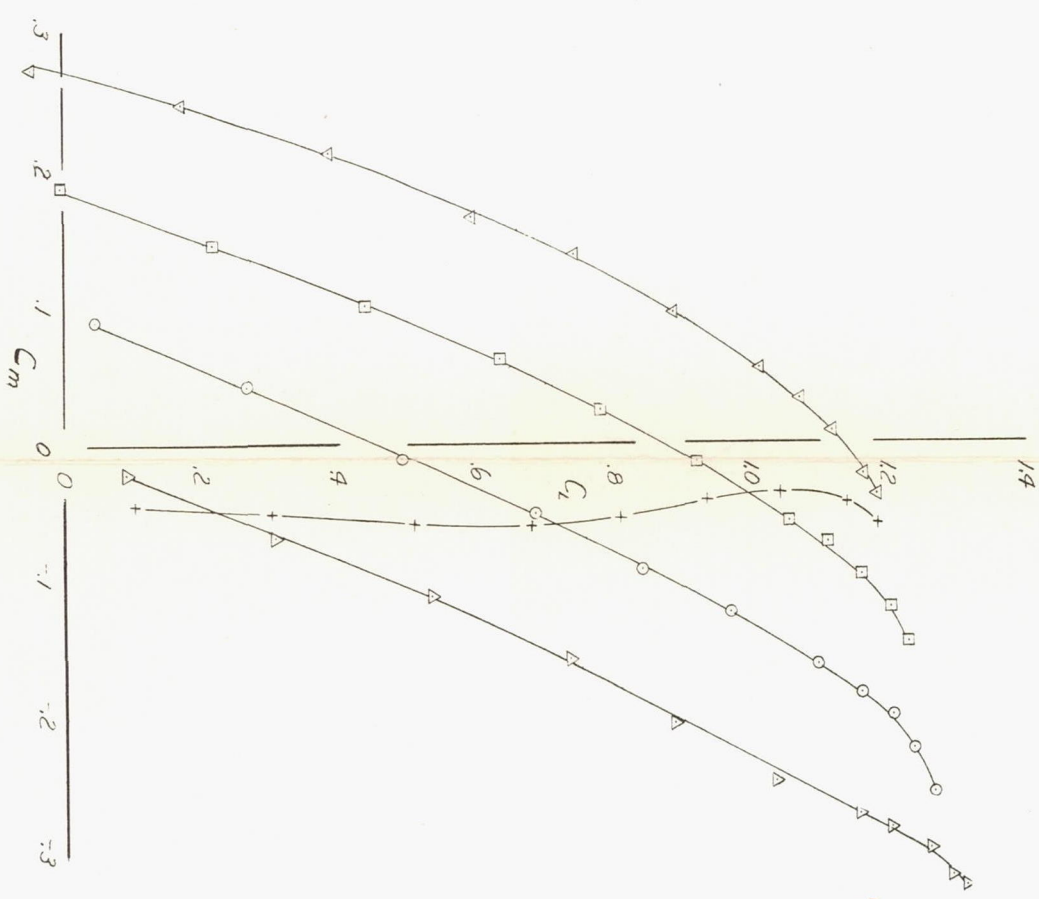
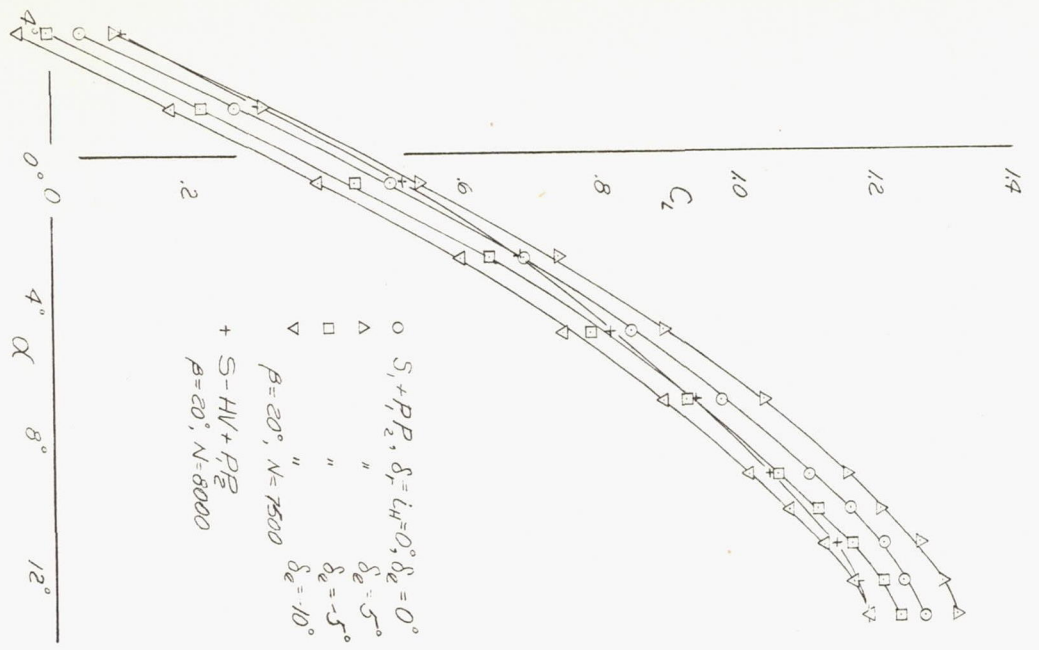
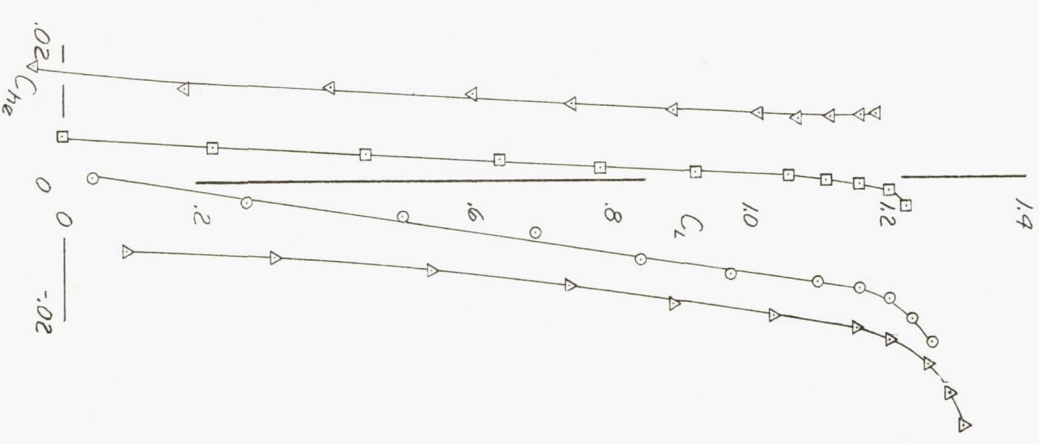


FIGURE 27.- VARIATION OF AERODYNAMIC CHARACTERISTICS WITH LIFT COEFFICIENT. FLAPS AND GEAR UP, POWER OFF ($T_c = 0$).

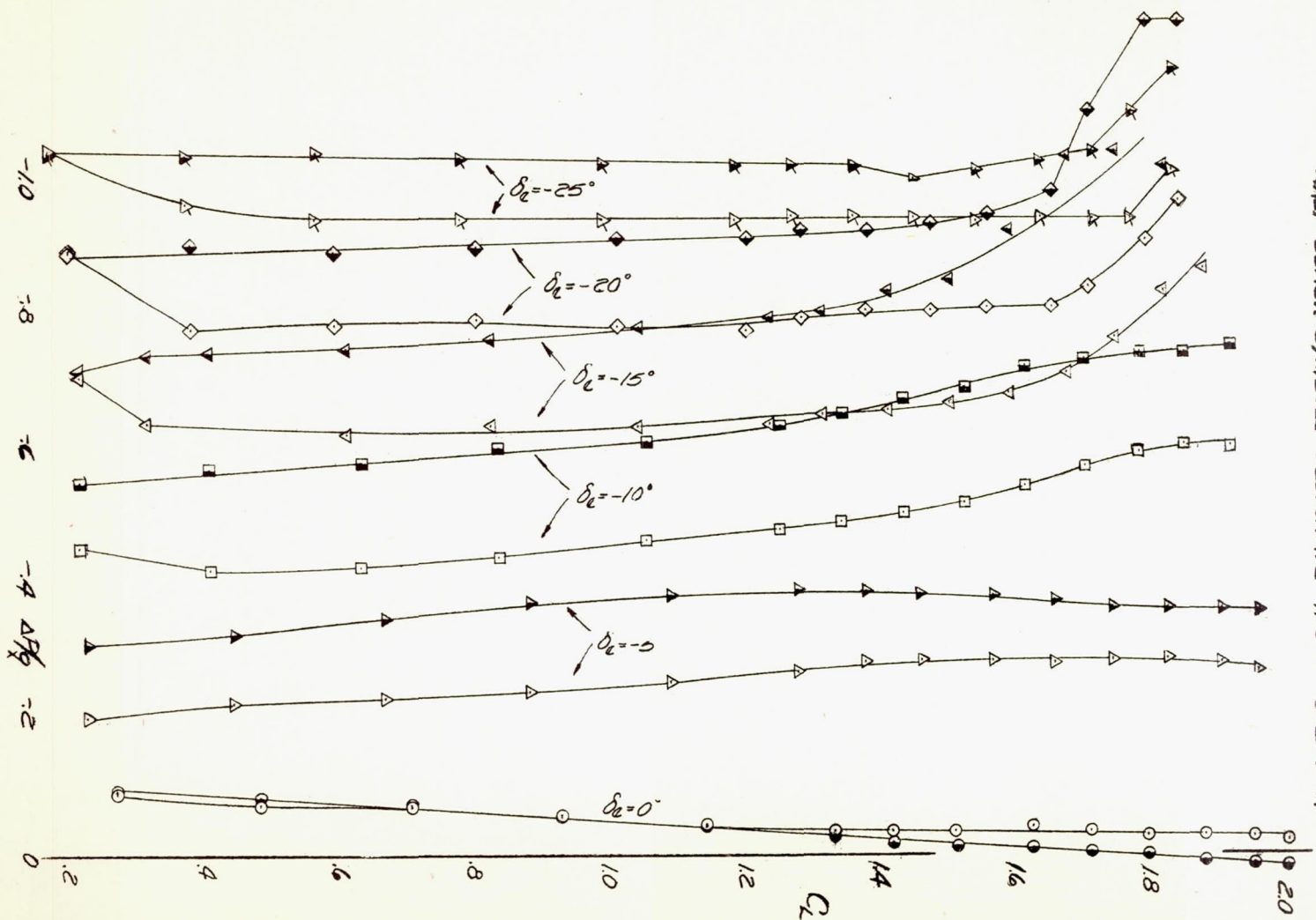


.443 C_L EFFECTIVE BALANCE



NATIONAL ADVISORY COMMITTEE FOR AERONAUTICS

FIGURE 28.- VARIATION OF AERODYNAMIC CHARACTERISTICS WITH LIFT COEFFICIENT. FLAPS AND GEAR UP, MILITARY POWER AT SL.

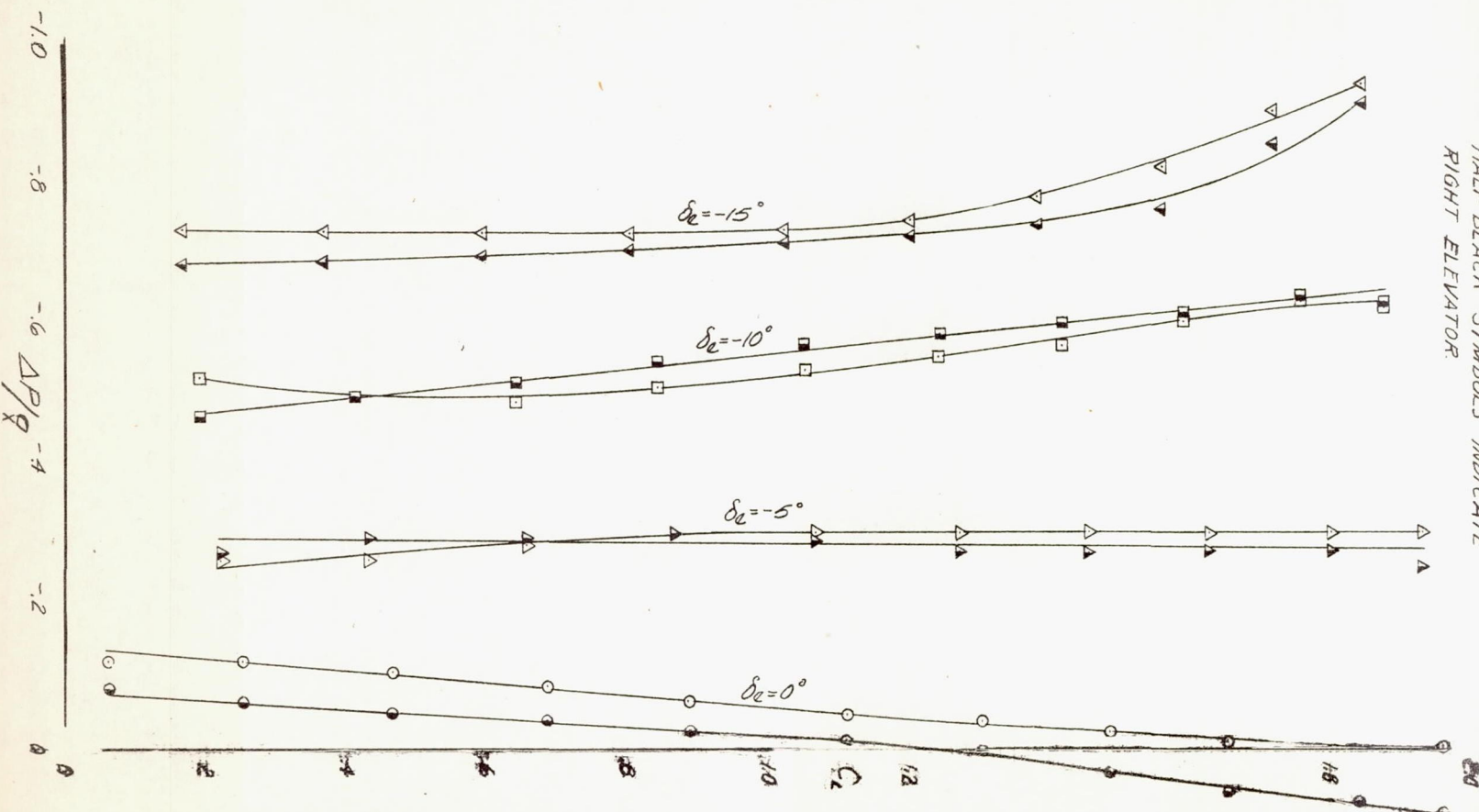


NOTE: SYMBOL LEGEND ON PRECEDING FIGURE. (29 a)
 HALF BLACK SYMBOLS DESIGNATE RIGHT ELEVATOR.

(b) $\Delta P/q$

FIGURE 29.- CONCLUDED

NOTE: SYMBOL LEGEND ON PRECEDING FIGURE (30A)
 HALF BLACK SYMBOLS INDICATE
 RIGHT ELEVATOR

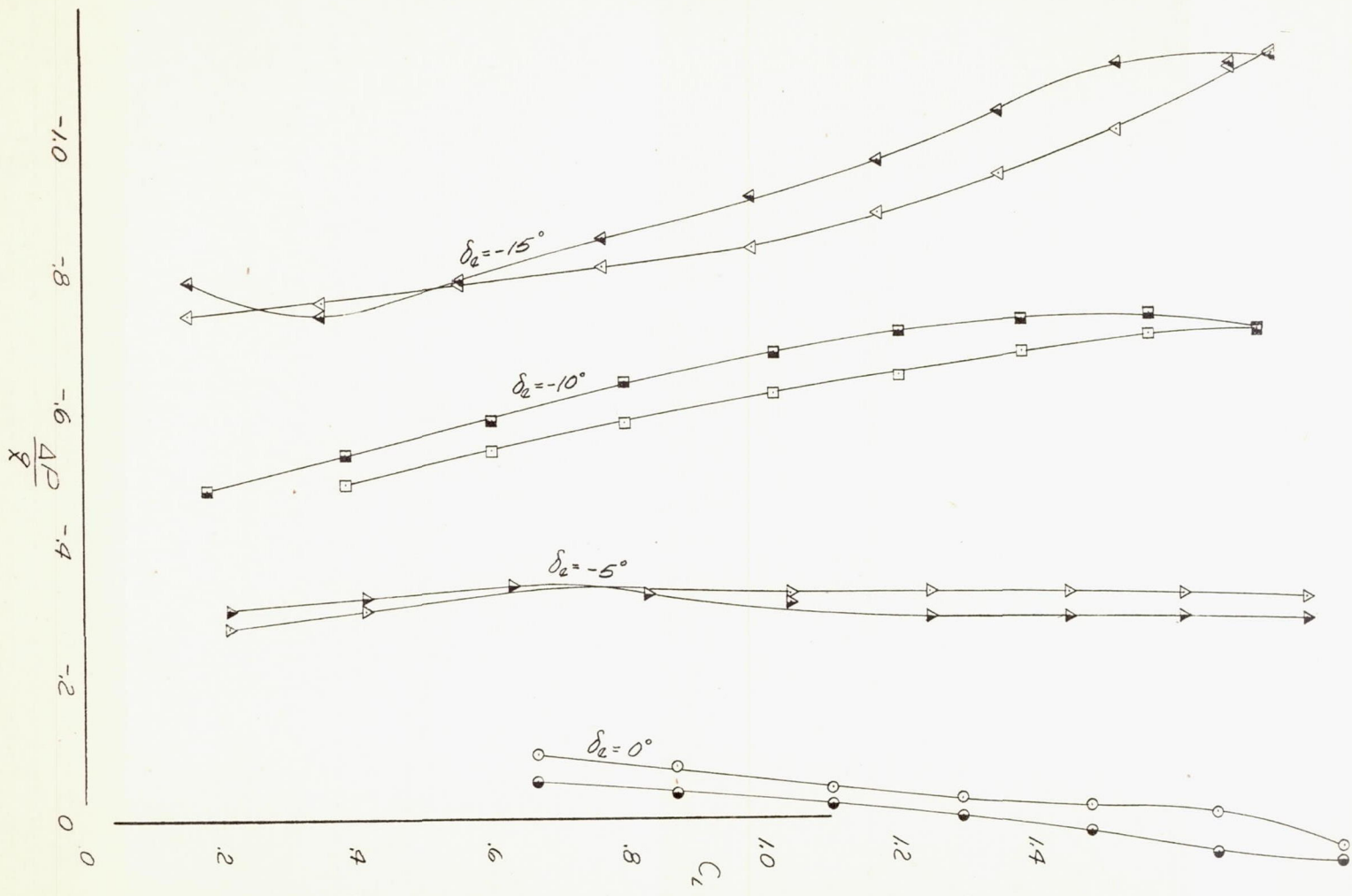


NATIONAL ADVISORY
 COMMITTEE FOR AERONAUTICS

MR NO. A5J12

(b) $\Delta P/q$
 FIGURE 30. - CONCLUDED

NOTE: HALF-BLACK SYMBOLS INDICATE RIGHT ELEVATOR
 SYMBOL LEGEND ON PRECEDING FIGURE (31a)

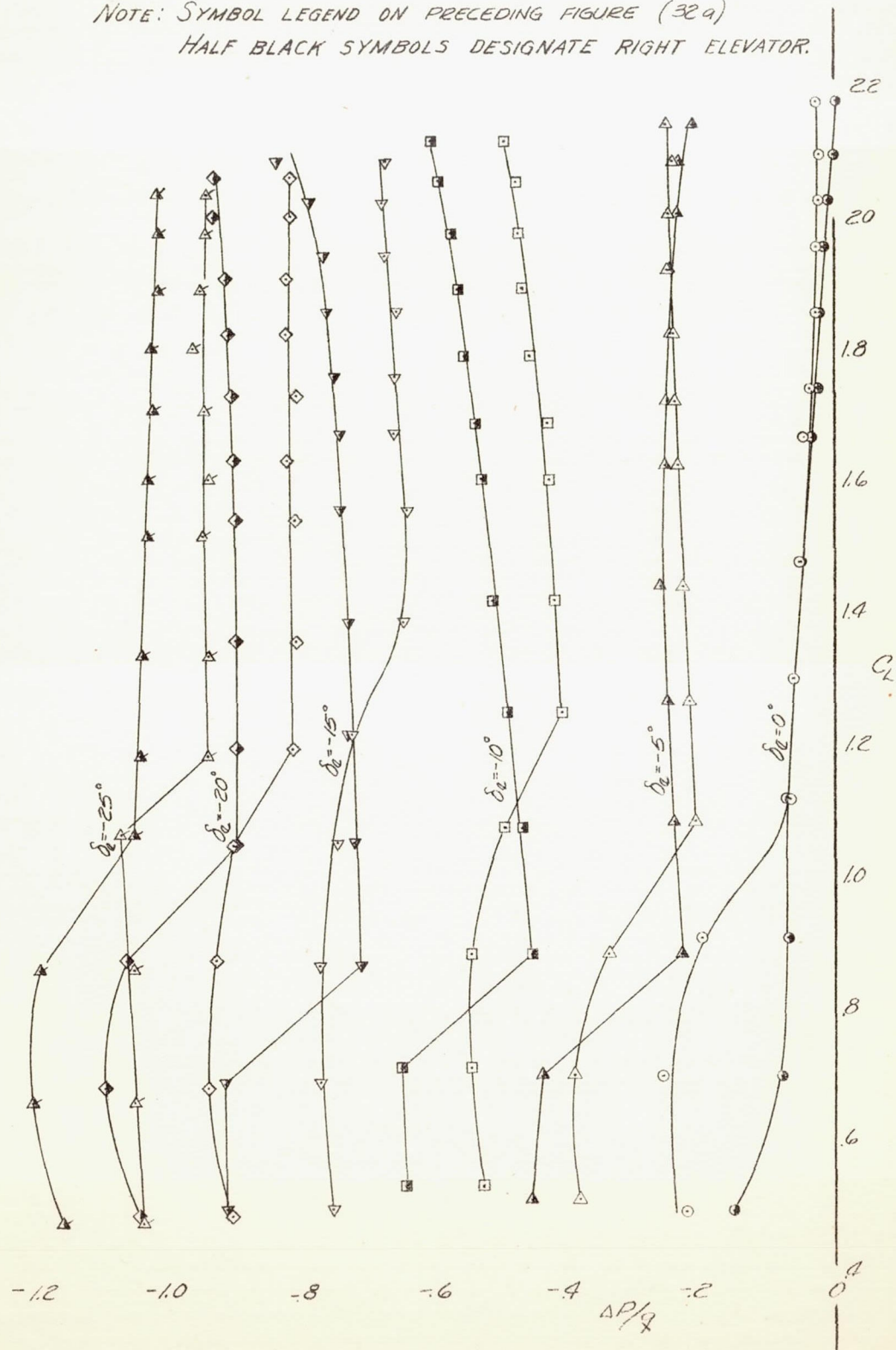


(b) $\Delta P/q$

FIGURE 31.- CONCLUDED.

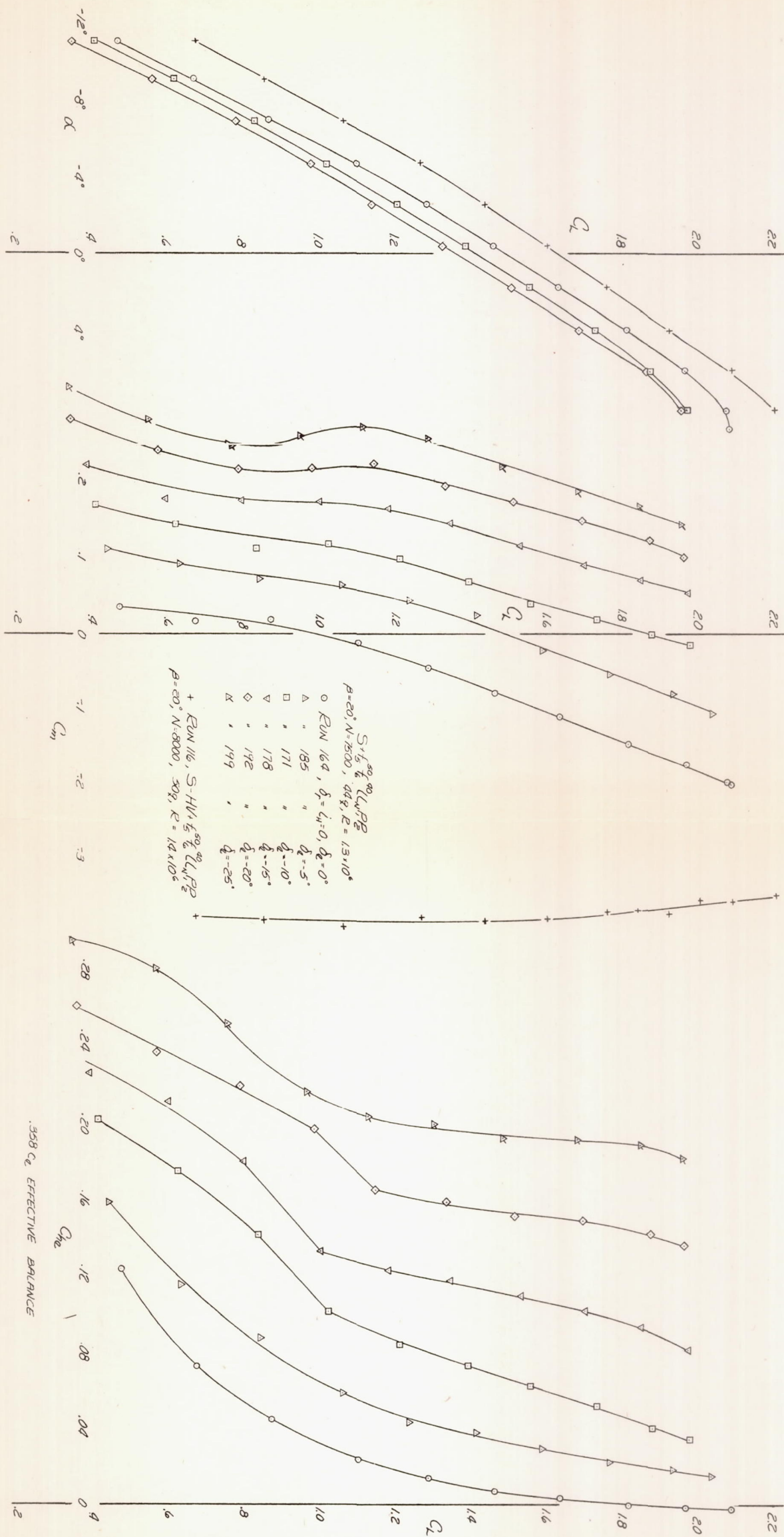
NATIONAL ADVISORY
 COMMITTEE FOR AERONAUTICS

NOTE: SYMBOL LEGEND ON PRECEDING FIGURE (32a)
HALF BLACK SYMBOLS DESIGNATE RIGHT ELEVATOR.



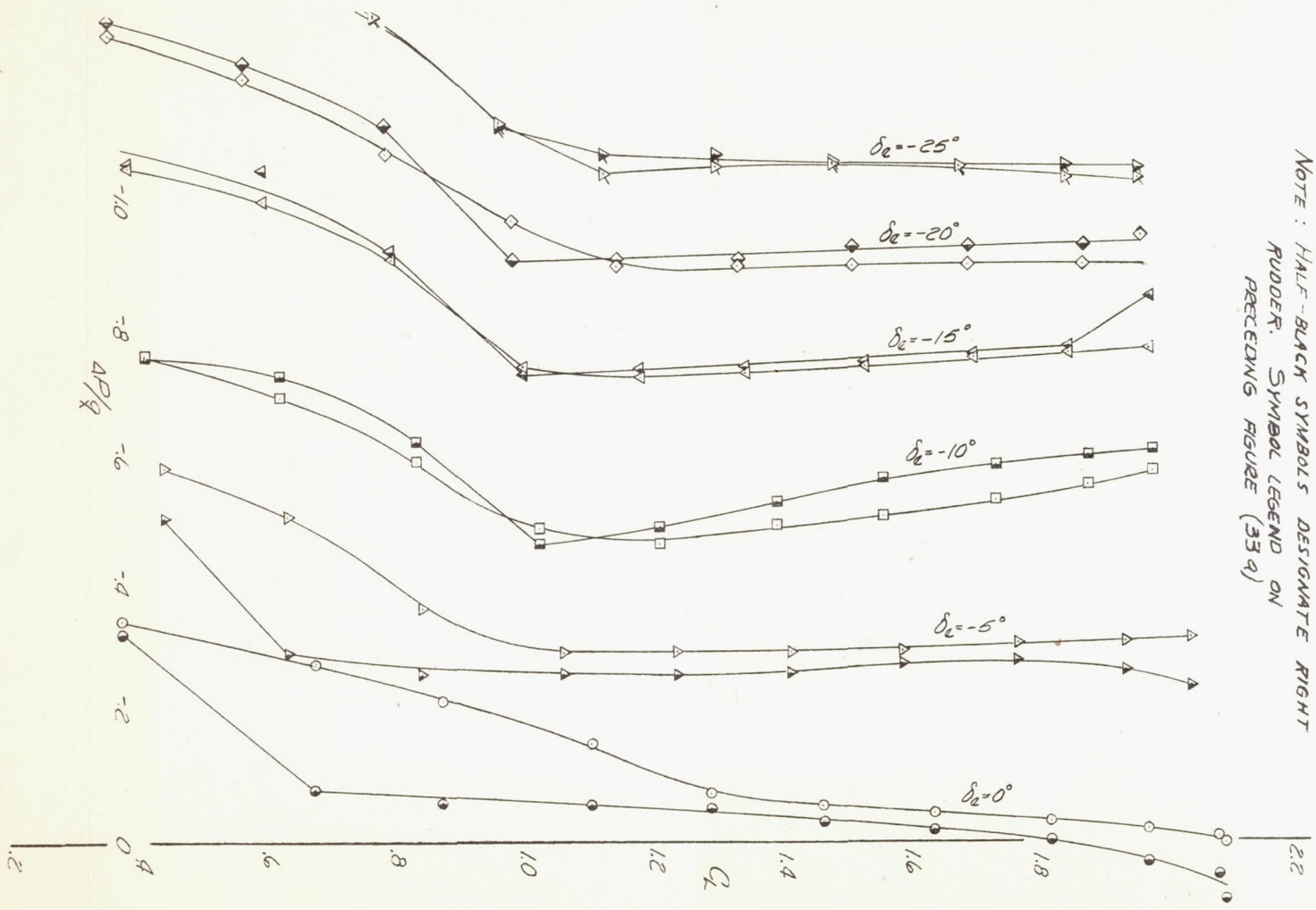
NATIONAL ADVISORY
COMMITTEE FOR AERONAUTICS

(b) $L/P/q$ CONCLUDED.
FIGURE 32. -



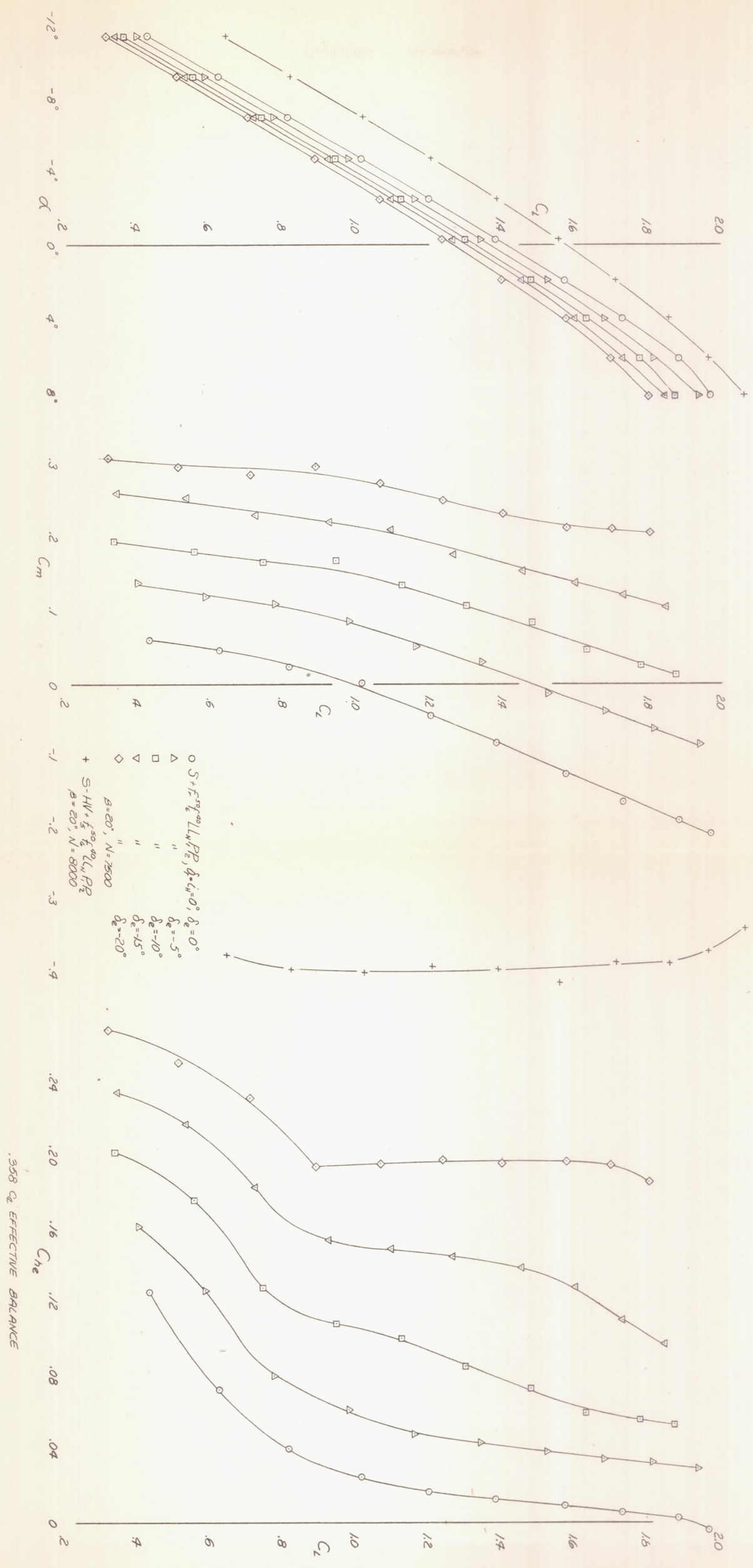
NATIONAL ADVISORY COMMITTEE FOR AERONAUTICS

(a) α, C_m, C_{he}
 FIGURE 33.- VARIATION OF AERODYNAMIC CHARACTERISTICS WITH LIFT COEFFICIENT
 FLAPS 50° , GEAR DOWN, POWER OFF ($T_e = 0$)



NOTE: HALF-BLACK SYMBOLS DESIGNATE RIGHT RUDDER. SYMBOL LEGEND ON PRECEDING FIGURE (33 a)

FIGURE 33 - (b) C_p/q CONCLUDED.



NATIONAL ADVISORY COMMITTEE FOR AERONAUTICS

(a) α, C_m, C_{he}
 FIGURE 34.- VARIATION OF AERODYNAMIC CHARACTERISTICS WITH LIFT COEFFICIENT. FLAPS 50° , GEAR DOWN, MILITARY POWER AT SL.

NOTE: SYMBOL LEGEND ON PRECEDING FIGURE (34 a)
HALF BLACK SYMBOLS DESIGNATE RIGHT ELEVATOR.

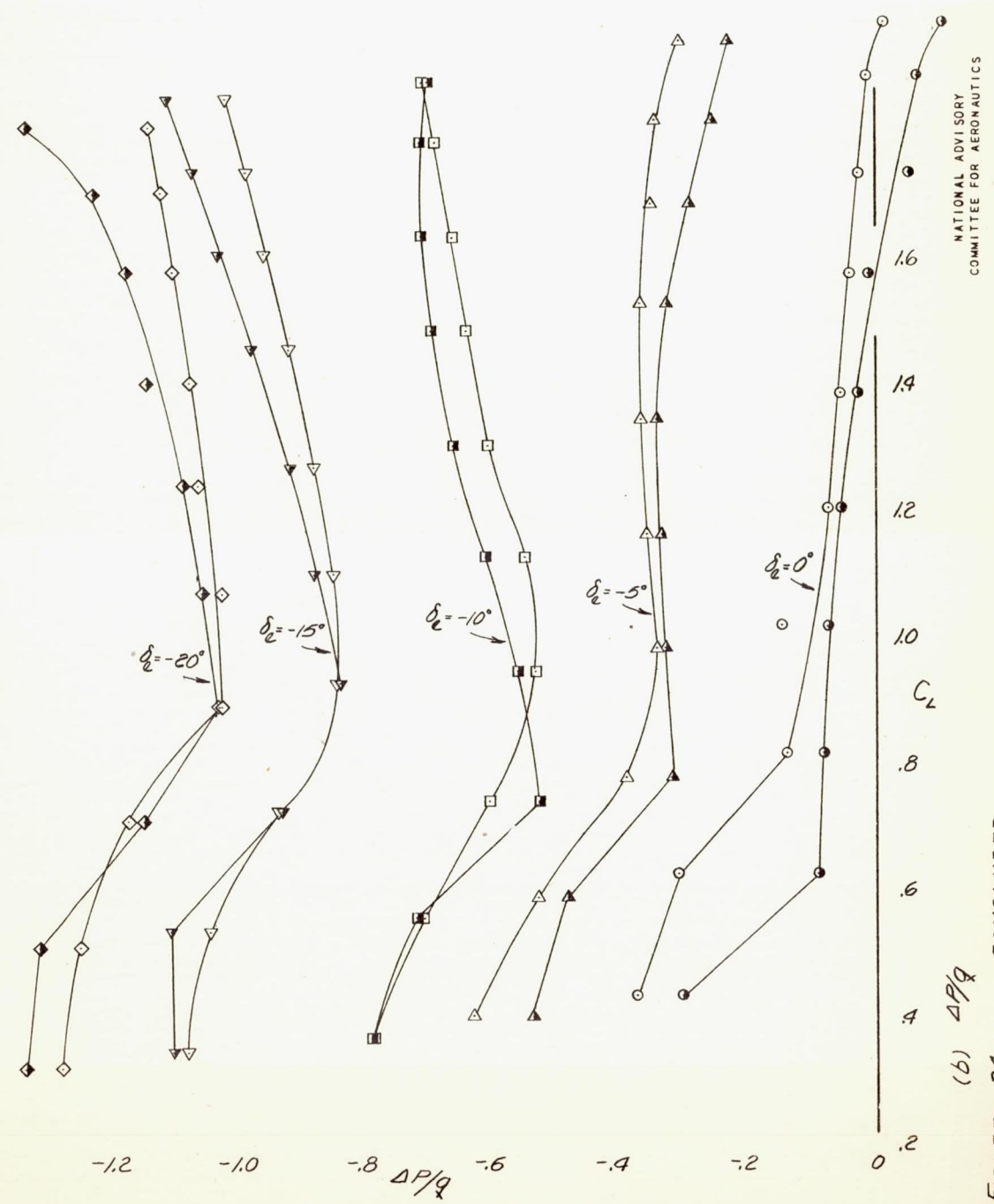


FIGURE 34 - CONCLUDED.

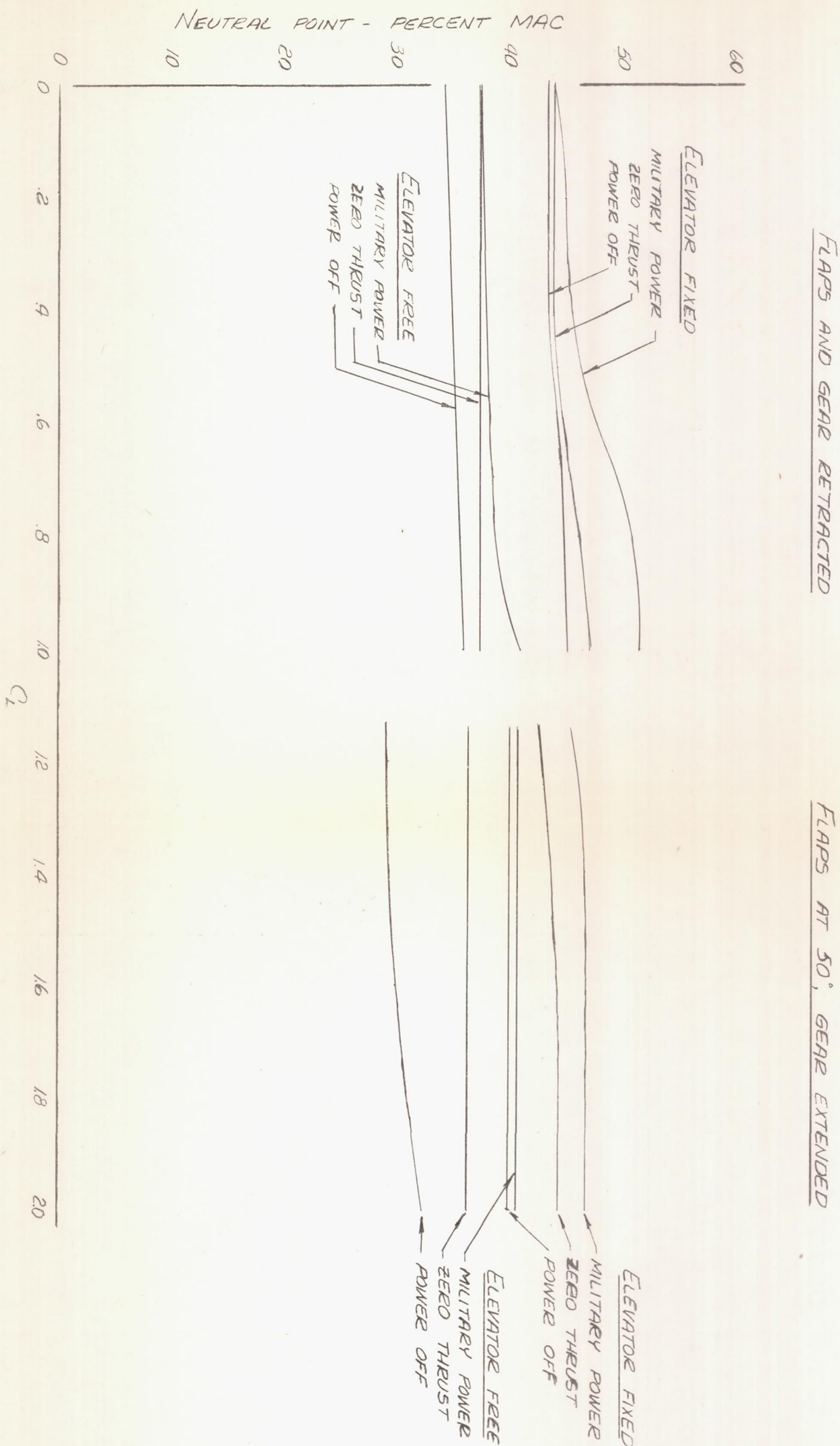
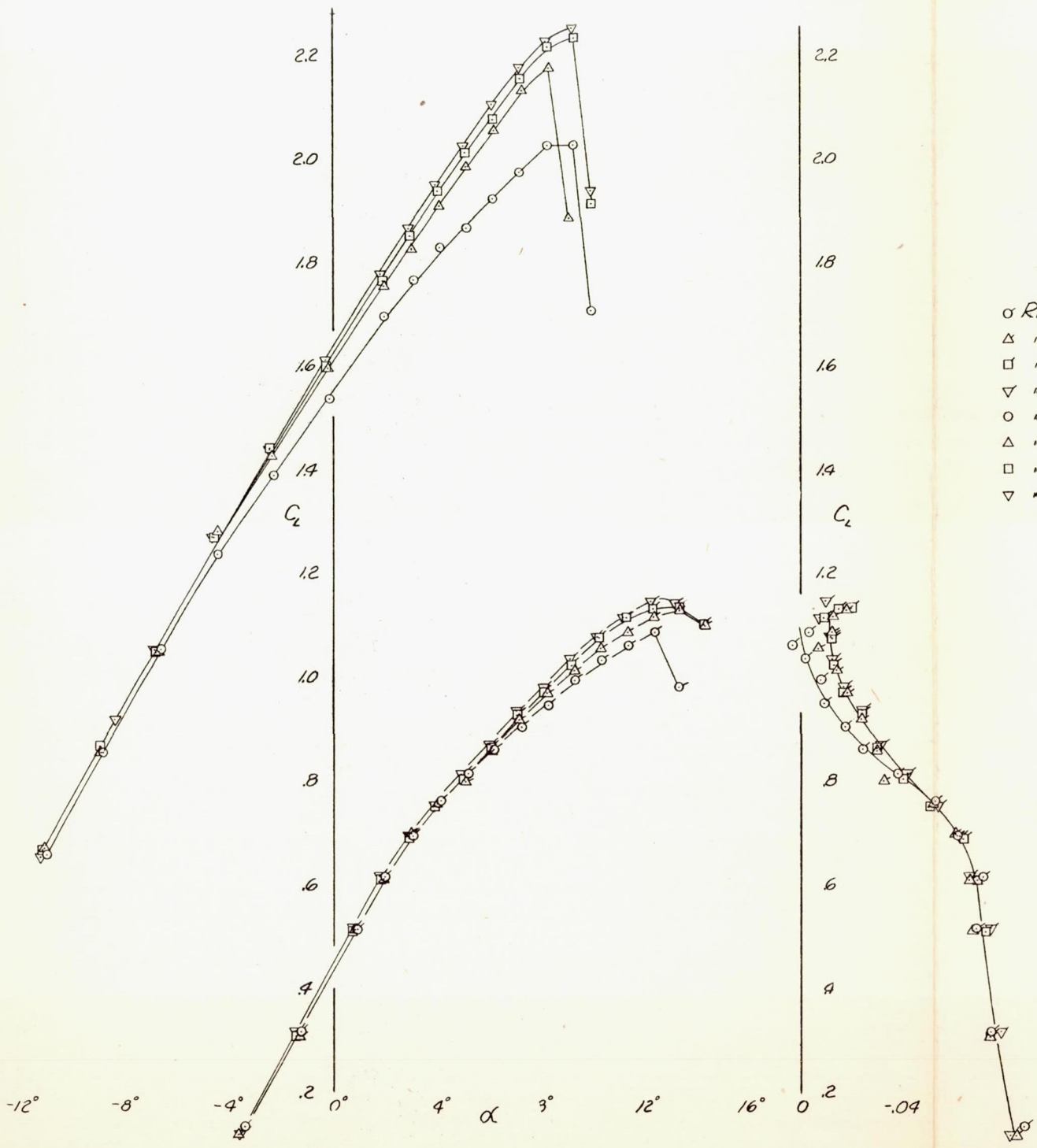
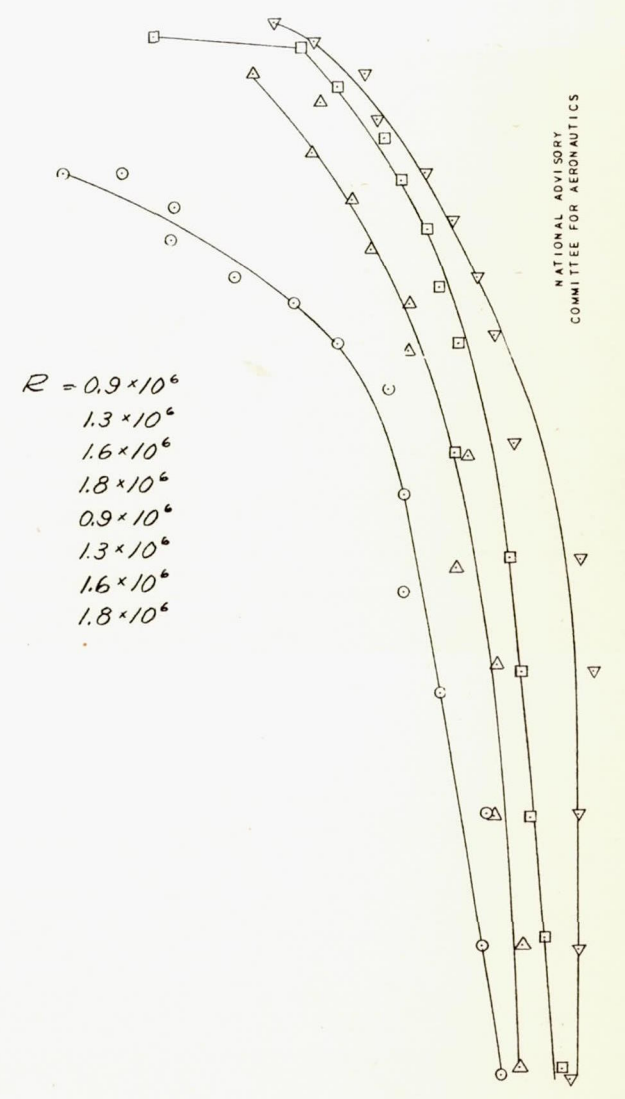


FIGURE 35.- EFFECT OF POWER ON NEUTRAL-POINT LOCATION



α	RUN 43, $W_2 G_3 B N_4 Z_6 X_2$	20	q
Δ	" 44 "	40	
\square	" 45 "	60	
∇	" 39 "	80	
\circ	" 46, $W_2 G_3 B N_4 Z_6 X_2 f_5^{50} f_6^{90}$	20	
Δ	" 47 "	40	
\square	" 48 "	60	
∇	" 49 "	80	



NATIONAL ADVISORY
COMMITTEE FOR AERONAUTICS

FIGURE 36.- EFFECT OF REYNOLDS NUMBER ON THE VARIATION OF AERODYNAMIC CHARACTERISTICS WITH LIFT COEFFICIENT. TAIL REMOVED.

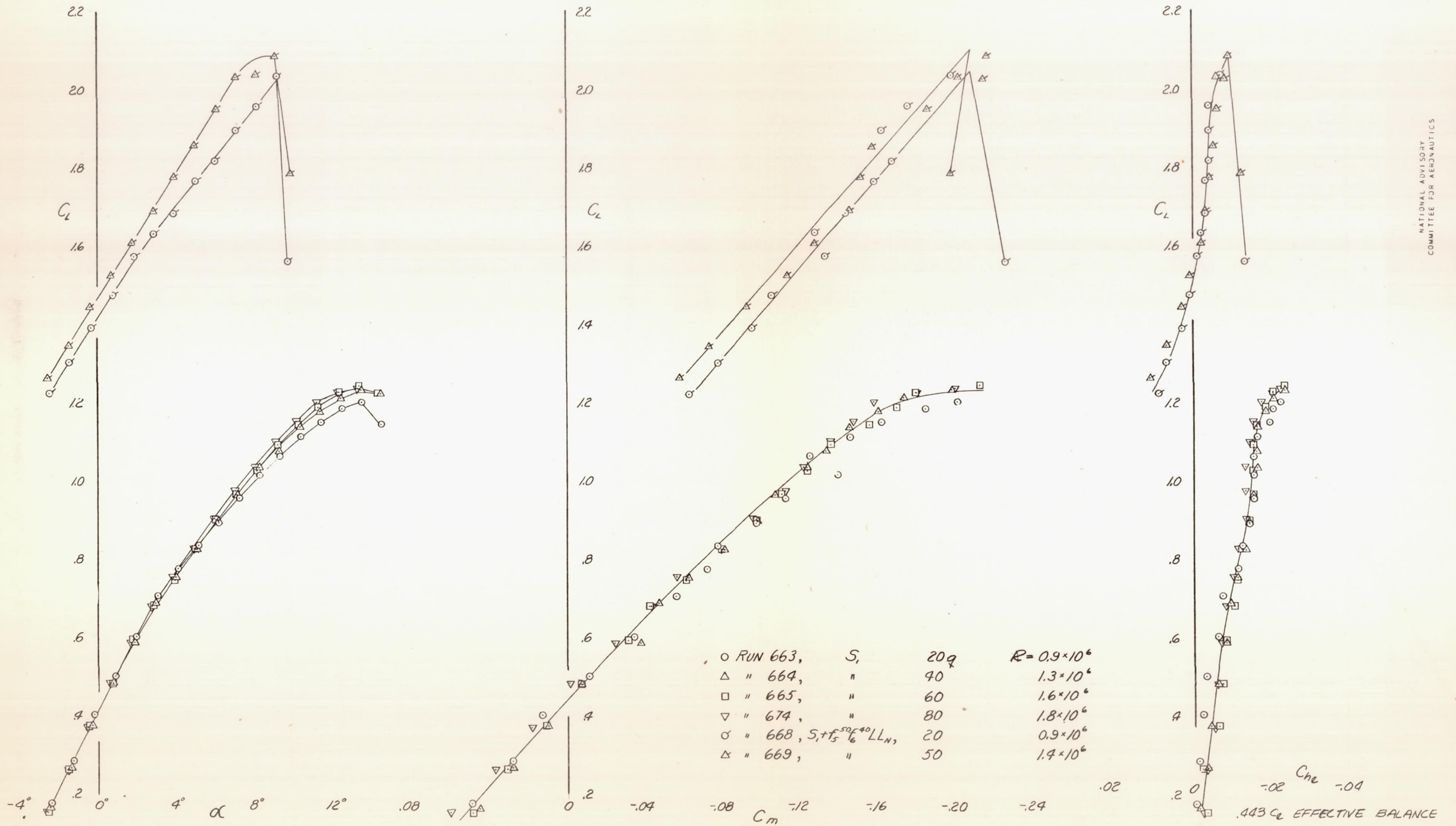


FIGURE 37. - EFFECT OF REYNOLDS NUMBER ON THE VARIATION OF AERODYNAMIC CHARACTERISTICS WITH LIFT COEFFICIENT. TAIL ON.

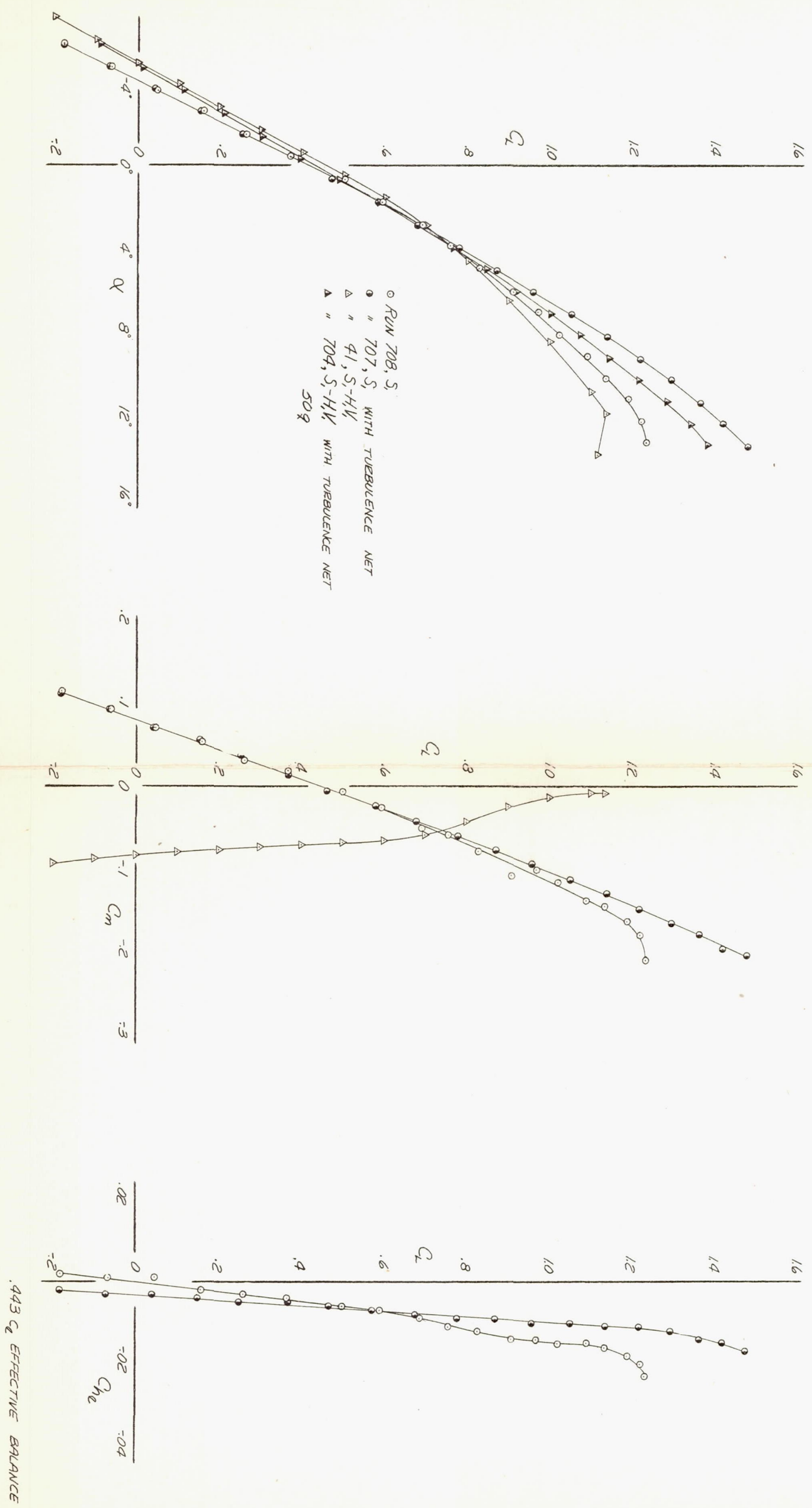


FIGURE 38.- EFFECT OF A TURBULENCE NET ON THE AERODYNAMIC CHARACTERISTICS
 FLAPS AND GEAR UP, PROPELLER OFF.

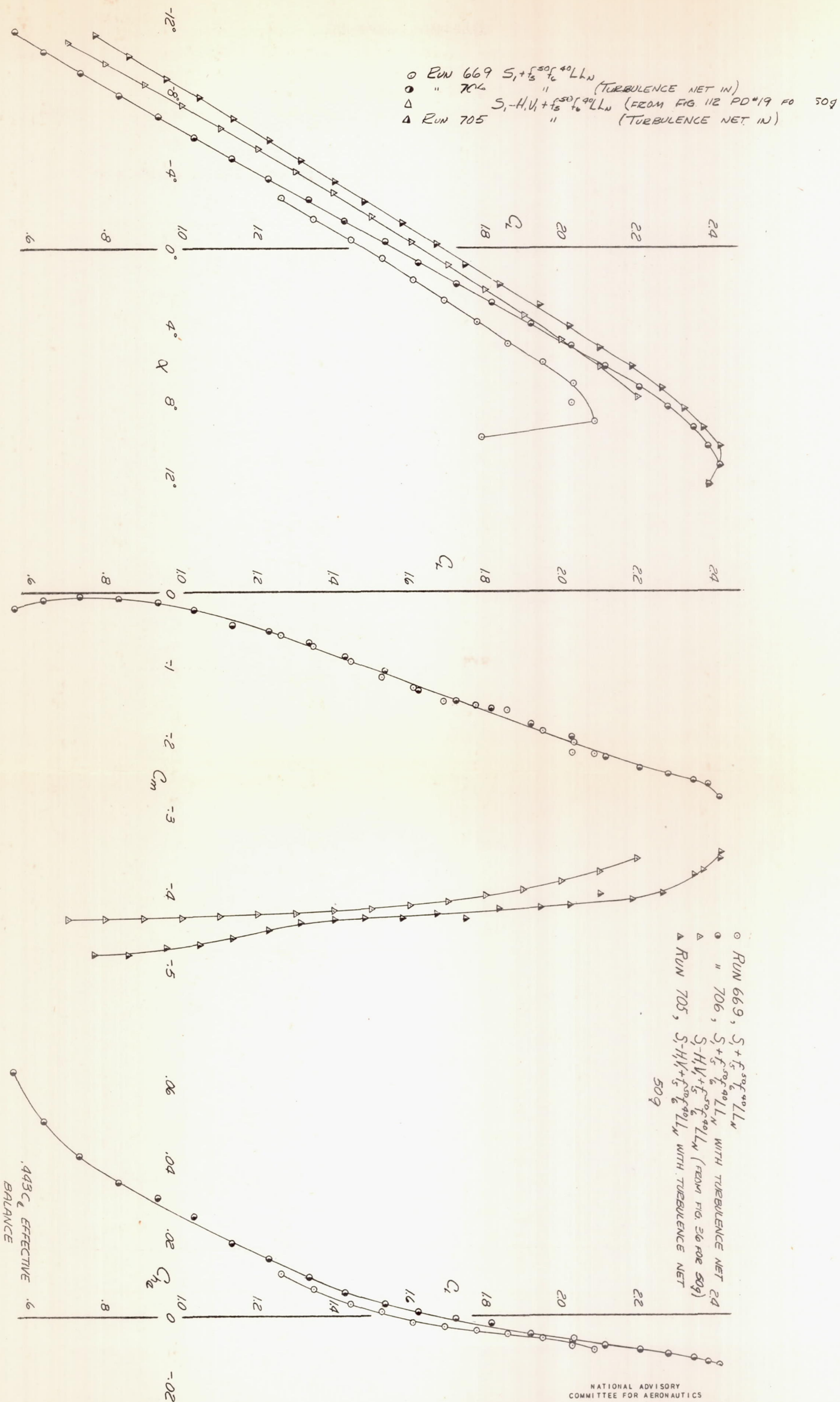
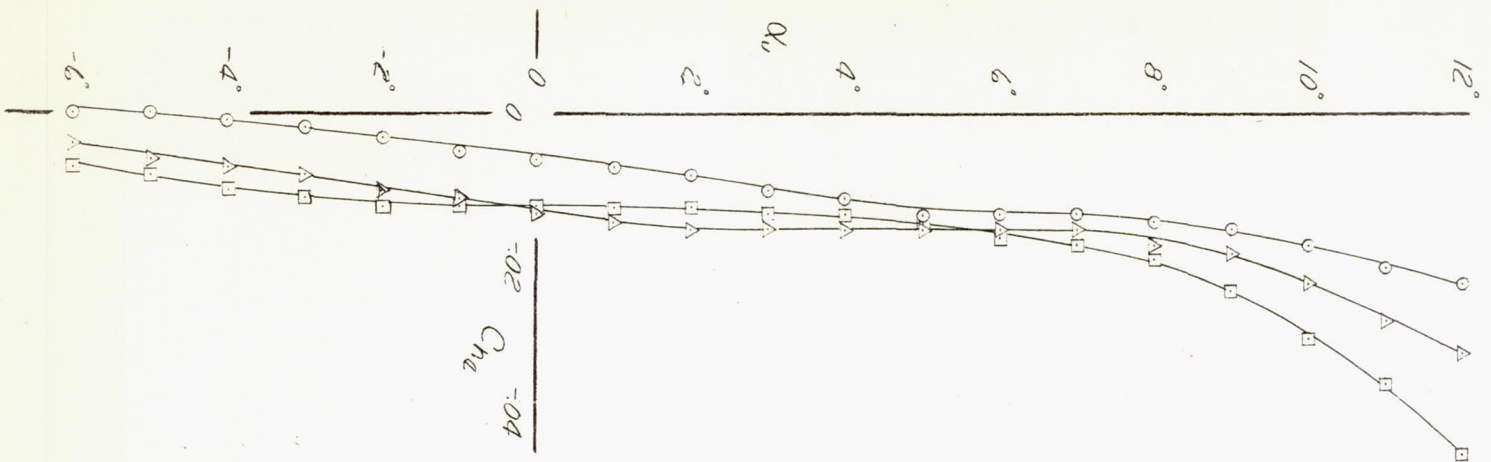
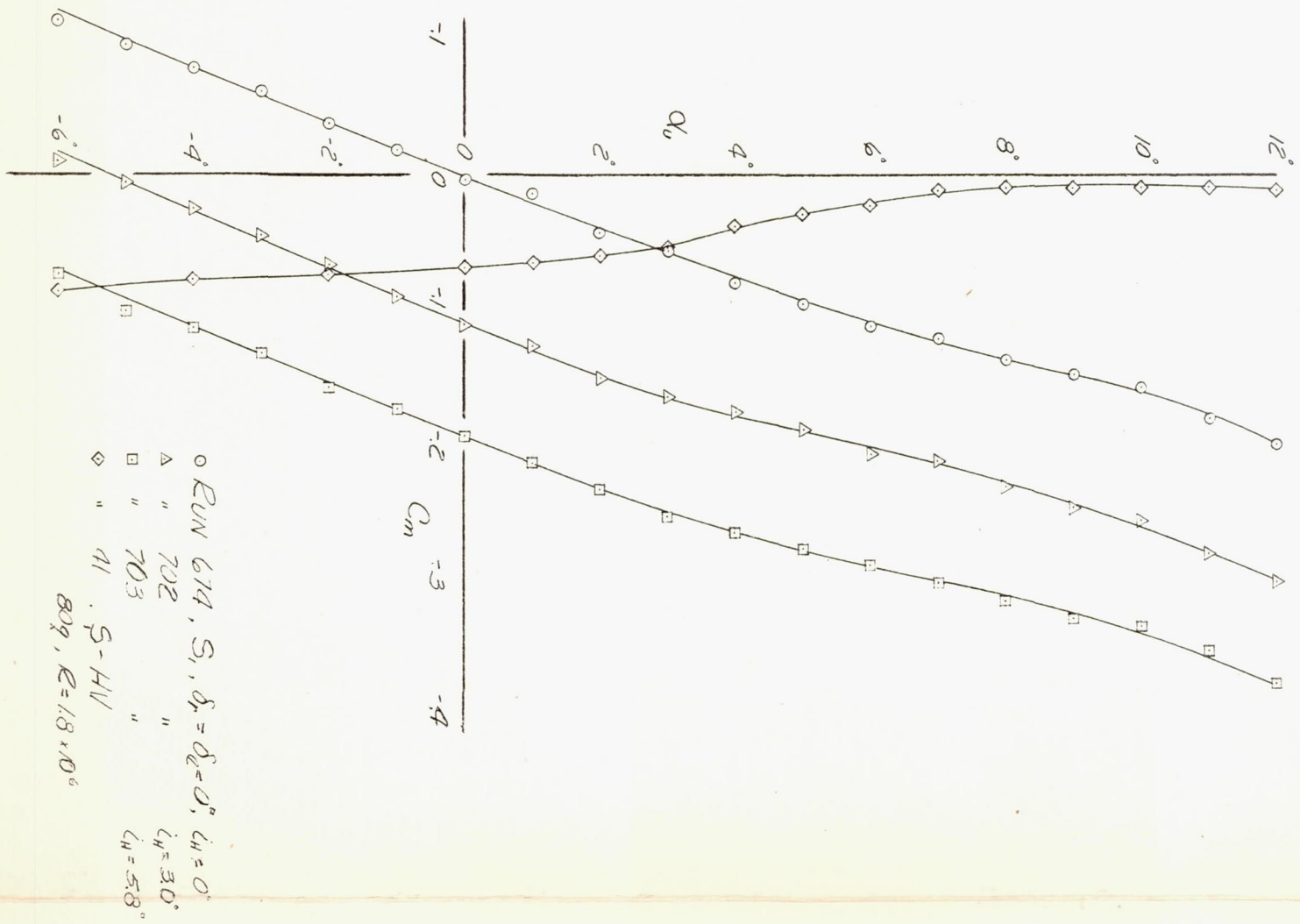


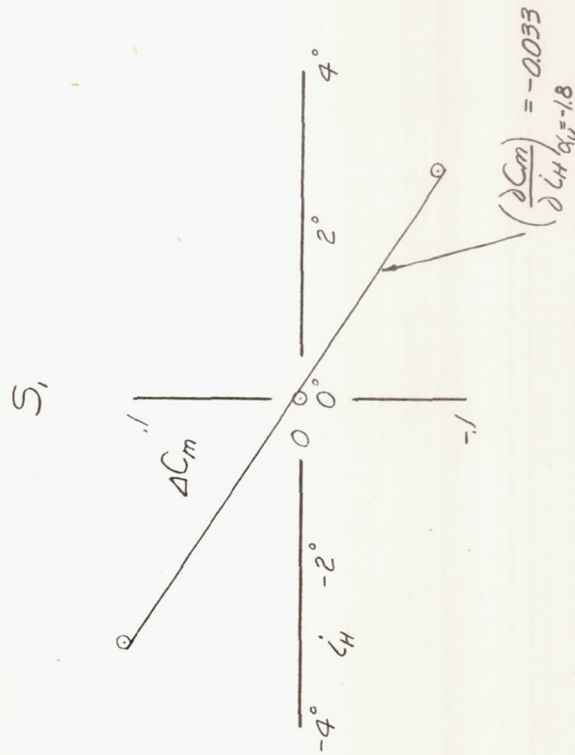
FIGURE 39.- EFFECT OF A TURBULENCE NET ON THE AERODYNAMIC CHARACTERISTICS. FLAPS 50° GEAR DOWN, PROPELLER OFF.



4430, EFFECTIVE BALANCE

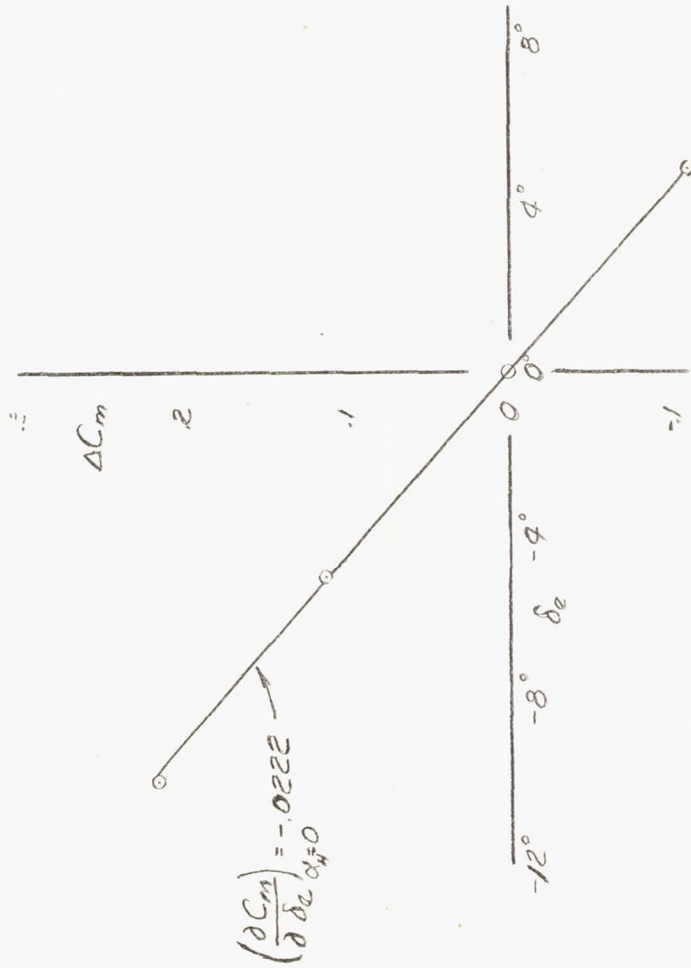
NATIONAL ADVISORY
COMMITTEE FOR AERONAUTICS

FIGURE 40.- VARIATION OF AERODYNAMIC CHARACTERISTICS WITH ANGLE OF ATTACK. STABILIZER INCIDENCE VARIED, FLAPS AND GEAR UP, PROPELLER OFF.



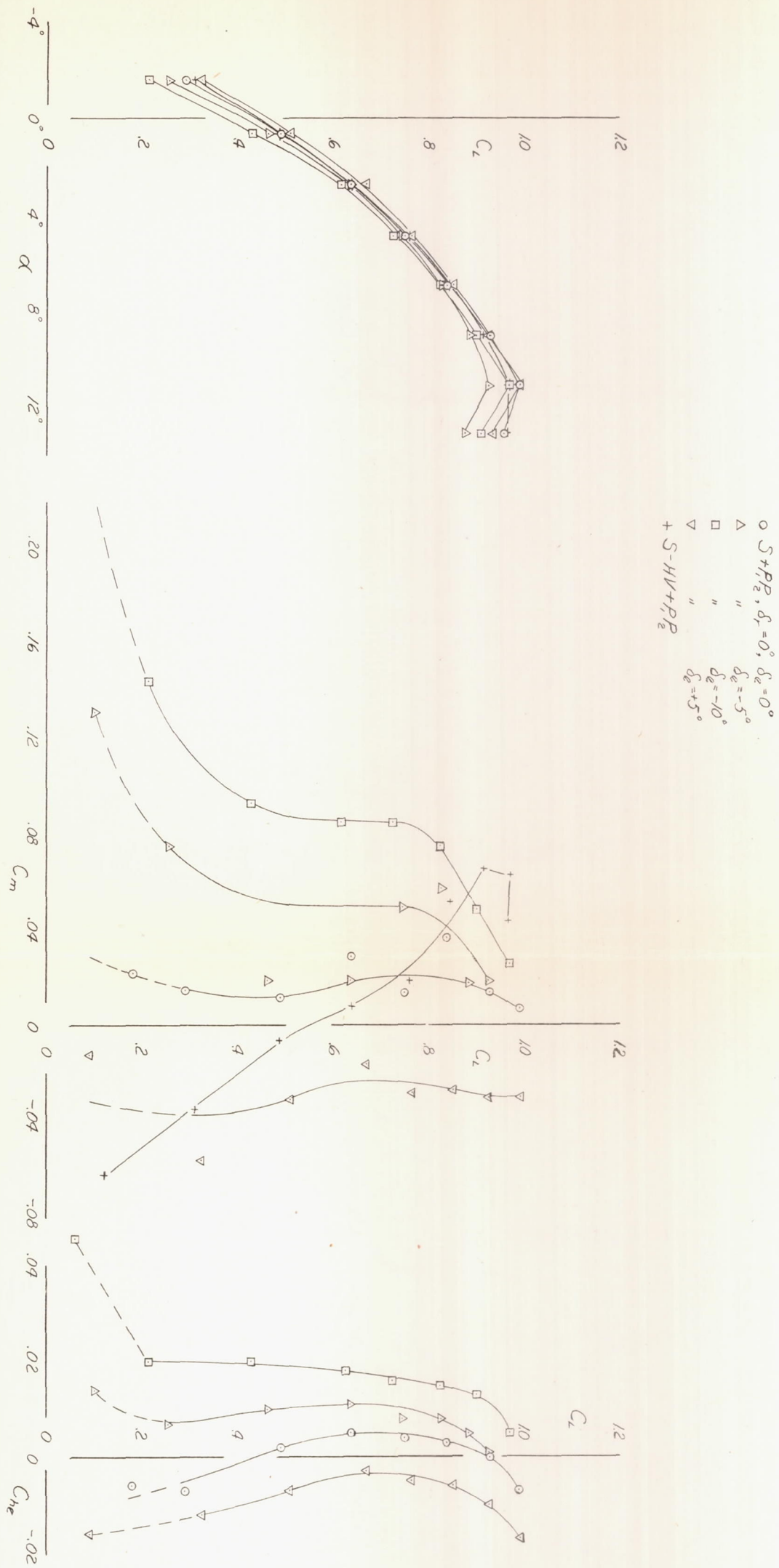
NATIONAL ADVISORY
COMMITTEE FOR AERONAUTICS

FIGURE 41.- STABILIZER EFFECTIVENESS. FLAPS AND GEAR UP, PROPELLER OFF



NATIONAL ADVISORY
COMMITTEE FOR AERONAUTICS

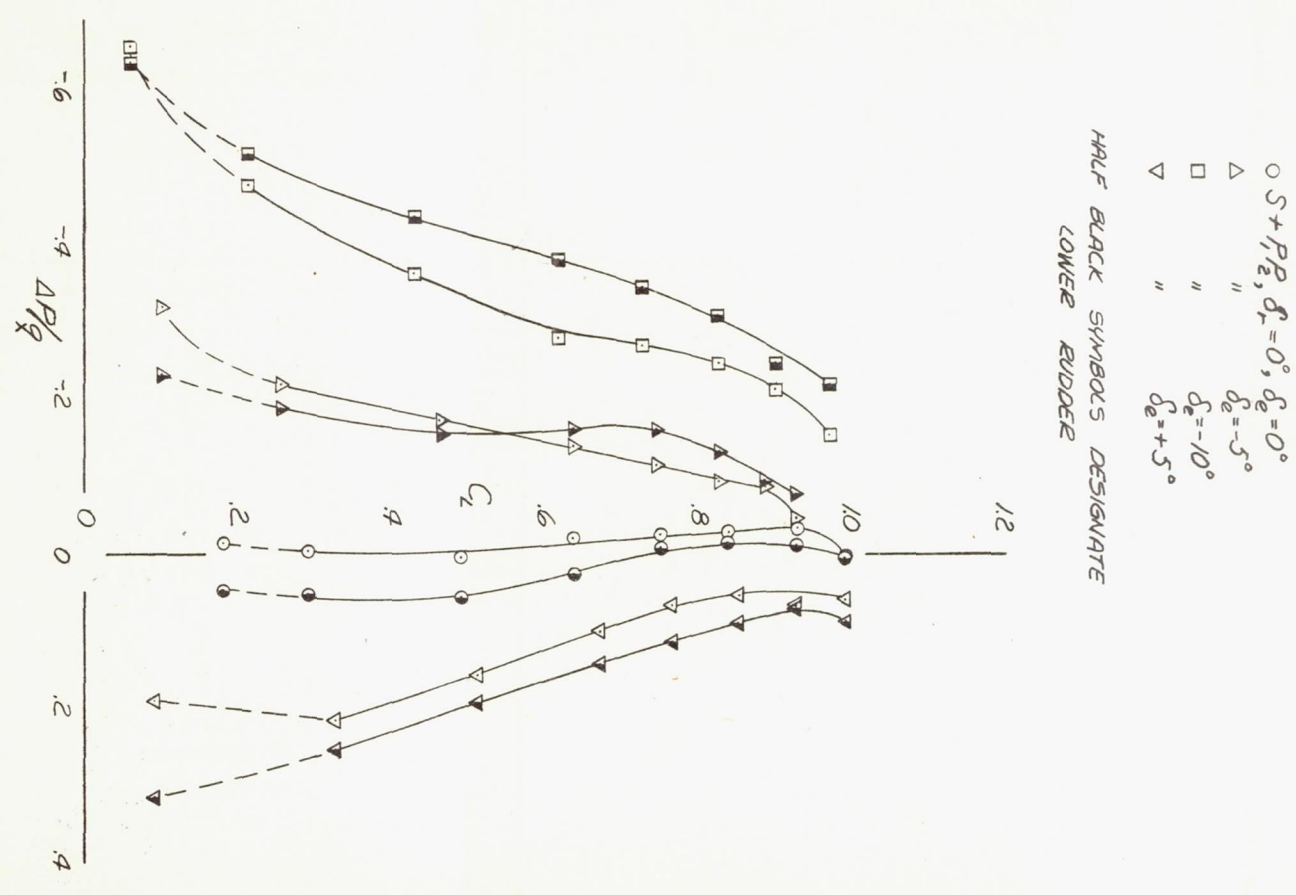
FIGURE 42.- ELEVATOR EFFECTIVENESS. FLAPS AND GEAR UP, PROPELLER OFF.



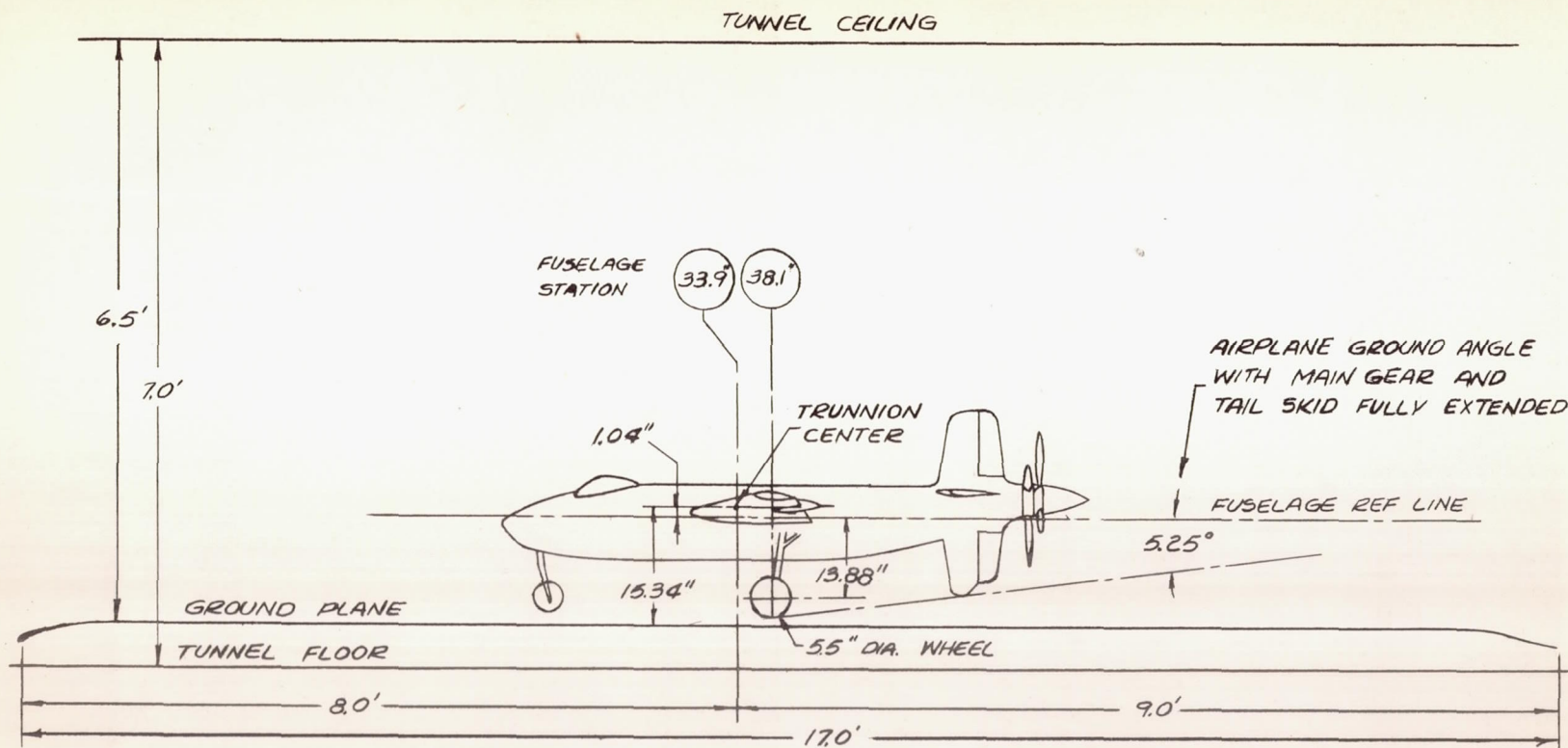
358 C_L EFFECTIVE BALANCE

NATIONAL ADVISORY COMMITTEE FOR AERONAUTICS

(a) C_L, C_m, C_{hz}
 FIGURE 43.- VARIATION OF AERODYNAMIC CHARACTERISTICS WITH LIFT COEFFICIENT.
 FLAPS AND GEAR RETRACTED, PROPELLER OPERATING AT
 NEGATIVE THRUST, MILITARY POWER AT SL., ELEVATOR DEFLECTED.



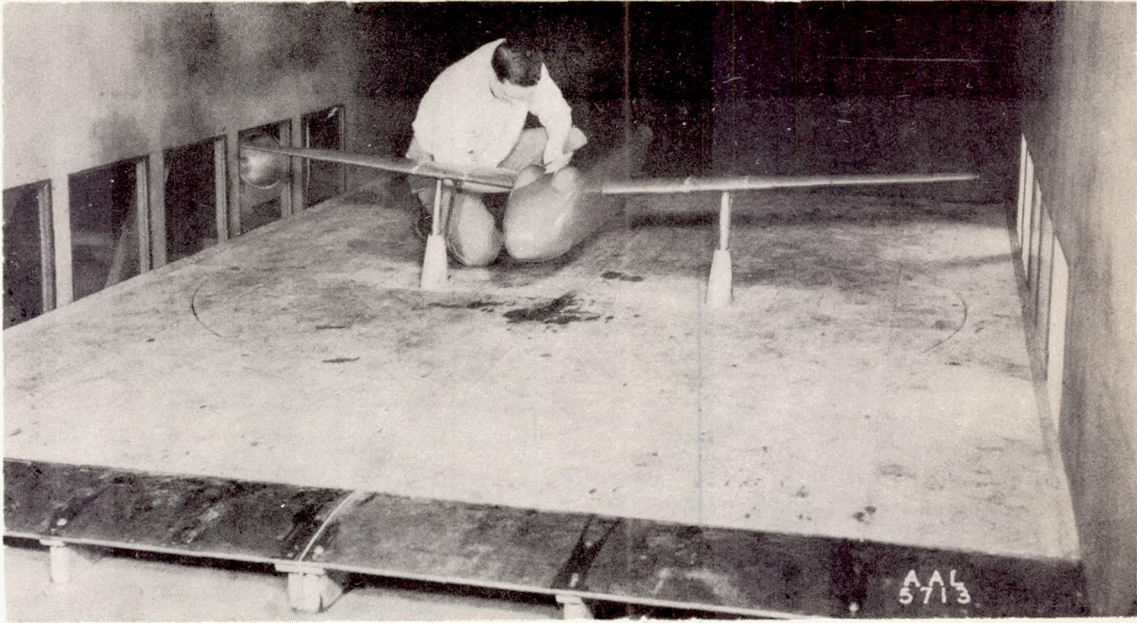
(b) $\Delta P/q$
FIGURE 43.- CONCLUDED.



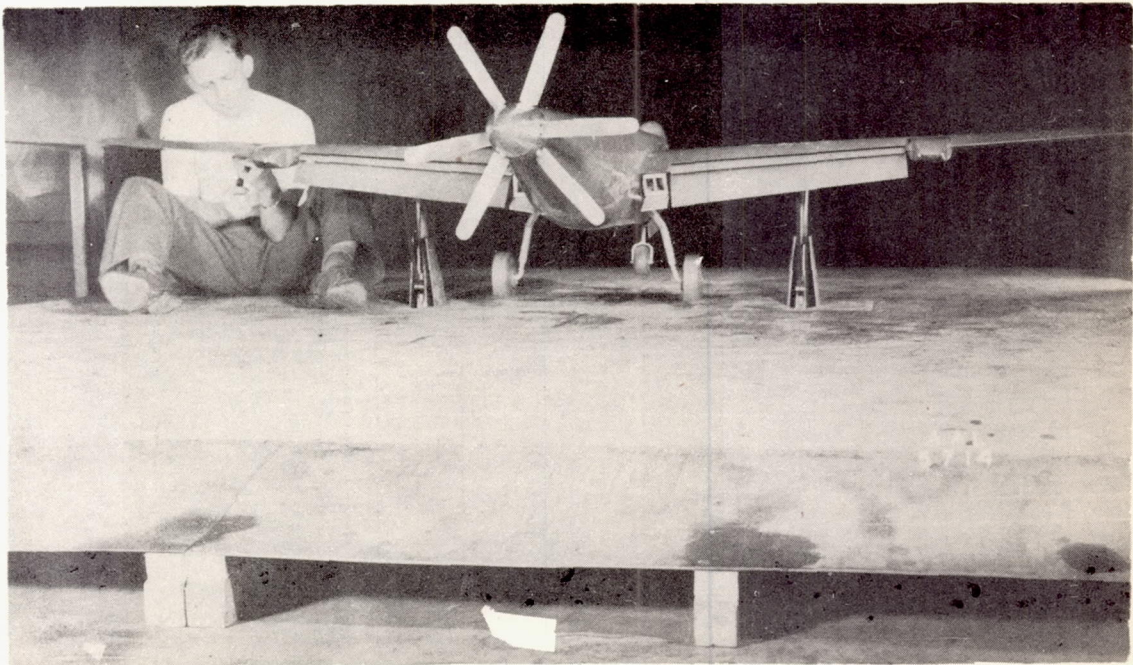
$\frac{1}{20}$ SCALE

NATIONAL ADVISORY
COMMITTEE FOR AERONAUTICS

FIGURE 44.- SIDE VIEW OF THE MODEL WITH GROUND-PLANE
INSTALLATION IN THE 7-BY 10-FOOT TUNNEL.

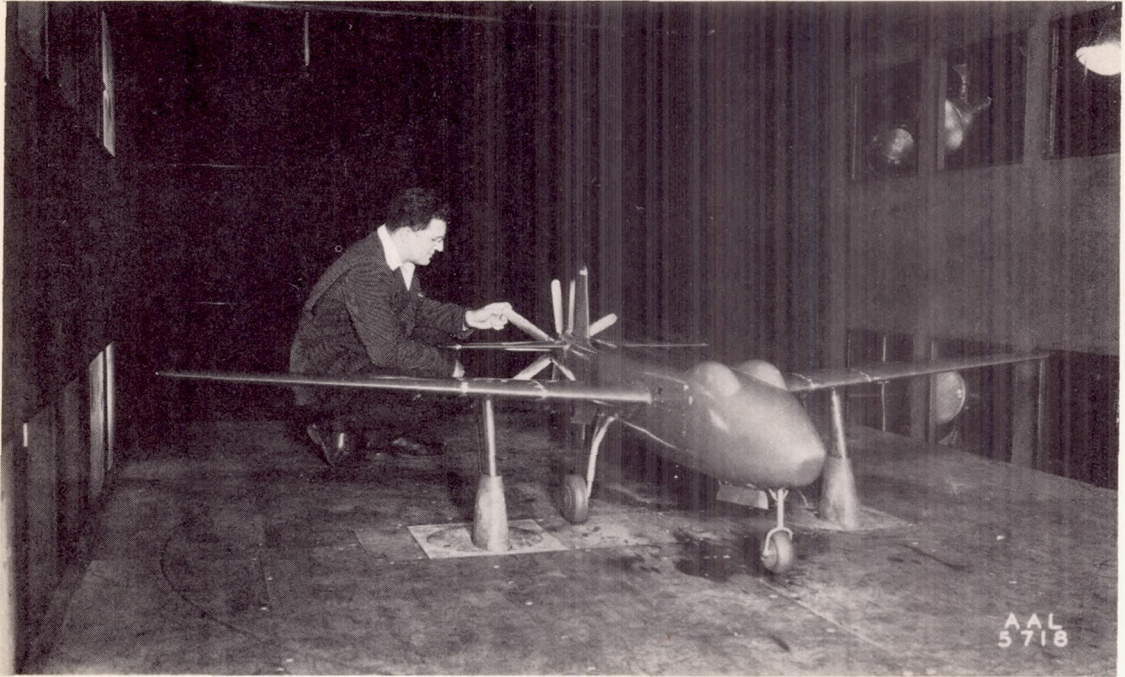


(a) Standard configuration with tail removed ($S_1 - H_1V_1 + GP$).



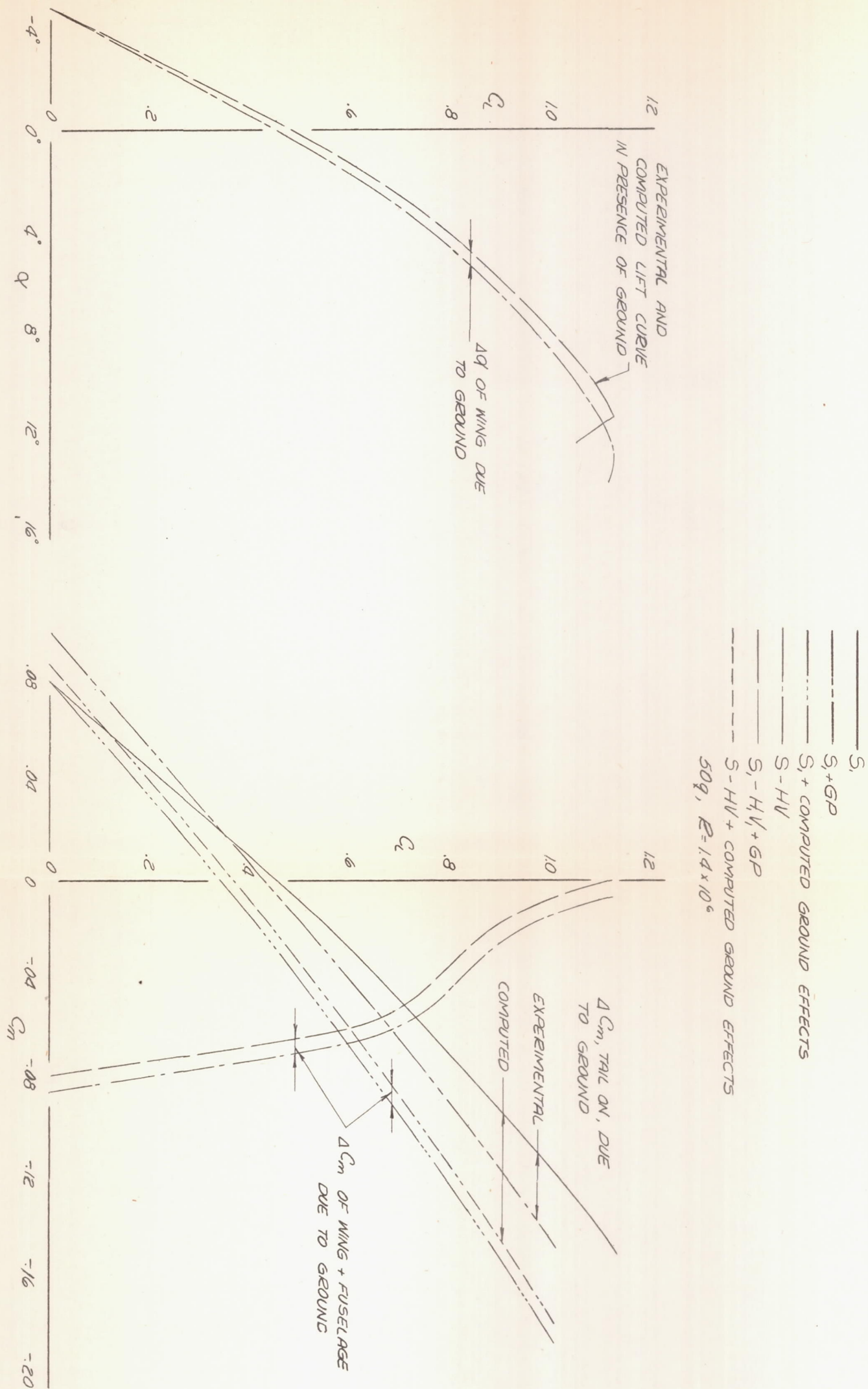
(b) Landing configuration with tail removed.
($S_1 - H_1V_1 f_s^{50} f_e^{40} LL_N P_1P_2 GP$).

Figure 45.- Views of the model in the presence of a ground plane.



(c) Take-off configuration ($S_1 + f_5^{30} f_6^{40} LLN P_1 P_2 + GP$).

Figure 45.- Concluded.



NATIONAL ADVISORY COMMITTEE FOR AERONAUTICS

FIGURE 46. - COMPARISON OF EXPERIMENTAL AND COMPUTED GROUND EFFECTS ON LIFT AND PITCHING MOMENT. FLAPS AND GEAR UP, PROPELLER OFF, ELEVATOR 0° .

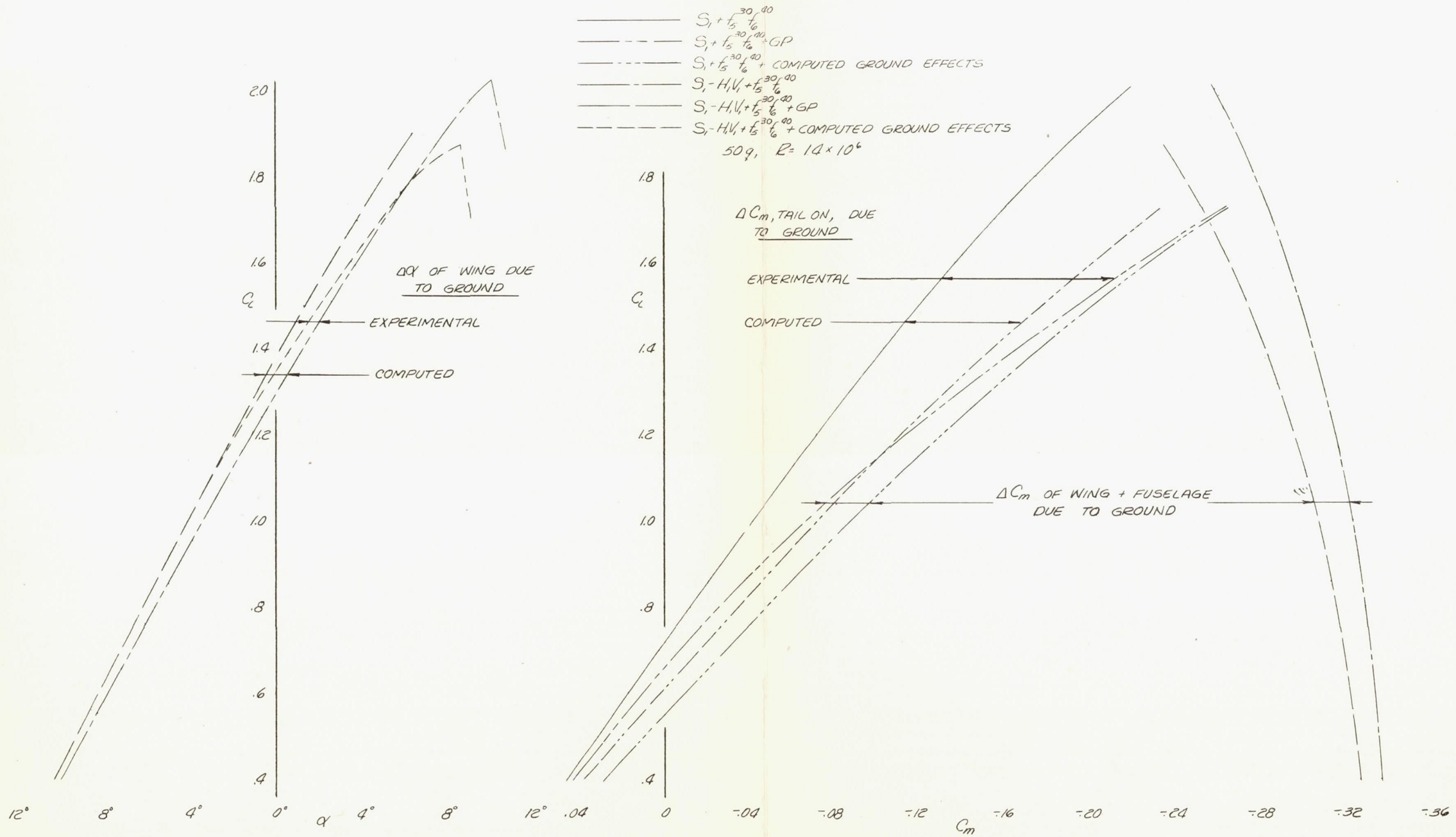
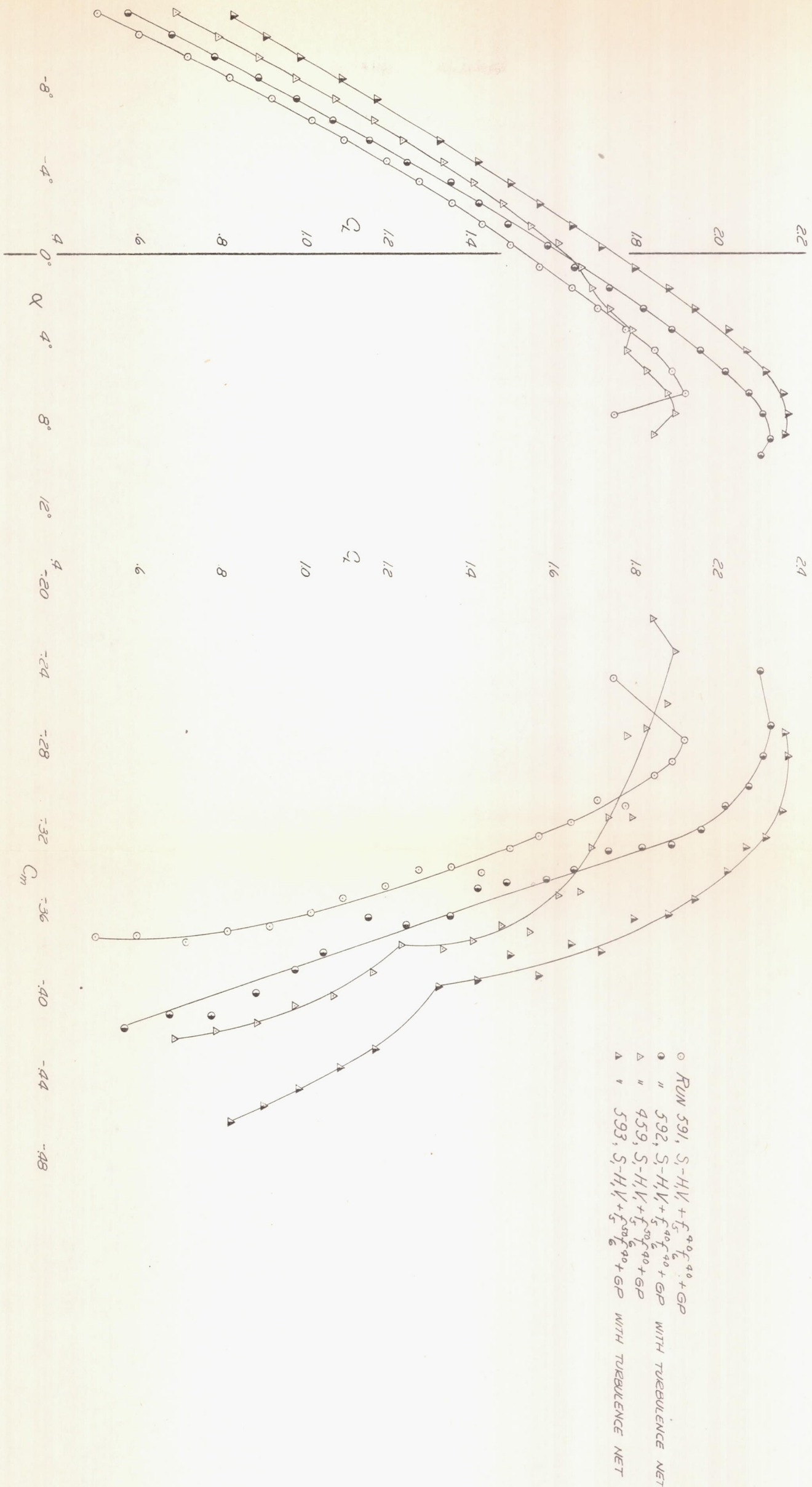
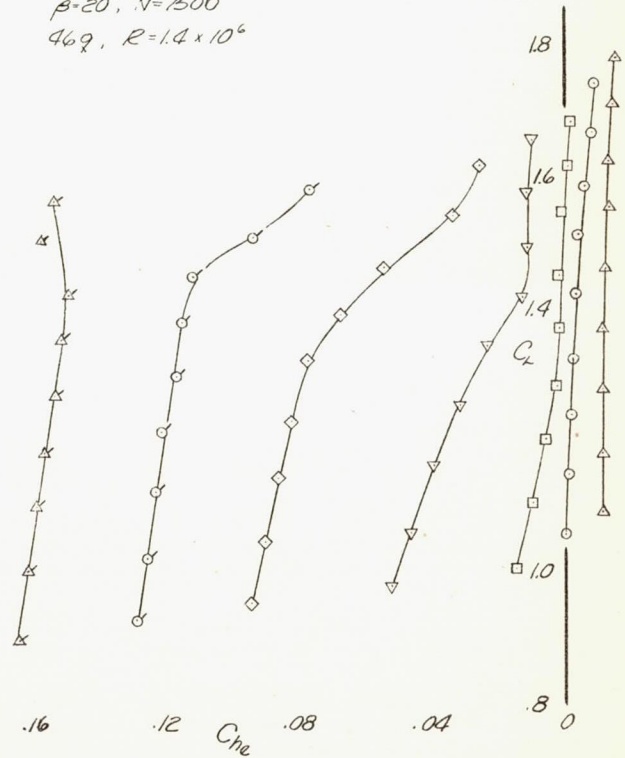
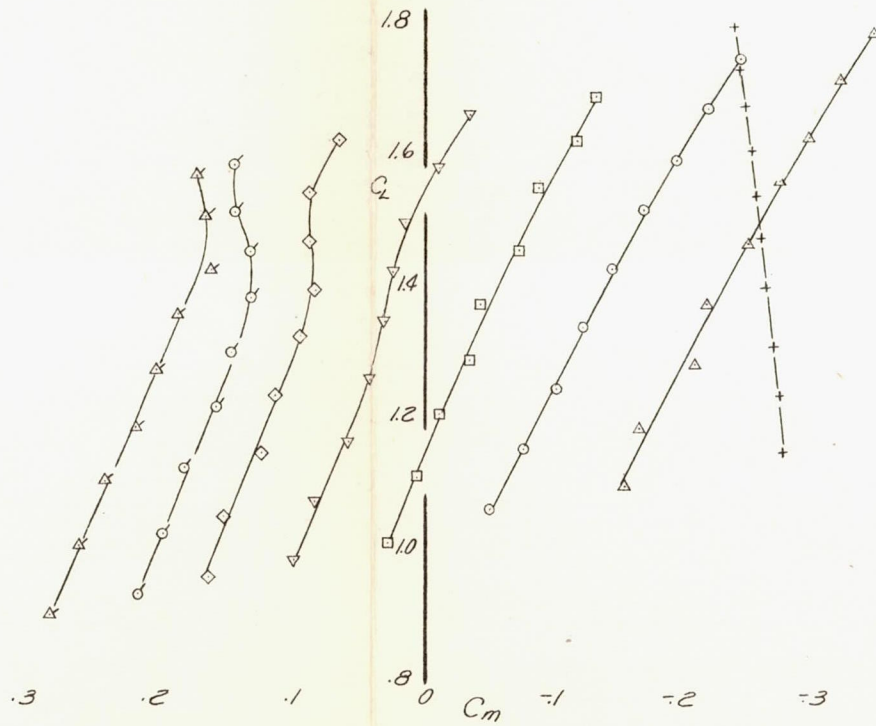
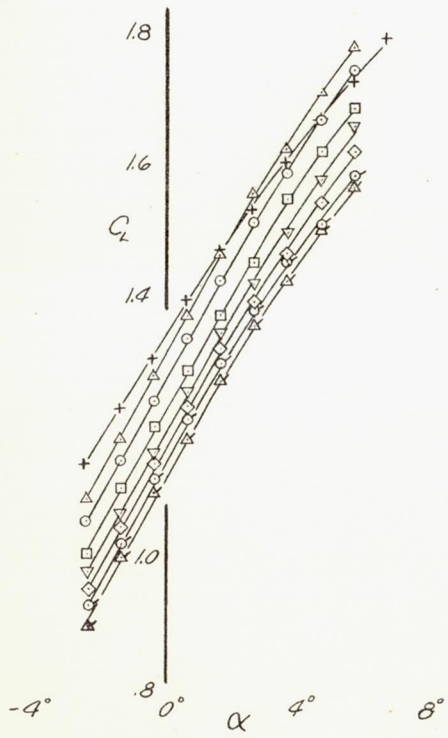


FIGURE 47.- COMPARISON OF EXPERIMENTAL AND COMPUTED GROUND EFFECTS ON LIFT AND PITCHING MOMENT. FLAPS 30°, GEAR UP, PROPELLER OFF, ELEVATOR 0°.



NATIONAL ADVISORY
COMMITTEE FOR AERONAUTICS

FIGURE 48. - EFFECT OF A TURBULENCE NET ON THE AERODYNAMIC CHARACTERISTICS OF THE MODEL IN THE PRESENCE OF A GROUND PLANE. FLAPS 40° AND 50°, GEAR UP, TAIL OFF, PROPELLER OFF.

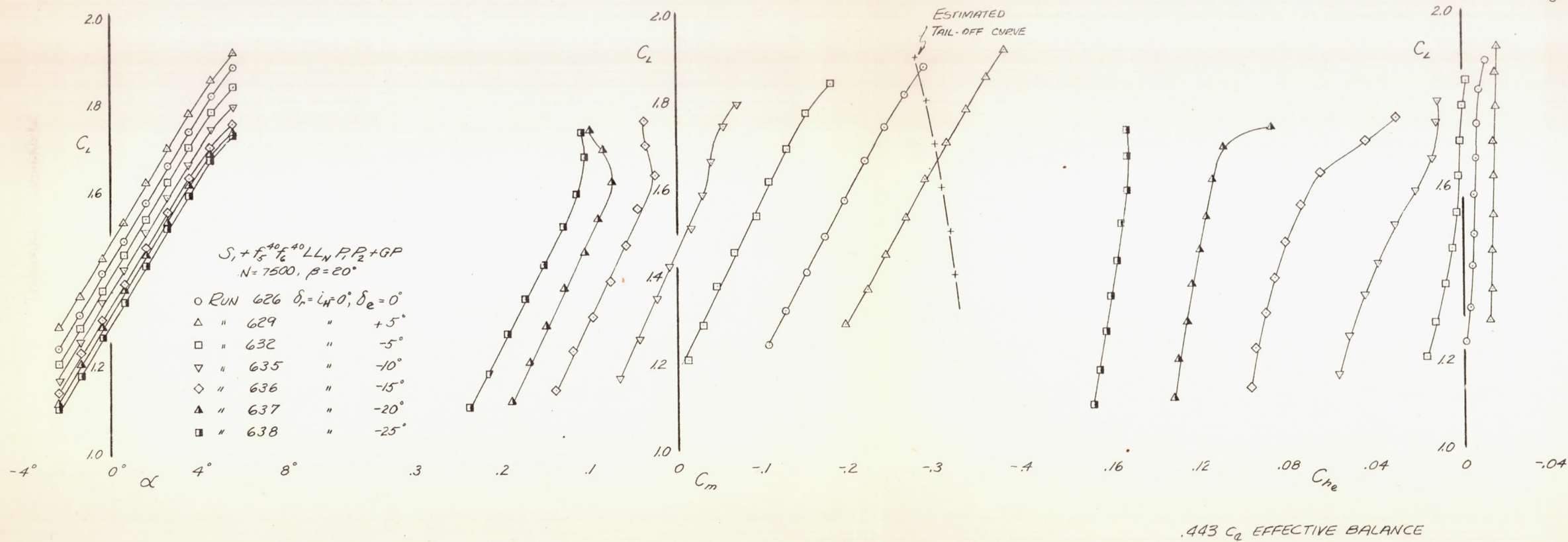


o RUN 540 $S_1 + f_s^{30,40} LL_N PP + GP$ $\delta_f = 44^\circ, \delta_e = 0^\circ$
 Δ " 584 " " $\delta_e = +5^\circ$
 □ " 585 " " $\delta_e = -5^\circ$
 ▽ " 551 " " $\delta_e = -10^\circ$
 ◇ " 586 " " $\delta_e = -15^\circ$
 ♂ " 562 " " $\delta_e = -20^\circ$
 ✕ " 573 " " $\delta_e = -25^\circ$
 + " 467 $S_1 - HV_1 + f_s^{30,40} LL_N PP + GP$
 $\beta = 20^\circ, N = 7500$
 $469, R = 1.4 \times 10^6$

.443 C_e EFFECTIVE BALANCE

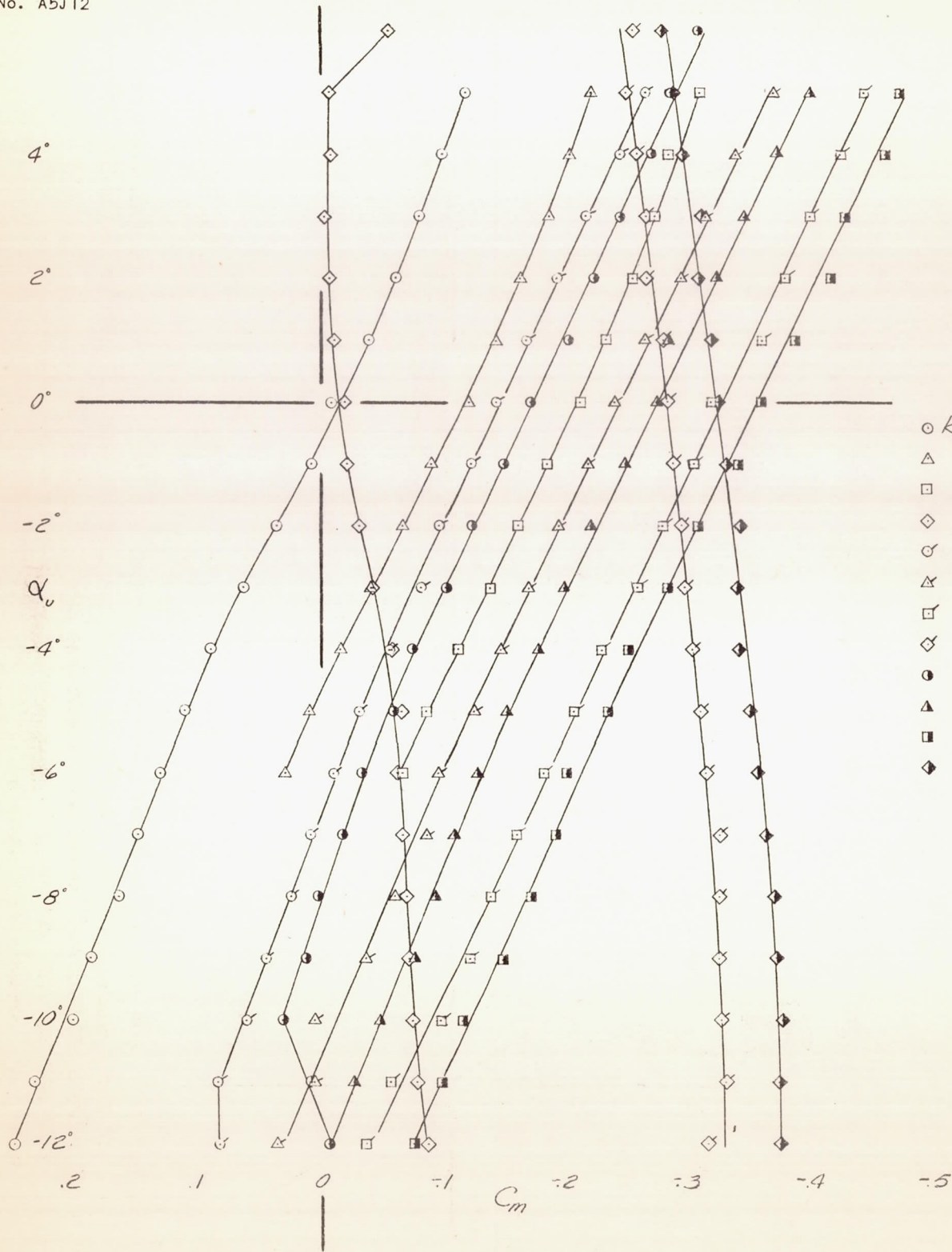
NATIONAL ADVISORY
COMMITTEE FOR AERONAUTICS

FIGURE 49. - VARIATION OF AERODYNAMIC CHARACTERISTICS WITH LIFT COEFFICIENT OF THE MODEL IN THE PRESENCE OF A GROUND PLANE. FLAPS 30°, GEAR DOWN, POWER OFF ($\xi = 0$).

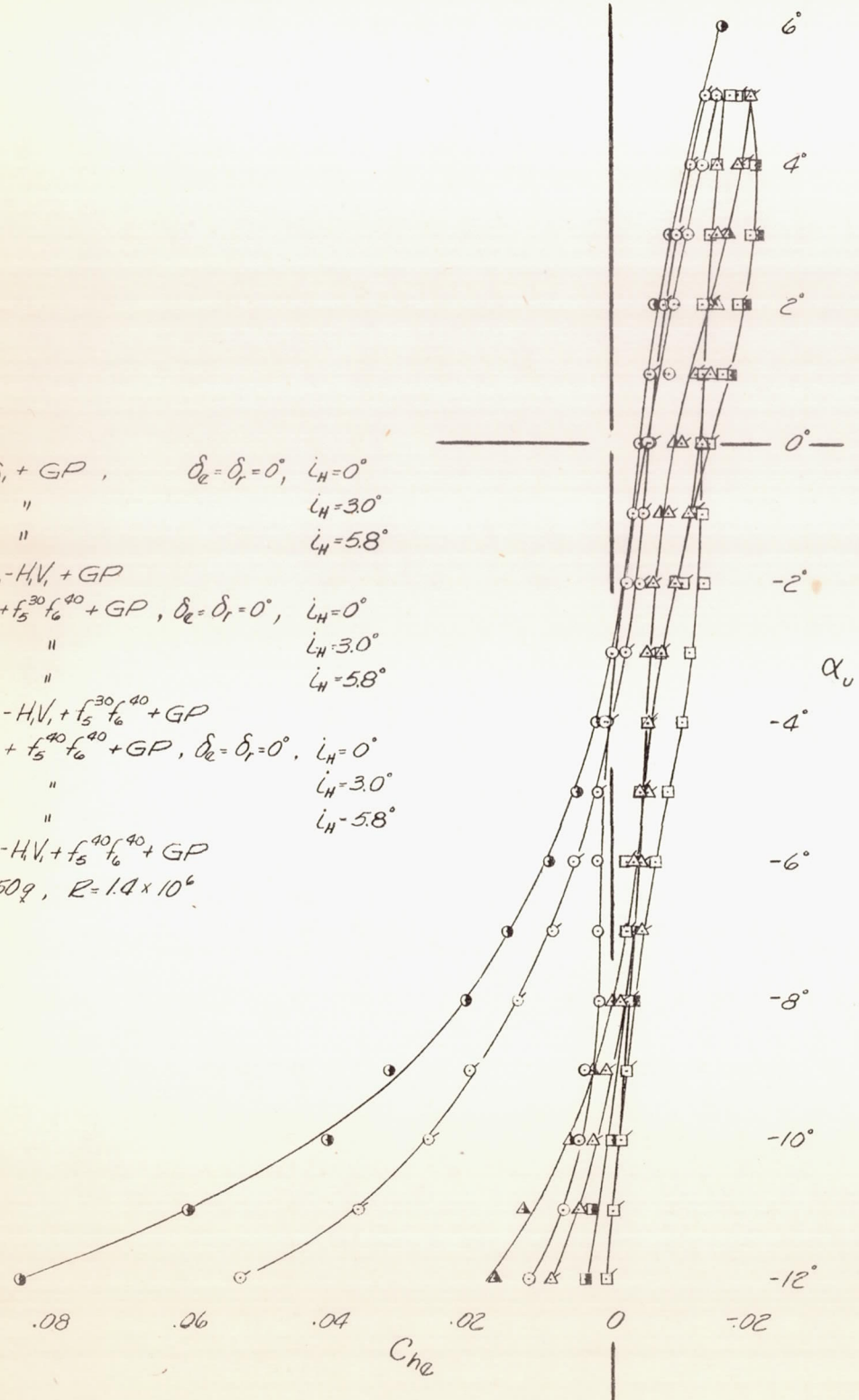


NATIONAL ADVISORY COMMITTEE FOR AERONAUTICS

FIGURE 50.- VARIATION OF AERODYNAMIC CHARACTERISTICS WITH LIFT COEFFICIENT OF THE MODEL IN THE PRESENCE OF A GROUND PLANE. FLAPS 40°, GEAR DOWN, POWER OFF ($T_c = 0$)

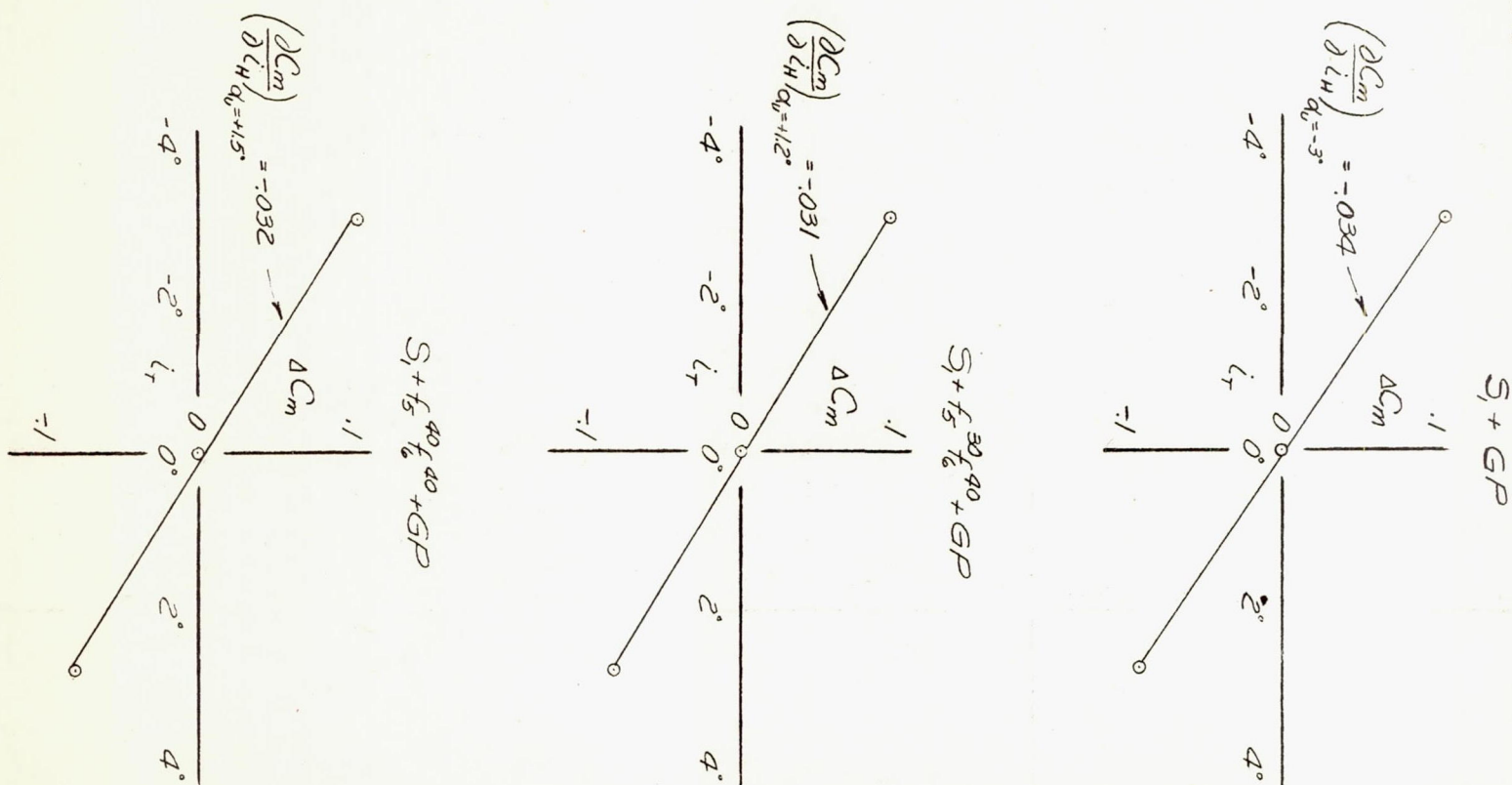


- RUN 507, $S_1 + GP$, $\delta_e = \delta_r = 0^\circ$, $i_H = 0^\circ$
 - △ " 623 " $i_H = 30^\circ$
 - " 624 " $i_H = 58^\circ$
 - ◇ " 451, $S_1 - HV_1 + GP$
 - ◊ " 500, $S_1 + f_5^{30} f_6^{40} + GP$, $\delta_e = \delta_r = 0^\circ$, $i_H = 0^\circ$
 - △ " 621 " $i_H = 30^\circ$
 - " 622 " $i_H = 58^\circ$
 - ◇ " 455, $S_1 - HV_1 + f_5^{30} f_6^{40} + GP$
 - " 612, $S_1 + f_5^{40} f_6^{40} + GP$, $\delta_e = \delta_r = 0^\circ$, $i_H = 0^\circ$
 - △ " 619 " $i_H = 30^\circ$
 - " 620 " $i_H = 58^\circ$
 - ◇ " 591, $S_1 - HV_1 + f_5^{40} f_6^{40} + GP$
- 50g, $R = 1.4 \times 10^6$



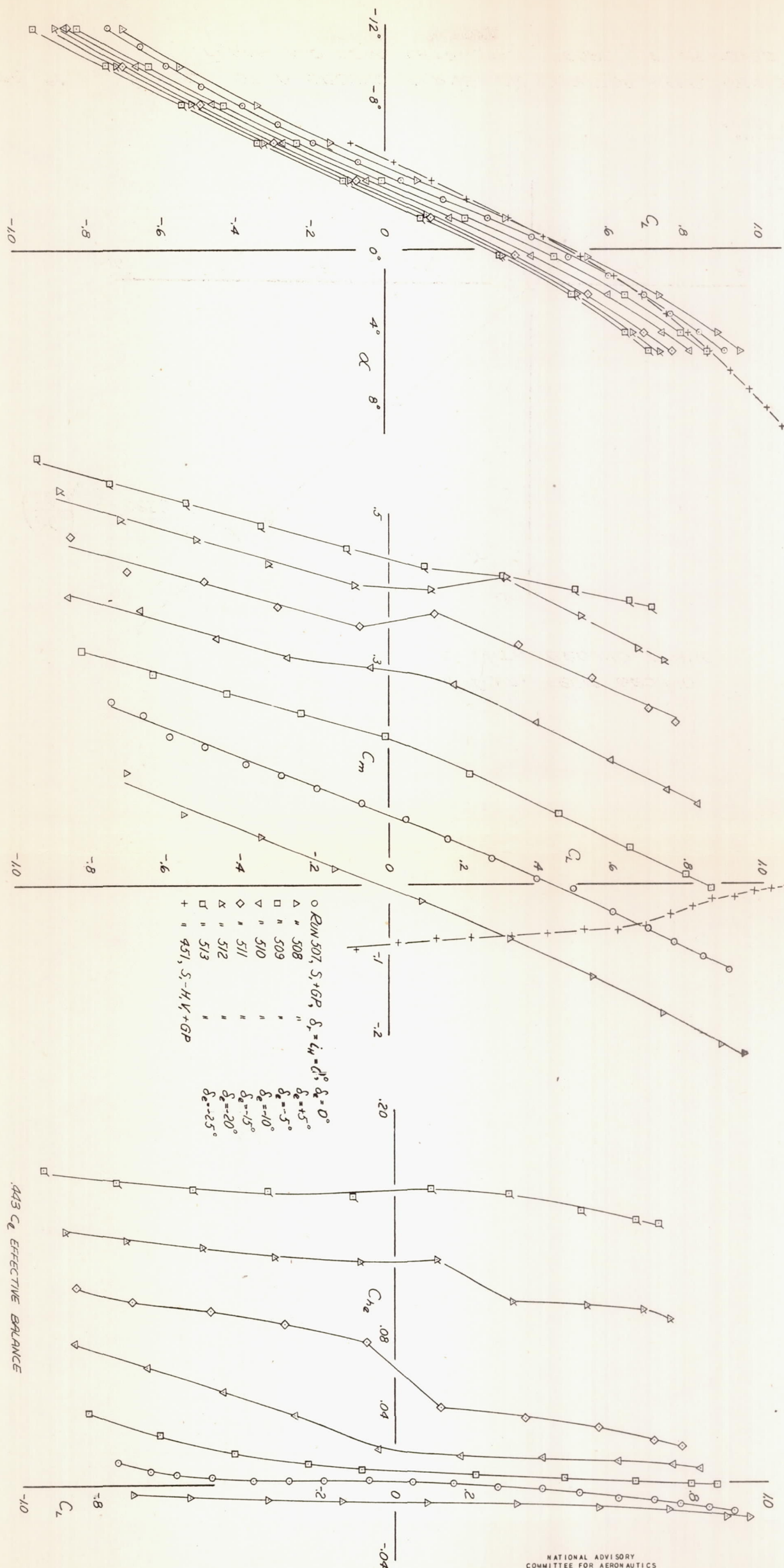
.443 C_D EFFECTIVE BALANCE

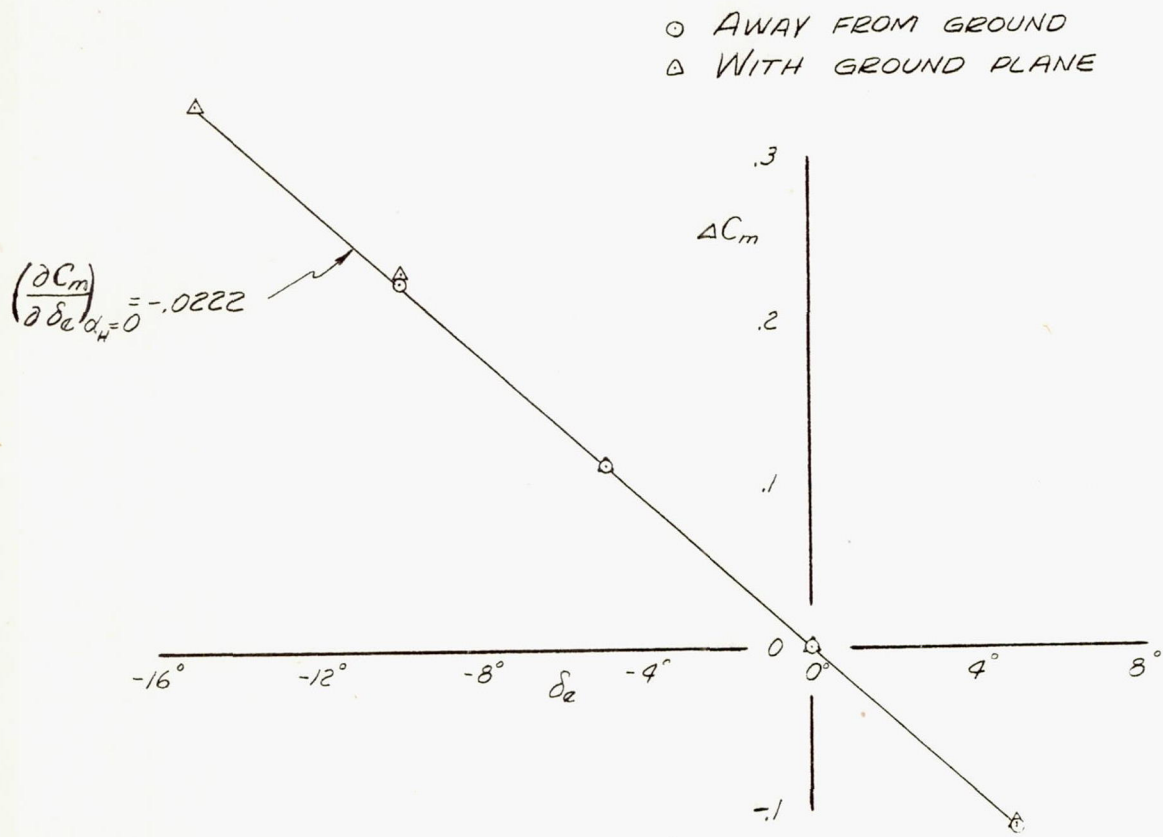
FIGURE 52.- VARIATION OF AERODYNAMIC CHARACTERISTICS WITH ANGLE OF ATTACK OF THE MODEL IN THE PRESENCE OF A GROUND PLANE. STABILIZER INCIDENCE VARIED, FLAPS $0^\circ, 30^\circ$, AND 40° , GEAR UP, PROPELLER OFF.



NATIONAL ADVISORY
COMMITTEE FOR AERONAUTICS

FIGURE 53.- STABILIZER EFFECTIVENESS OF THE MODEL IN THE PRESENCE OF A GROUND PLANE. FLAPS 0° , 30° , AND 40° , GEAR UP, PROPELLER OFF.





NATIONAL ADVISORY
COMMITTEE FOR AERONAUTICS

FIGURE 55. - EFFECT OF A GROUND PLANE ON ELEVATOR EFFECTIVENESS.
FLAPS AND GEAR RETRACTED, PROPELLER REMOVED.

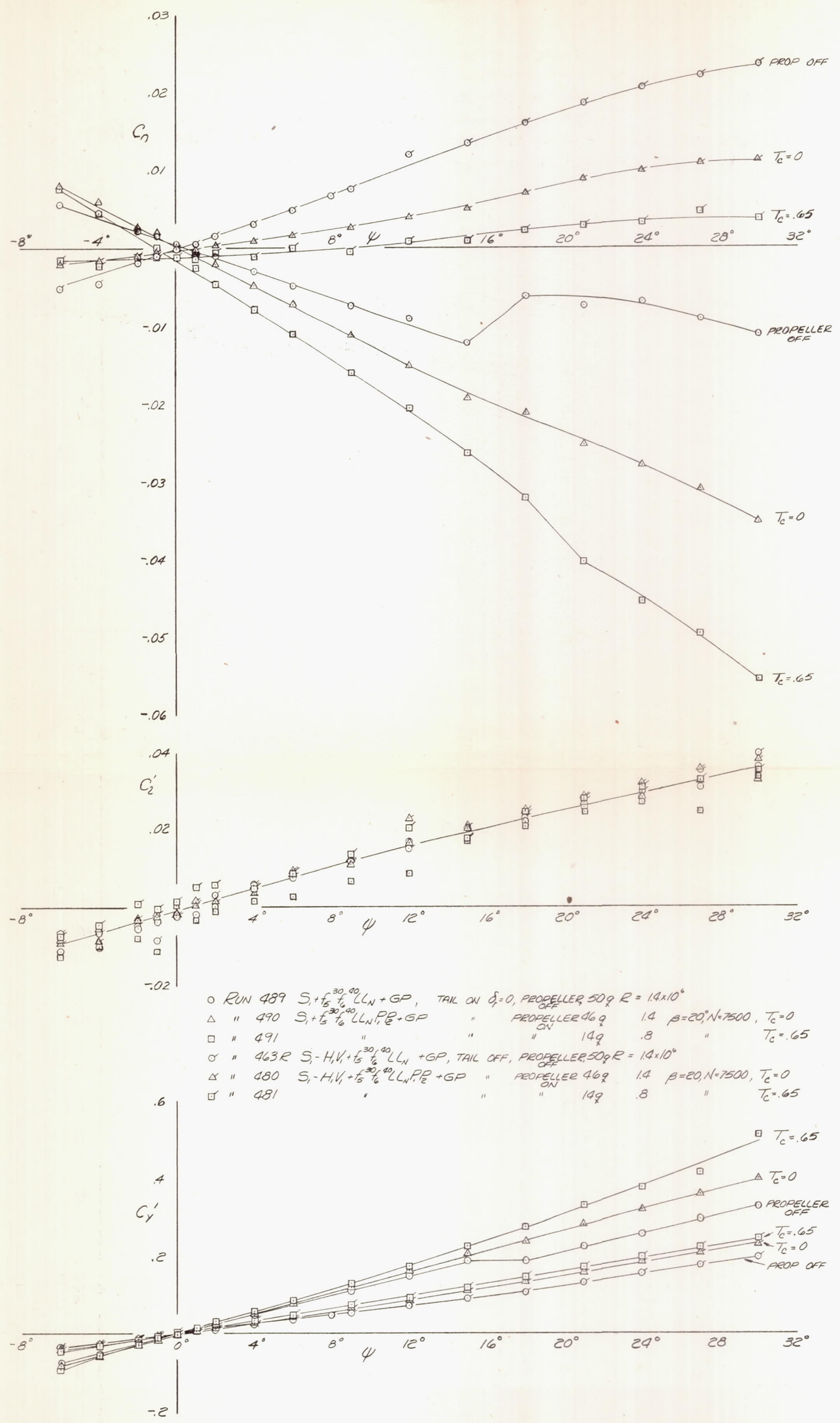
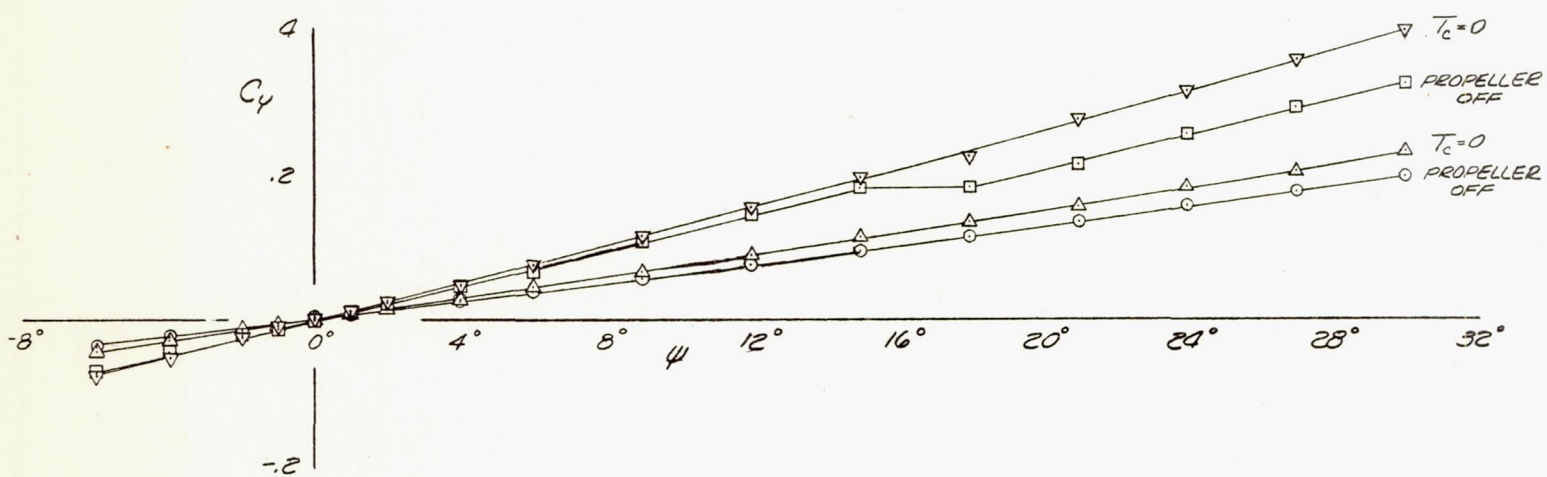
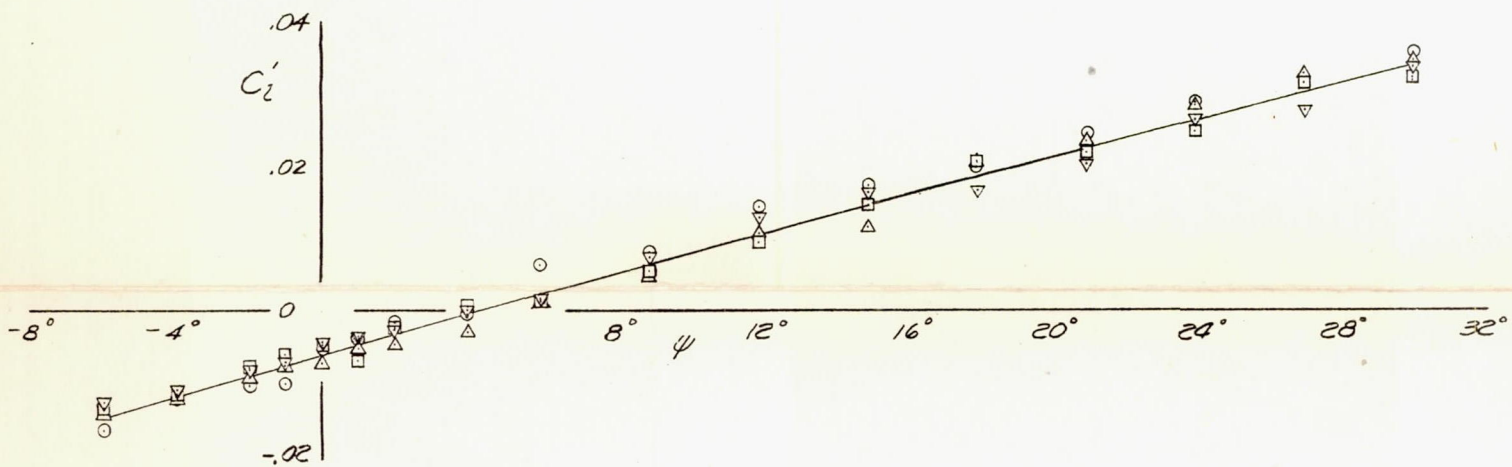
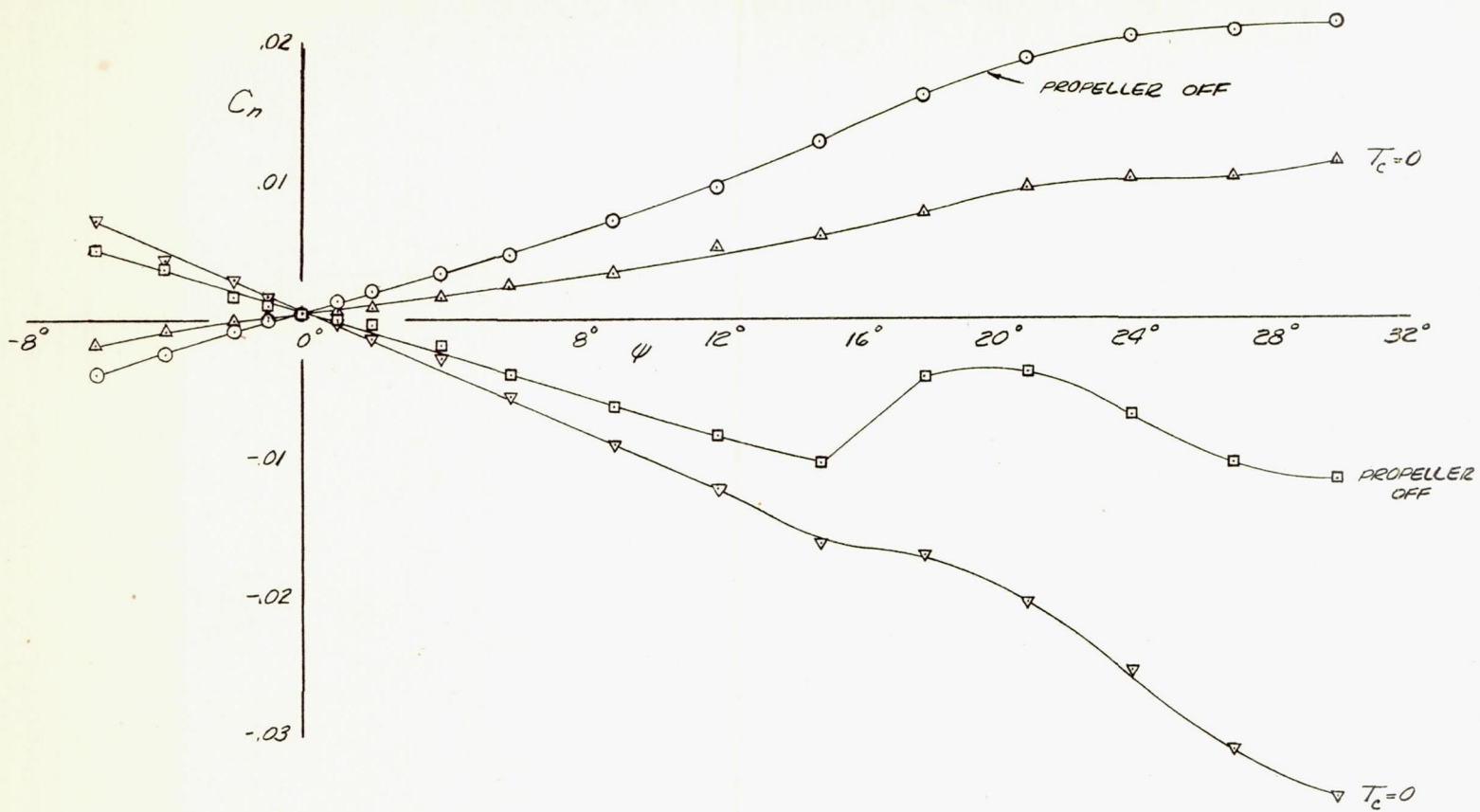


FIGURE 56.- VARIATION OF AERODYNAMIC CHARACTERISTICS WITH ANGLE OF YAW OF THE MODEL IN THE PRESENCE OF A GROUND PLANE. FLAPS AT 30° , GEAR DOWN, $\alpha_u = 2^\circ$



- RUN 462R $S_1-H.V. + f_5^{50} f_6^{40} LL_N + GP$, TAIL OFF, PROPELLER OFF, 50g $R=1.4 \times 10^6$
- △ " 479 $S_1-H.V. + f_5^{50} f_6^{40} LL_N P_2 + GP$ " PROPELLER ON, 46g " $\beta=20^\circ, N=7500, T_c=0$
- " 488 $S_1 + f_5^{50} f_6^{40} LL_N + GP$ TAIL ON, PROPELLER OFF, 50g "
- ▽ " 492 $S_1 + f_5^{50} f_6^{40} LL_N P_2 + GP$ " PROPELLER ON, 46g " $\beta=20^\circ, N=7500, T_c=0$

FIGURE 57.- VARIATION OF AERODYNAMIC CHARACTERISTICS WITH ANGLE OF YAW OF THE MODEL IN THE PRESENCE OF A GROUND PLANE. FLAPS AT 50° GEAR EXTENDED, $\alpha_0 = -1^\circ$